# CHARACTERIZATION OF A NOVEL SORBENT POLYMER FOR THE TREATMENT OF SEPSIS

by

**Isabella Elfriede Valenti**

B.S. in Bioengineering, The Pennsylvania State University, 2008

Submitted to the Graduate Faculty of

Swanson School of Engineering in partial fulfillment

of the requirements for the degree of

Master of Science in Bioengineering

University of Pittsburgh

2010

UNIVERSITY OF PITTSBURGH

SWANSON SCHOOL OF ENGINEERING

This thesis was presented

by

Isabella Elfriede Valenti

It was defended on

June 29, 2010

and approved by

William R. Wagner, Ph.D.
Professor, Departments of Surgery, Chemical & Petroleum Engineering, and Bioengineering

John A. Kellum, M.D., FACP, FCCM
Professor, Departments of Critical Care Medicine and Bioengineering

Thesis Advisor: William J. Federspiel, Ph.D.
William Kepler Whiteford Professor, Departments of Chemical & Petroleum Engineering, Critical Care Medicine, and Bioengineering

**CHARACTERIZATION OF A NOVEL SORBENT POLYMER FOR THE TREATMENT OF SEPSIS**

Isabella Elfriede Valenti, M.S.
University of Pittsburgh, 2010

Severe sepsis is defined as a systemic inflammation leading to organ failure and is characterized by the release of pro- and anti-inflammatory markers called cytokines. Current clinical techniques used to treat sepsis such as early goal-directed therapy, specific-target drug therapies, and hemofiltration have had limited success and inconsistent outcomes. A newly investigated therapy, hemoadsorption, has proven to be nonselective and therefore broad-spectrum (i.e. restores homeostasis to the system as a whole); more efficient and cost-effective than affinity-based removal; and is auto-regulating in that solutes at higher concentrations are removed more rapidly than those at lower, safer concentrations. The goal of this thesis was to characterize and compare adsorption profiles of several cytokines in our cytokine adsorption device (CAD) for use in the treatment of sepsis. To do this, we first characterized capture of our three main cytokines of interest in the original lot of CytoSorb resin for buffer and serum. This polymer is a highly porous polymer manufactured by Cytosorbents, Inc. (Monmouth Junction, NJ) and consists of a polystyrene divinylbenzene (PSDVB) copolymer covered in a biocompatible polyvinylpyrrolidone coating. We then detailed changes in adsorption profiles over a manufacturer's lot change and re-established our baseline capture rates with the main cytokines of interest as well as a secondary group of cytokines in both buffer and serum. Further investigation into a lot of smaller diameter polymer followed and a re-design of our CAD ensued. Finally, we tested the polymer in three distinct red blood cell suspensions in order to

methodically increase the degree of complexity of the capture suspension. With the information included in this thesis, further optimization and development to our CAD and the polymer will be done. Additionally, the characterization of the resin is crucial for our in-house mathematical model as well as the development and calibration of a systems model of sepsis. This model will be used to simulate the development and progression of sepsis in humans and the integration of a therapeutic CAD intervention protocol into the timecourse of sepsis to improve patient outcomes.

## TABLE OF CONTENTS

## LIST OF TABLES

## LIST OF FIGURES

# PREFACE

As my time in graduate school has come to an end, I would like to take the time to thank those who have contributed, mentored, and supported me during my studies. First and foremost, I would like to thank my advisor, Dr. William Federspiel, for his mentorship the past two years. With your support, patience, and knowledge, I have been able to develop the research, writing, and presentation skills crucial to an engineer. I am grateful for the chance to work on a demanding and fulfilling research project that has greatly prepared me for my future career in medical device development.

I would also like to thank my committee members, Dr. John Kellum and Dr. William Wagner. Their expertise has not only aided me in my research, but also the development of the SEPsIS project as a whole.

Over the past two years, I certainly would not have come as far as I have without the technical support and friendship of those in the Medical Devices Lab. I'd like to thank all of those members of the lab, past and present, for your friendship and support made my time in the lab so much more enjoyable. I wish you all the best of luck in everything you do.

Lastly, I would like to thank my wonderful family for their support and love throughout my time in school. To my soon-to-be husband: your patience, kindness, support, and encouragement helped me though the ups and downs of graduate school, thank you for always believing in me and what I could accomplish. I love you and cannot wait to start our life

together. To my mom: thank you for your love and encouragement; your strength never ceases to amaze me and allows me to work through even the toughest of days. To my dad: although only here in spirit, your kindness, love, and encouragement will never be forgotten; I miss you always. And to my four younger sisters who have always been my best friends, thank you for your love and always finding a way to bring a smile to my face.

This work was funded by the National Institutes of Health (NIH), National Heart, Lung, and Blood Institute (Grant Number *HL080926-02*). Thanks goes to the additional support from Cytosorbents, Inc. (Monmouth Junction, NJ) for manufacturing the polymer used in these studies as well as technical support provided. Finally, my gratitude goes to the McGowan Institute for Regenerative Medicine for additional funding and the CRISMA Laboratories (UPMC) for their contributions to the project.

# 1.0 INTRODUCTION

In noncardiac intensive care units, sepsis represents the largest cause of death [1]. Severe sepsis is defined as an infection that results in systemic inflammation, resulting in organ failure and death [2]. In the United States alone, more than 750,000 people each year are affected with a mortality rate greater than 30% [3, 4]. In addition, total annual costs associated with care for septic patients in the United States were greater than $16.7 billion in 2001 [4], and because sepsis affects the elderly at the highest rates, the incidence and cost of sepsis will continue to rise [5]. For survivors, detrimental effects of sepsis such as increased risk of death and increased medical costs associated with repeated hospitalizations remain for many years, resulting in a poor quality of life [4, 6]. Despite advances in medicine and research, understanding of the pathophysiology of sepsis and septic shock remains incomplete. Due to its high incidence, high mortality and morbidity, high cost, and complexity, sepsis is a major challenge faced in clinical medicine today.

## 1.1 OVERVIEW OF SEPSIS

As with most diseases and syndromes, sepsis is a progressive disorder and includes several stages, the definitions of which were laid out by the American College of Chest Physicians (ACCP) and the Society of Critical Care Medicine (SCCM) at a conference in 1991 in Chicago.

These stages, describing the inflammatory response to infection, include *systemic inflammatory response syndrome* (SIRS), *sepsis, severe sepsis,* and *septic shock* [2, 4].

Systemic inflammatory response syndrome or SIRS is the first stage of sepsis that is diagnosed. Patients with two or more of the following vitals are described as having SIRS: heart rate greater than 90 beats per minute, body temperature less than 36 $^{o}$C (96.8 $^{o}$F) or greater than 38 $^{o}$C (100.4 $^{o}$F), respiratory rate greater than 20 breaths per minute or a $PaCO_2$ less than 32 mm Hg on a blood gas analyzer, and a white blood cell count less than 4000 cells/mm$^3$ or greater than 12000 cells/mm$^3$ or the presence of greater than 10% immature neutrophils [4]. These criteria are nonspecific and general, reflecting the numerous and divergent individual diseases that can lead to a systemic inflammatory response that make studying and understanding the disease such a challenge. As a result, the incidence of SIRS is extremely high, with estimates of 30% of all in-hospital patients, greater than 50% of all ICU patients, and more than 80% of surgical patients in any given hospital meeting the criteria for SIRS [7].

A landmark study by Rangel-Frausto et al. examined the incidence and progression of SIRS in three ICUs and three hospital wards over seven months at academic medical centers, substantiating the high incidence estimates. Of 3708 patients admitted, more than 68% met criteria for SIRS; patients with SIRS had a 26% chance of developing sepsis, 18% chance of developing sever sepsis, and a 4% chance of developing septic shock. Patients with two SIRS criteria at admission had a mortality of 6% compared to 3% without SIRS, while patients with three criteria had a mortality of 9%, and those meeting all four criteria had a mortality of 18% [8].

Sepsis is defined as a patient who meets SIRS criteria in response to a known infection source, as diagramed in Figure 1, with typical vital signs including: fever, tachypnea,

tachycardia and hypotension [1]. In most epidemiological studies, pulmonary, gastrointestinal, urinary tract, and bloodstream infections are the most common sources of infection in patients with sepsis or severe sepsis, accounting for approximately 80% of all sites. In addition to infection site, incidence by which sepsis is acquired has also been examined. Specifically, community acquired infections account for more than 55% of severe sepsis that requires hospitalization, while the remaining 44% are nosocomial and are caused by infections acquired in the hospital [4].

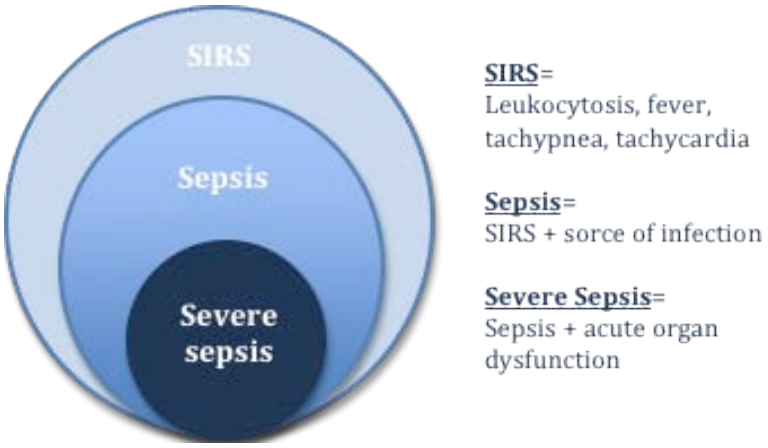


**Figure 1:** Representation of overlap between SIRS, sepsis, and severe sepsis [4]

The high incidence and numerous causes of SIRS and sepsis are reflected in the varying degrees of susceptibility of patients, with demographic variables and co-morbidities accounting for some of the variability. Demographic traits that put a patient at a higher risk include being male, African American, elderly (over 65 years of age), and living in poverty. Risk factors for increased susceptibility for the disease include co-morbidities such as diabetes, cancers, alcoholism, HIV infection, and immunosuppression agents. Also, studies have identified a seasonal change in the incidence of sepsis, with winter months having higher rates [4, 9, 10].

Severe sepsis is the progression of the systemic response to inflammation and infection to the point where the patient develops acute organ dysfunction. Organs typically affected include lung, kidney, and cardiovascular systems with clinical indications outlined in Table 1, below. Septic shock is defined for those patients with severe sepsis and acute cardiovascular dysfunction [1, 7].

**Table 1:** Affected organs and clinical indications in severe sepsis [1]

| | |
|---|---|
| **Central Nervous System** | Encephalopathy<br>Delirium |
| **Cardiopulmonary** | Increased cardiac output<br>Decreased systemic vascular resistance<br>Hypotension<br>Metabolic acidosis hyperlacatemia<br>Acute lung injury, hypoxemia<br>Acute respiratory distress syndrome (ARDS) |
| **Renal** | Decreased urinary output<br>Acute tubular necrosis |
| **Gastrointestinal** | Ileus<br>Elevated bilirubin |
| **Dermatology** | Ecthyma gangrenosum<br>Symmetrical peripheral gangrene<br>Acrocyanosis<br>Toxic erythema<br>Rash |
| **Other** | Metabolic<br>Hyperglycemia, hypoglycemia<br>Hematologic<br>Leukocytosis, leucopenia<br>Thrombocytopenia<br>Disseminated intravascular coagulation |

In order to better manage sepsis and develop more effective treatment options, an understanding of the pathophysiology and cellular mechanisms is important. Although understanding is incomplete, it is generally accepted that two mechanisms result in sepsis, severe sepsis, and

septic shock: extrinsic: toxins, endotoxin, protein particles from gram-positive bacteria, viruses, fungi; and intrinsic (or endogenous); pro-inflammatory mediators released into the blood stream [11].

Endotxin, a lipopolysaccharide (LPS), can directly activate macrophages, endothelial cells, and complement. This activation results in the release of proinflammatory mediators, or proinflammatory cytokines, such as: tumor necrosis factor (TNF), interleukin-1 (IL-1), interleukin-6 (IL-6), high mobility group box-1 protein (HMG-B1), macrophage migratory inhibitory factor (MIF), platelet activating factor (PAF), nitric oxide (NO), complements, and eicosonoids. Similarly, gram-positive bacteria may cause septic shock that is impossible to differentiate from gram-negative bacteria. The binding of LPS or proteins from gram-positive bacteria to the surface molecule CD14 on macrophages, monocytes, and neutrophils relays a signal through a transmembrane protein called the toll-like receptor (TLR). Signals from the CD14/TLR complex activate nuclear factor κB (NK- κB) by phosphorylation cascades, causing NK- κB to move from the cytoplasm to the nucleus. This translocation of NK- κB promotes the production of cytokines by target genes. Cytokines are defined as small proteins approximately 25 kDa that are released by cells in response to a stimulus and induce a signaling pathway through receptors. A chemokine is a subgroup of cytokines that have chemoattractant properties, causing cells to migrate towards the chemokine [12]. The systemic release of cytokines into the bloodstream is characteristic of sepsis and is strongly correlated to organ failure and death [13]. This organ damage then leads to further cytokine release, which further damages organs, resulting in more cytokine production. The production of cytokines, then, is redundant and difficult to manage.

Viruses, which can cause injury to host cells, do so by direct lysis of host cells, lysis of distant organ cells due to activated complement pathway, or are the result of circulating proinflammatory cytokines released in response to the presence of the virus. Particles on viruses can also bind CD14 directly, activating the NK- κB pathway. Finally, particles of fungi can activate macrophages, endothelial cells, and complements, with some fungal infections directly interacting with TLRs on cell membranes, activating the NK- κB pathway and therefore inducing the production of cytokines [11].

Intrinsic factors are released as a result of activation of the immune system by external stimuli such as severe infections, burns, trauma, and hemorrhage and include cytokines/chemokines (TNF, IL-1, IL-6, IL-8, HMG-B1, and MIF) and noncytokine mediators (NO, PAF, and complements) [11]. Important cytokine and chemokine mediators for this study will be outlined in section 1.2.

Noncytokine mediator nitric oxide (NO) is a free radical with cytotoxic properties and can be formed by synthesis in cendothelial cells, in the brain, and by macrophages (which is triggered by TNF, IL-1, or PAF). The action of NO results in decreased intracellular calcium, causing vascular and nonvascular smooth muscle relaxation. In sepsis, this relaxation of smooth muscles results in hypotension. Additionally, NO inhibits platelet adhesion and aggregation as well as polymorphonuclear (PMN) chemotaxis. Another noncytokine mediator, platelet activating factor (PAF), is synthesized by endothelial cells, macrophages, and neutrophils. In the presence of endotoxin, it is released and promotes aggravation and adhesion of platelets, thrombosis, and vascular injury as well as enhancing PMN chemotactic responses [11].

In addition to the release of cytokines, sepsis is complicated by other cellular mechanisms. For example, when infection is introduced into the body, activation of complement

via the alternate pathway may take place. Here, LPS is able to activate C3, signaling the start of the cascade. Activated C3 and C5 are anaphylatoxins and potent vasodilators. Excessive activation of complement can result in organ damage and has been hypothesized to contribute to hemodynamic collapse in septic shock [11].

## 1.2 INFLAMMATORY MEDIATORS OF INTEREST

As described above, sepsis is characterized by a surplus of inflammatory mediators called cytokines in the bloodstream. This release of cytokines, both pro- and anti-inflammatory, is associated with organ failure and death [13]. Several published studies have examined which cytokines may be most important in effectively identifying the disease, identifying patients at higher risk of mortality, and guiding treatment options over the course of the disease [11, 14-16]. The presence and concentration of specific cytokines and chemokines can then be considered biomarkers, or "characteristics objectively measured and evaluated as indicators of normal biological processes, pathogenic processes, or pharmacological responses to a therapeutic intervention," to be measured and carefully monitored over the timecourse of the patient [16]. These biomarkers, in addition to being ideally rapidly available and easy to assay, would also be potential targets for therapy.

In our laboratory, three important cytokine mediators of sepsis to be studied were chosen based on data from the largest sepsis study to date, the results of an observational study called GenIMS at the University Of Pittsburgh School Of Medicine, Department of Critical Care. This study, which analyzed more than 1600 patients at 30 sites in the Eastern United States, found that plasma levels of interleukin 6 (IL-6), tumor necrosis factor (TNF), and interleukin 10 (IL-10) on

the day of presentation were higher in those patients that died in the hospital compared to those that were discharged alive [17]. A conclusion of the GenIMS study was that those three cytokines were important for predicting outcomes in sepsis and were, therefore, significant to modulate using hemoadsorption (discussed in section 1.4.1) [17]. For that reason, our laboratory focuses on the removal kinetics of IL-6, TNF, and IL-10, with each cytokine suspended by itself in solution to avoid possible effects of competition. These three cytokines as well as additional secondary cytokines such as IL-1, IL-8, and HMG-B1 will be characterized thoroughly in the following chapters in several different suspensions and devices.

IL-6 is a 21-26 kDa glycoprotein and is considered both a pro- and anti-inflammatory mediator, involved in the immune response, inflammation, and hematopoiesis [18]. It is produced by activated B cells, activated T lymphocyte, activated monocytes, and endothelial cells and has a relatively long half-life, making measurements in serum reliable and uncomplicated. It is one of the initial cytokines released in inflammation, making it a potential early predictor in the time course of sepsis [11, 16]; however, it is a comparatively nonspecific marker of infection, elevated in many inflammatory states [16]. The release of IL-6 induces T-cell and B-cell proliferation, as well as the production of acute-phase proteins. These proteins, produced in the liver, are the result of inflammation or tissue injury, although their actual roles are not well understood [11].

TNF is a 51.9 kDa trimer classified as a pro-inflammatory cytokine and is secreted in large quantities by activated macrophages during sepsis and septic shock. It is an important mediator of inflammation, causing fever, hypotension, shock-like syndrome, organ dysfunction, and activation of PMN and endothelial cells and has been indicated in the development certain

types of cancer [19]. The production of TNF results in production of complement components, NO, cell adhesion molecules, and IL-1, IL-6, IL-8, and IL-10 [18].

Finally, IL-10 is a 17-21 kDa dimeric protein classified as an anti-inflammatory cytokine that can down-regulated activated macrophages. Produced by epithelial cells, monocytes, and lymphocytes during inflammatory states, its plasma levels have been shown to correlate to state of shock, TNF plasma concentrations, and organ injury [18].

## 1.3 CURRENT CLINICAL THERAPIES

Clinical treatment for severe sepsis has been approached several ways, each to varying degrees of success and failure. In general, patients have been treated using hemodynamic support and intensive care; early goal-directed therapy (EGDT); specific and broad-spectrum drug therapies; and hemofiltration. Typically, the use of one therapy over another is varied, with location of care and knowledge of the attending physician guiding therapy choice [20]. Unfortunately, each therapy currently used clinically has limitations associated with its use as indicated by the high mortality rate of sepsis despite these treatments being accessible to most. The individual therapies and their limitations will be discussed further in the following section.

### 1.3.1 Hemodynamic support and intensive care

Before innovative techniques such as drug therapies and filtration, the standard of care for sepsis included hemodynamic support and intensive care. For many ICUs, this is still the most common method of care practiced and includes monitoring vital signs, central venous pressure,

and urinary output to achieve specific hemodynamic endpoints [21]. According to a publication by a panel of the American College of Critical Care Medicine of the Society of Critical Care Medicine regarding practice parameters for hemodynamic support, there are three main components in treating sepsis and septic shock: the first priority is to achieve and maintain a reasonable mean arterial pressure and cardiac output to maintain vitals; next, infection should be identified and eliminated; finally, a later goal includes disrupting the progression of the disease to septic shock. During the time the patient is in the ICU, organ perfusion and function must be maintained and monitored [21].

From the guidelines of the ACCM, the following basic principles for hemodynamic support were established [21]:

1. Resuscitate patients quickly and actively. Perfusion of organs and tissues should be addressed early on for improved outcomes.
2. Treatment of patients with severe sepsis of septic shock should take place in an ICU with continuous EKG and arterial oxygen monitoring.
3. Arterial cannulation is recommended in order to provide more accurate monitoring of intra-arterial pressure and beat-to-beat analysis. More accurate monitoring allows for physicians to adjust therapy quickly and effectively.
4. End points of arterial pressure, heart rate, urine output, skin perfusion, mental status, and indexes of tissue perfusion (blood lactate concentration and venous oxygen saturation) should be met by adjusting therapy accordingly.
5. Proper assessment of cardiac filling pressures may require catheterization. Echocardiography may also be used for ventricular volume and cardiac performance assessment.

In addition to the above guidelines, the ACCM also recommended three forms of therapy in order to achieve the end points in guideline 4 of proper arterial pressure, heart rate, urine output, skin perfusion, mental status, and indexes of tissue perfusion. These therapies include fluid resuscitation, vasopressor therapy, and inotropic therapy.

Recommendations of fluid therapy include the following: fluid infusion is the first step in treating a septic patient; isotonic crystalloids or iso-oncotic colloids may also be effective if titrated to endpoints; invasive hemodynamic monitoring may be required for those patients not responding to initial fluid infusions and should be used to monitor complications such as pulmonary edema; finally, hemoglobin concentrations should be monitored and maintained at recommended levels, especially in patients with low cardiac output, lactic acidosis, venous oxygenation desaturation, or cardiac or pulmonary disease. Complications of fluid resuscitation include pulmonary and systemic edema resulting from increases in hydrostatic pressures, decreases in colloid osmotic pressures, and increases in microvascular permeability associated with septic shock [21].

ACCM recommendations for vasopressor therapy include the use of dopamine and norepinephrine to increase arterial blood pressure once the patient is adequately fluid resuscitated. Phenylephrine is an alternative to increase blood pressure if tachyarrhythmias are present. While low doses of dopamine to maintain renal function are not recommended. Replacement does steroids for those patients with hypotension may be beneficial, and low doses of vasopressors as a hormone replacement may also aid in raising blood pressure, although data has not been well established. Complications of vasopressor therapy include significant

tachycardia, possible myocardial ischemia or infarction, decreased stroke volume and cardiac output, limp ischemia or necrosis, and impaired blood flow [21].

Finally, the first of several recommendations for inotropic therapy describes that dobutamine is a first choice for patients with low cardiac index and/or low mixed venous blood saturation after fluid resuscitation. For patients with hypoperfusion, doutamine may help increase cardiac index and vasodpressors such as norepinephrine may be titrated separately from one another to maintain mean arterial pressure and cardiac output. Complications of inotropic therapies include significant tachycardia or other cardiac arrhythmias, possible myocardial ischemia or infarction, necrosis of myocardial tissue, reduction in blood pressure, or possible impaired blood flow [21].

Hemodynamic support and intensive care has been and continues to be a prominent method for caring for patients with sepsis, severe sepsis, and septic shock. Unfortunately, this method includes many complications and, according to several published studies, does not result in a consistent, significant improvement in the mortality and morbidity of sepsis [19, 22].

### 1.3.2 Early goal-directed therapy (EGDT)

Early goal-directed therapy is a therapy designed to address inconstancies and deficiencies in hemodynamic support and intensive care. The argument against hemodynamic support and intensive care is based upon the fact that vital signs, venous pressure, urinary output, and physical findings are inadequate to detect global tissue hypoxia. To address these inadequacies, EGDT includes goal-oriented management of cardiac preload, afterload, and contractility to maintain equilibrium between systemic oxygen delivery and oxygen demand [19, 23].

One study conducted by Rivers et al. investigated the potential benefit of EGDT in sepsis patients compared to controls (hemodynamic support and intensive care) [22]. In this study 263 patients were randomly assigned to EGDT or control groups, with no significant differences in either group concerning baseline characteristics at admittance. During the course of the study, those patients in the control group were given care at the attending doctors' discretion following a protocol for hemodynamic support, similar to that found in section 1.3.1, and were admitted to inpatient beds as soon as possible. Those patients in the experimental group received EGDT therapy as shown in Figure 2 for at least six hours in the emergency department before being transferred to inpatient beds. The study found that those patients with EGDT had an in-hospital mortality of 30.5% compared to 46.5% for the control. Additionally, patients in the EGDT group had significantly higher mean central venous oxygen saturation, lower lactate concentration, lower base deficit, and a higher pH, and less severe organ dysfunction than those in the control group.

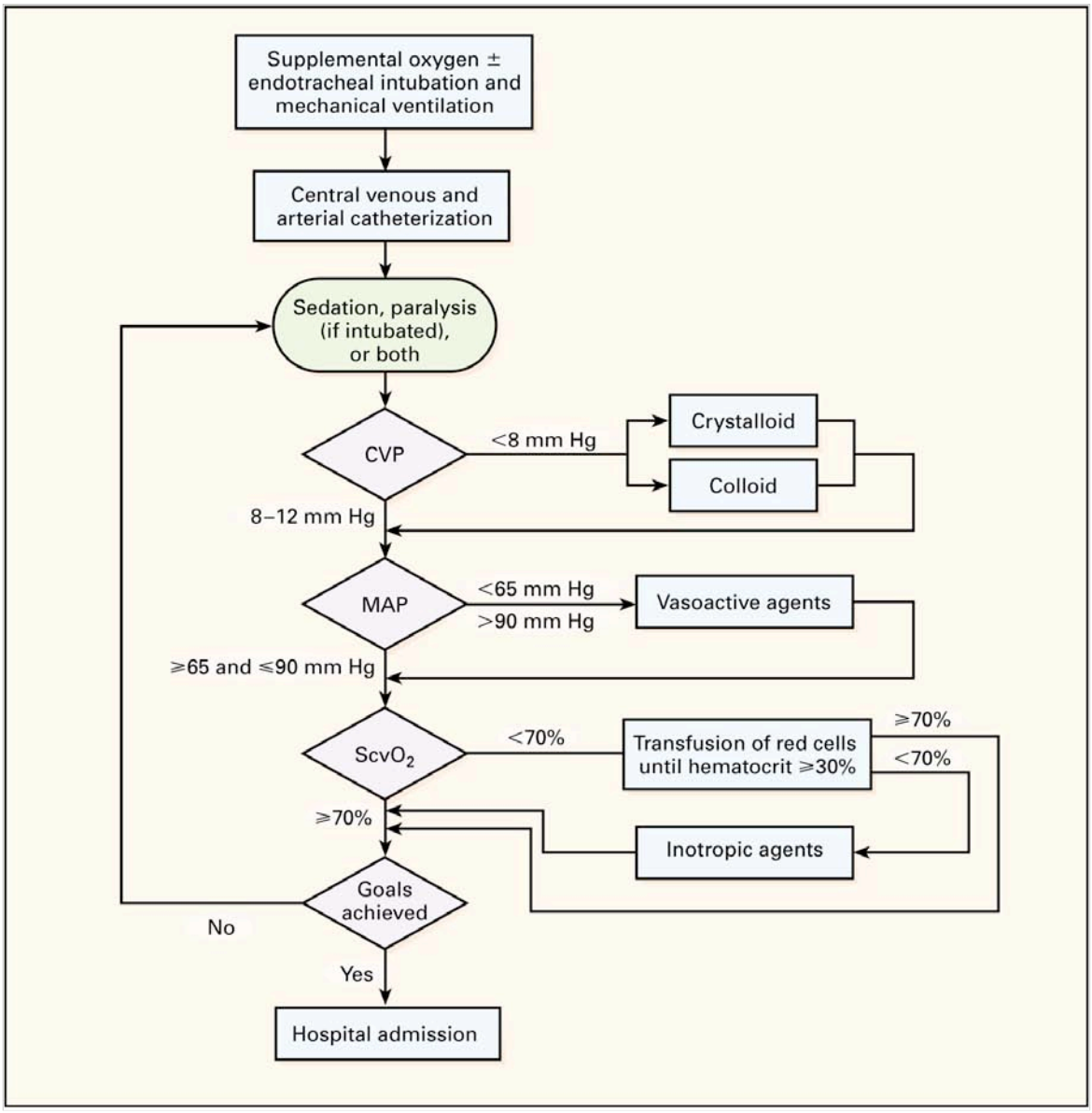


**Figure 2:** Protocol for EGDT [19, 22]

Although EGDT in this one study did seem to significantly increase the rate of survival, debate still exists concerning the diagnostic and therapeutic interventions used and this method is not used universally. Additionally, as with many studies on the mortality of sepsis, further and broader studies should be implemented in order to discover the true significance of the method [19, 24].

### 1.3.3 Drug therapies

In sepsis, drug therapies traditionally pursue one specific target in an attempt to down-regulate pro-inflammatory markers or limit the response of the immune system. For example, a clinical trial by Abraham et al. focused on the use of a specific antagonist of TNF, murine TNF monoclonal antibody (TNF mAb), for the treatment of sepsis. In this study 1879 patients were randomly assigned a single infusion of TNF mAb or a placebo consisting of human serum albumin with mortality at 28 days being the main outcome measurement. The group determined that there was no association between the use of the therapy and increased reversal of symptoms and deemed the drug ineffective in the treatment of sepsis [25]. Similarly, Fisher et al. conducted a clinical trial to test the efficacy of interleukin 1 receptor antagonist for the treatment of sepsis, specifically targeting IL-1 in an attempt to down-regulate that cytokine. In this study 99 patients were randomly assigned to be given one of three different doses of IL-1RA or placebo in addition to standard supportive care outlined in section 1.3.1 with mortality at 28 days the main outcome. This group determined that a slight dose-dependent survival advantage existed for those that were treated; however, the small n-value in this study was a major limitation in the evaluation of the results. For both of these trials, failure of the specific antagonist is a result of the inability of the drugs to attenuate the entire response of sepsis [26].

Other specific mediators have also been used as a source for drug therapies. For example, drotrecogin alfa (activated protein C) and corticosteroids have all been used for the treatment of sepsis to little success. Studies by Bernard et al. and Agnus et al. showed a significant reduction in mortality using drotrecogin alfa, a protein with antithrombotic, antiinflammatory, and profibrinolytic properties; however in the first study the risk of bleeding

was also significantly increased and the second study indicated that the positive effects of the drug were only observed until discharge, with little effect after [3, 27].

Finally, Annane et al. reported on the results of a study using low doses of corticosteroids in order to treat septic shock. In this study, 300 patients were randomly assigned to receive hydrocortisone and fludrocortisones or placebo to determine if improvement to 28-day survival were made. This group concluded that there was a significant increase in survival [28]; however, a subsequent publication in rebuttal of those results indicate that the patient population in the Annane et al. study was unfairly skewed and biased the results [29].

The lack of definite success in improving patient outcomes in the above randomized clinical trials of sepsis led to the development of more broad-spectrum cytokine modulation such as hemofiltration and hemoadsorption, discussed in the following sections.

### 1.3.4 Hemofiltration

Hemofiltration is the removal of solutes from the plasma by convection generated by a concentration gradient across a semi-permeable membrane. This therapy is advantageous over those therapies targeting specific antagonists since it can restore homeostasis by nonspecific removal of both pro- and anti-inflammatory mediators [30, 31]. Additionally, this type of treatment is concentration-regulated, meaning that mediators of higher concentrations are eliminated at a higher rate compared to those mediators at a lower plasma level [32]. The regulation inherent in hemofiltration is important since it does not completely deplete levels of all inflammatory mediators in a septic patient, which may reduce the ability of the patient to fight infection. Several studies utilizing hemofiltration have been able to demonstrate an early

decrease in cytokine concentration followed by a plateauing of removal with time [33-35]. With limited available surface area, it is clear that filters become saturated over time.

Several studies have been able to demonstrate the hemofiltration using porous fibers is able to remove many different mediators of inflammation and thereby influence the plasma concentration of those mediators [33-35]. In one such study, circulating TNF concentrations in a small population of septic patients decreased during continuous veno-venous hemofiltration using an AN69 hemofilter (Hospal Multiflow 60, Cobe Renal Intensive Care, Lakewood, CO). The mechanism by which the TNF was removed by the filter was not through diffusive transport but by convective means. Upon analysis of the ultrafiltrate, however, low cytokine concentrations were found. This indicated that adsorption of the cytokines to the filter membrane was the main mechanism by which TNF was removed [35]. Another study monitoring plasma levels of circulating IL-6 in septic rats during hemofiltration with a fiber module also came to the conclusion that the cytokines were being removed by nonspecific adsorption onto the fibers in the filter [34]. Finally, a clinical study in Belgium using hemofiltration with an AN69 hemofilter (Multiflow 100, Hospal, France) determined that concentrations of IL-6, TNF, and IL-1β were significantly reduced and that the main mechanism of removal was through nonspecific adsorption to the membrane [33].

These studies using hemofiltration were able to demonstrate that the removal of cytokines by adsorption was an important mechanism involved in modulating the inflammatory response of a patient. These filters are not designed for adsorption, however, and are severely limited by the lack of surface area of the fibers. Accordingly, devices utilizing porous beads as an absorbent, with far greater available surface area, are more likely to succeed.

## 1.4 BEAD-BASED CYTOKINE ADSORPTION DEVICE

### 1.4.1 Hemoadsorption

Hemoadsorption involves perfusion of whole blood or plasma directly through a device with a sorbent material such as porous beads. Blood purification by hemoadsorption is broad-spectrum due to the nonselective and concentration-dependant removal of both pro- and anti-inflammatory mediators (i.e. restores homeostasis to the system as a whole) [6]; is more efficient and cost-effective than affinity-based removal; and is auto-regulating in that solutes at higher concentrations are removed more rapidly than those at lower, safer concentrations [32].

One type of hemoadsorption currently used clinically is the Lixelle polymer developed by a group in Japan. This polymer has been shown to adsorb not only endotoxin, but also IL-1β, IL1-RA, IL-6, IL-8, and TNF with moderate efficiency both in rats and humans. The binding of both the endotoxin and the inflammatory mediators has been shown to significantly improve patient outcomes [15, 36-38]. From the same group, the development of a new column for the treatment of sepsis is also underway. This device, known as CTR, works along the same principal as the Lixelle column but contains larger, porous cellulose beads that are able to remove hydrophobic substances circulating in the blood. This polymer has a higher efficiency in adsorption of middle- to high-molecular weight molecules such as IL-6 and TNF due to carefully manufactured pore sizes that minimize adsorption of albumin and other high molecular weight proteins and preferentially targets smaller cytokines [36, 37].

Another adsorptive resin currently being developed is the CytoSorb™ polymer, used by our group for the development of a hemoadsorption device for the treatment of sepsis. This polymer and its use in this work will be discussed thoroughly in the following section.

### 1.4.2 CytoSorb™ polymer

The resin used in our device, CytoSorb™, is a highly porous polymer manufactured by Cytosorbents, Inc. (Monmouth Junction, NJ) [39]. The bead consists of a polystyrene divinylbenzene (PSDVB) copolymer covered in a biocompatible polyvinylpyrrolidone coating and is approximately 300-600 μm in diameter with a density of 1.02 g/cm$^3$ and a porosity 67.7%. Pore sizes in the beads range from 8-50 Å, allowing only smaller proteins to access the inside of the bead and excluding larger molecules such as albumin and fibrinogen. Figure 3 shows both a close-up of the polymer (left) and an image of the inner pore structure of the bead (right).

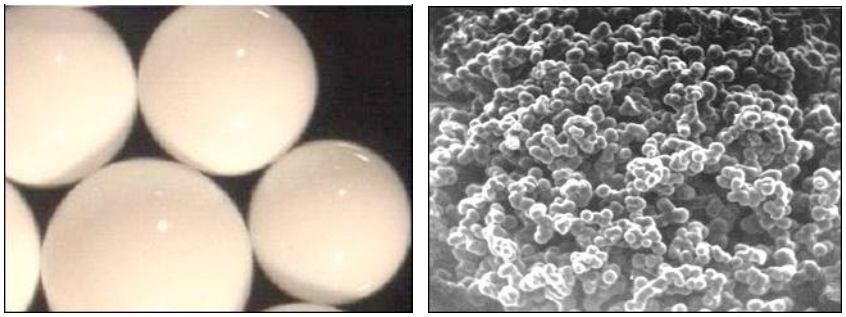

**Figure 3:** Images of CytoSorb™ polymer (left) and inner pore structure (right)

The use of a device that incorporates a biocompatible bead for nonspecific removal of cytokines is beneficial for several reasons. Specifically, whole blood may be perfused directly through the packed column, eliminating the need for plasma separation. Additionally, the surface area of CytoSorb™ polymer far exceeds that of fibers, with 850 m$^2$/g compared to 0.5-2 m$^2$/g. Finally, nonspecific and concentration dependant removal of inflammatory mediates is a broad-spectrum approach that increases efficiency and decreases costs that would be associated with a system for specific removal [32]. Kellum et al. showed that columns packed with CytoSorb™ polymer

were able to remove over 50% of circulating IL-6, TNF, and Il-10 concentrations in one hour in a study of septic rats. This removal was positively associated with increased survival times for animals of 21% compared to animals receiving sham treatment [40]. Another study using septic rats indicated a positive correlation between reduction in IL-6 and IL-10 with the CytoSorb™ polymer and mean survival times in septic rats [41]. Finally, a more recent study by Kellum et al. investigated the use of CytoSorb™ to remove cytokines from the blood of brain-dead humans. In this study, results indicated that the polymer was able to remove significant levels of IL-6 and TNF, but not IL-10 [42].

These studies indicate the significant removal of cytokines from the bloodstream as well as the positive effect hemoadsorption with the CytoSorb™ polymer has on survival outcomes for sepsis. In order to develop and optimize this polymer and device, a greater understanding of the adsorptive profiles of cytokines in suspension is needed. To do this, several different suspensions of increasing complexity from plain buffer to whole blood are needed to evaluate baseline polymer adsorption characteristics. Additionally, alterations in bead lots and polymer characteristics need to be fully understood and developed. Therefore, the goals of this thesis were to:

- Characterize adsorption profiles of cytokines in buffer and serum in baseline polymer
- Characterize and compare adsorption profiles across a change in bead lot and provide additional adsorption profiles for secondary cytokines of interest
- Characterize and compare adsorption profiles of several cytokines in the CAD and newly engineered reCAD and modify an existing mathematical model to produce more a accurate model fitting

- Characterize adsorption profiles of several cytokines spiked into red blood cells resuspended in plasma and serum as well as cytokines spiked into whole blood

In this thesis, Chapter 2.0 discusses the design and fabrication of our CAD as well as results of cytokine capture in buffer and serum for our original bead lot. Chapter 3.0 includes characterization and comparisons of changes in adsorption profiles over a manufacturer bead lot change. Chapter 4.0 then investigates a change in the sorbent polymer, with a focus on change in diameter with smaller diameter beads characterized and examined. Also in this chapter is the development and characterization of a newly engineered device, the reCAD, for use with small diameter polymer. Chapter 5.0 discusses cytokine capture in red blood cell suspensions and healthy whole blood in detail. Finally, Chapter 6.0 outlines the summary and conclusions of this work.

This characterization data is crucial not only for the validation and development of our own in-house mathematical model that will be discussed later, but also for the development and calibration of a systems model of sepsis developed by our colleagues [43]. This systems model will ultimately simulate the development and progression of sepsis in humans and the integration of a therapeutic CAD intervention protocol into the timecourse of sepsis to improve patient outcomes.

# 2.0 BASELINE BEAD CHARACTERIZATION

As discussed in Chapter 1.0 nonspecific removal of cytokines from whole blood using a hemoadsorption device is broad-spectrum, more efficient and cost-effective, and auto-regulating compared to other more traditional therapies. The development of a clinically used device, however, that utilizes biocompatible beads for direct blood perfusion has been absent from the literature. Our group has been investigating a novel porous, biocompatible sorbent polymer for use in such applications and has developed a device called the Cytokine Adsorption Device, or CAD, for use in the treatment of sepsis. In order to fully characterize such a polymer and device, recombinant human cytokines were spiked into suspensions of increasing complexity: buffer, serum, and red blood cell suspensions of buffer, serum, or whole blood. The more simplified suspensions allow us to understand the basic characteristics of cytokine removal with the polymer independent of the complexities inherent to whole blood perfusion, specifically biologically active molecules and soluble cytokine receptors in present in whole blood. This chapter focuses on the first set of characterization capture experiments for the original lot of CytoSorb$^{TM}$ polymer, #101003, in both buffer and serum.

A mathematical model was previously developed in-house in order to guide development of the device and characteristics of the polymer used. Our mathematical model was derived in order to quantify and compare removal of cytokines from suspensions using different bead sizes, flow rates, reservoir volumes, suspensions, etc., and was developed by graduate student Morgan

Fedorchak and Dr. William Federspiel. This model accounts for both macroscale transport in the device as well as diffusion and adsorption within the beads. The analysis published by DiLeo et al. yielded the following simple analytic expression for the removal rate of individual cytokines:

$$-\frac{dC_i}{dt} = \frac{Q}{V_r}\left[1 - \exp\frac{-3}{\sqrt{\pi}}\frac{m_b}{Q}\frac{1}{R}\sqrt{\frac{\Gamma_i}{\rho t}}\right]C_i(t) \qquad \textbf{(1)}$$

where Q is the volumetric flow rate, $V_r$ is the suspension reservoir volume, $m_b$ is the mass of beads in the column, $R$ is the radius of bead in the column, and ρ is the density of the polymer [44]. The unknown parameter $\Gamma_i$, which is specific to the cytokine *i* and the particular polymer, is defined as

$$\Gamma_i \equiv D_i q_i^{\max} K_i \qquad \textbf{(2)}$$

where $D_i$ is the effective diffusion coefficient of cytokine *i* in the beads, $q_i^{max}$ is the maximum capacity of cytokine *i* per unit mass of bead, and $K_i$ is the affinity constant from the Langmuir equilibrium adsorption isotherm [44].

To fit capture data to the model, concentrations of cytokines were normalized to initial concentration. Capture data was then fit to the model by integrating the above equation using a program written for MATLAB® R2009a (The MathWorks, Inc., Natick, MA), found in Appendix A1, so that reduction in reservoir volume due to sampling could be accounted for. Integration in MATLAB® was subject to the constraint that at t=0, the

normalized concentration is 1. The unknown parameter $\Gamma_i$ was determined by another program for nonlinear regression written in MATLAB®, also found in Appendix A.1.

Using this model and its lumped dimensionless output parameter, $\Gamma_i$, data sets between the different suspensions were compared and contrasted statistically for each of several cytokines in buffer and serum. Results for capture in buffer and serum in this chapter are presented for the three main cytokines of interest: IL-6, TNF, and IL-10. These baseline experiments were then used to make comparisons for other data sets presented later in this thesis.

## 2.1 CAD DESIGN AND FABRICATION

### 2.1.1 Design

The Cytokine Adsorption Device (CAD) is a commercially available 1 mL Rezorian™ cartridge (Supleco, Bellefonte, PA) with in-house modifications (see section 2.1.2) that is packed with our biocompatible polymer, Figure 4 (top). The bead bed within the cartridge is approximately 1 cm in diameter and 3 centimeters in length, which is approximately 300 times smaller than a clinically used device, Figure 4 (bottom) [45]. This scaling factor was also used to scale our recirculation experiment set-up, specifically reservoir volume and flow rate. From flow rates of 150 to 300 mL/min for hemoadsorption used clinically [45] and total blood volume in a human being 4 to 6 L, plasma flow rate and reservoir (plasma) volume are scaled to 0.8-1.0 mL/min and 8 mL, respectively (unless otherwise noted).

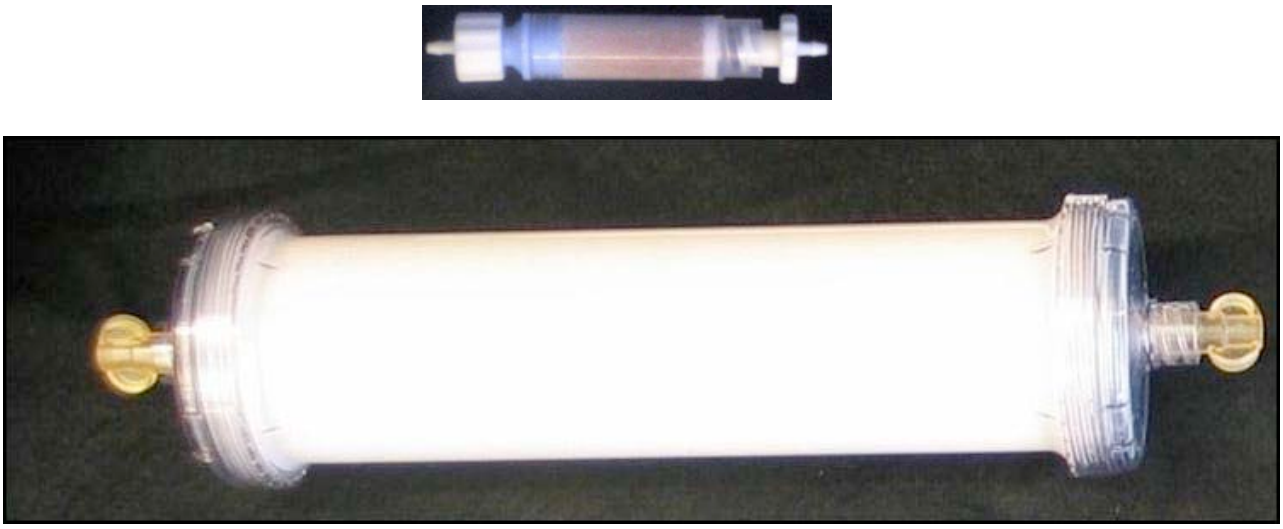

**Figure 4:** CAD (top) and full-sized cartridge (bottom), not to scale

### 2.1.2 Fabrication

Fabrication of the device requires modification of a commercially available cartridge to ensure a properly packed and secured bead bed. To do this, a 3/16" diameter hole is punched through the center of a filter included in the 1 mL Rezorian tube kit (Supleco, Bellefonte, PA) using a stainless steel hand punch. With a small amount of clear RTV silicone adhesive sealant (Permatex, Solon, OH), a 5/16" in diameter 250 μm polyurethane mesh (Small Parts, Inc., Miramar, FL) disc is then glued to one side of the filter. Using a small amount of clear RTV silicone adhesive sealant (Permatex, Solon, OH), a 1/4" in diameter 250 μm polyurethane mesh (Small Parts, Inc., Miramar, FL) disc is then glued to the inner side of the blue end cap. Once the adhesive was completely dried, the CAD was assembled as shown in Figure 5, below, with caps screwed onto the ends of the device.

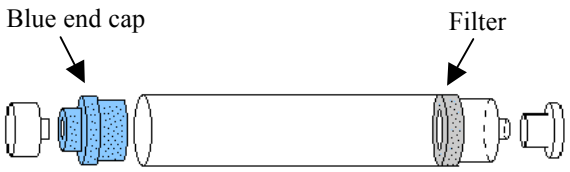


**Figure 5:** Schematic of CAD

To ensure repeatability, devices were weighed before and after packing. The mass was then compared to a set average mass established in-house, plus or minus one standard deviation, of 1.49 g ± 0.075 g (1.416 g – 1.565 g). This is to ensure that all of the cartridges are packed to the same specifications based on mass.

### 2.1.3 Determination of polymer radius

Using particle size distribution histograms provided by the manufacturer for each bead lot, we determined a weighted average radius of the beads supplied. This weighted average was used in order to provide a better fit for our model since bead radius distributions are not normally distributed and provide a poorer fit. An example of a mock histrogram used is shown in Figure 6. To determine the average bead radius, we first averaged the radius size ranges for each of the histogram bins provided and transformed the data with the equation:

$$1 - \exp\left(\frac{1}{R}\right) \qquad (3)$$

This value was then weighted by multiplying it with the percent volume given in the histogram. The average of the weighted values was then computed and transformed back using the inverse

of the natural log. This value, our in-house weighted average radius, was then used in our mathematical modeling to compare lots of beads.

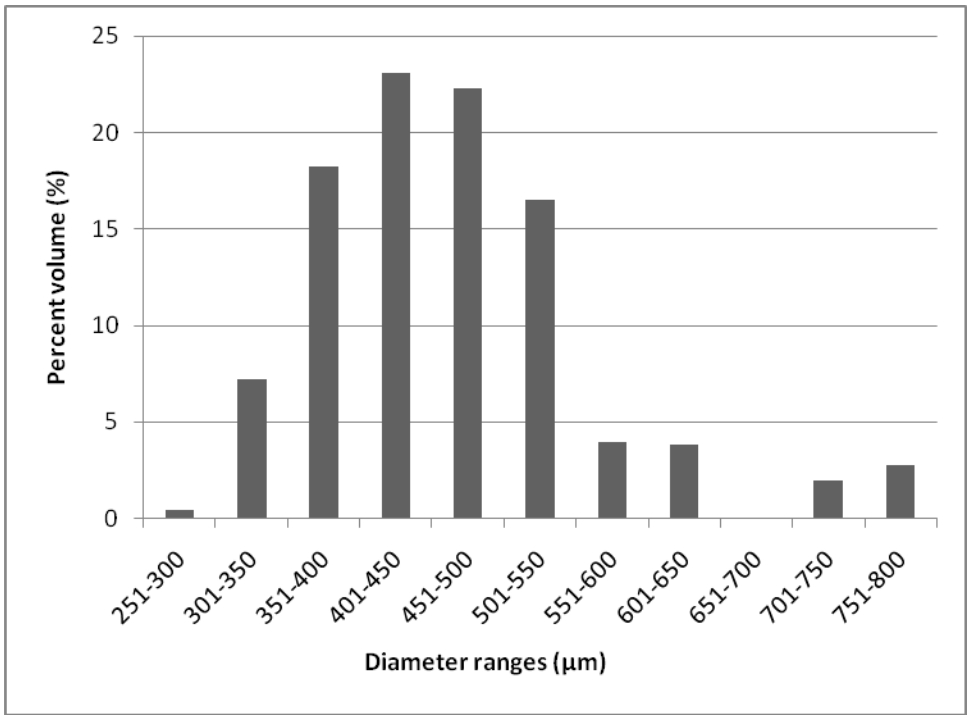


**Figure 6:** An example of a mock histogram used for determining the weighted bead radius

## 2.2 CAPTURE EXPERIMENTS

### 2.2.1 Materials and methods

In general, recirculation (capture) experiments in buffer and serum were done as follows. A fabricated CAD was filled with CytoSorb$^{TM}$ polymer lot #101003 from Cytosorbents, Inc. (Monmouth Junction, NJ). The mass of the device before and after filling was measured and recorded in order to ensure repeatability between trials, as described in section 2.1.2. To connect

the CAD to tubing, a female 3/32” leur lock with a 5” piece of 3/32” ID (5/32” OD) Tygon tubing and a male 3/32” leur lock with a 5” piece of 3/32” ID (5/32” OD) Tygon tubing were connected to the appropriate ends of the CAD. This was then connected to a 3/32” fitting for ready connection to a low-flow peristaltic pump (Fisher Scientific, Waltham, MA) and the other end of the fitting was connected to a 10” piece of 3/32” ID (5/32” OD) Tygon tubing, Figure 7.

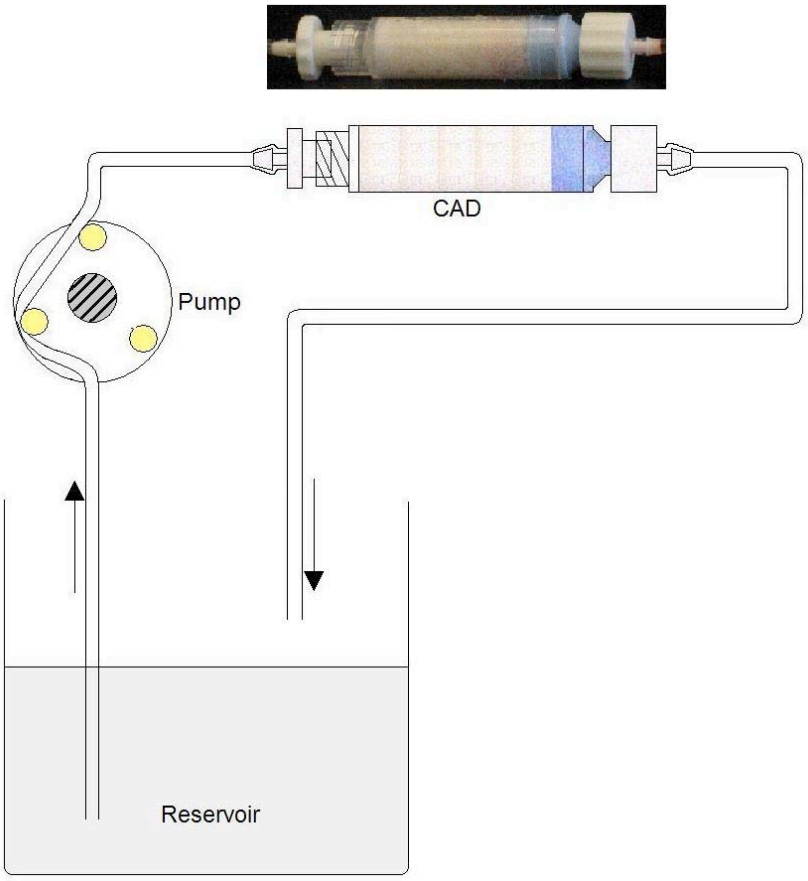


**Figure 7:** Schematic of capture experiment set-up [46]

Once the tubing was attached to the pump head, the inlet end was placed in a beaker containing approximately 20 mL of PBS (pH 7.4) and the tubing and CAD were primed for at least 20 minutes. During this time, the pump was calibrated to the appropriate flow rate of 0.8-1.0

mL/min, unless otherwise stated. Additionally, the reservoir, containing 8 mL thawed horse serum or 8 mL PBS with 5% BSA was spiked with the appropriate recombinant human cytokine. Spiked concentrations of recombinant cytokines mimicked physiological concentrations for a septic patient, approximately 1000-5000 pg/mL.

Once the tubing and CAD were fully primed, the inlet end of the tubing was removed from the reservoir to create approximately a 3 inch bubble of air in the tubing so that PBS would not enter the reservoir. The tubing inlet was then placed in the reservoir containing the suspension of interest. The experiment began when the first drop of buffer/serum entered the reservoir from the outlet end of the tubing. Sampling was done by pipetting 200 μL volumes from the reservoir and transferring to a labeled eppendorf tube for time points: 0 (baseline, before recirculation begins), 15, 30, 60, 90, 120, 180, and 240 minutes for all capture experiments. Samples were then frozen at -80$^{o}$C until they could be assayed. All samples were assayed using a solid phase sandwich Enzyme Linked Immunosorbent Assay (ELISA) purchased commercially, according to the instructions from the manufacturer (Invitrogen, Camarillo, CA or other, as noted).

### 2.2.2 Statistical analysis

To compare data sets for different cytokines or different suspensions, the average $\Gamma_i$ value and standard deviation was calculated for each set of experiments, with n=3 unless otherwise stated. $\Gamma_i$ values were then compared using an independent t-test with $p < 0.05$ considered significant. A one-way analysis of variance (ANOVA) was used to determine the significance of the mean $\Gamma_i$ values between all three cytokines in each suspension. When a significant F value was obtained,

further analysis with posthoc testing consisting of a Bonferroni correction was completed to determine significance.

## 2.3 RESULTS AND DISCUSSION

### 2.3.1 Capture of test cytokines in buffer

As the simplest form of suspension, recombinant cytokines were spiked into 8 mL of PBS with 5% BSA. Figure 8 shows the results of IL-6 capture in buffer. Error bars in this and all of the following figures for capture experiments indicate the standard deviation of three trials (n=3), unless otherwise specified. The average $\Gamma_i$ value obtained over those three trials was 1.00E-4 ± 1.8E-5 $cm^2 \cdot mL \cdot min^{-1} \cdot g^{-1}$. Total cytokine reduction was more than 90% at the end of the four hour capture experiment, with more than 50% of the initial cytokine concentration depleted in the first 30 minutes of capture.

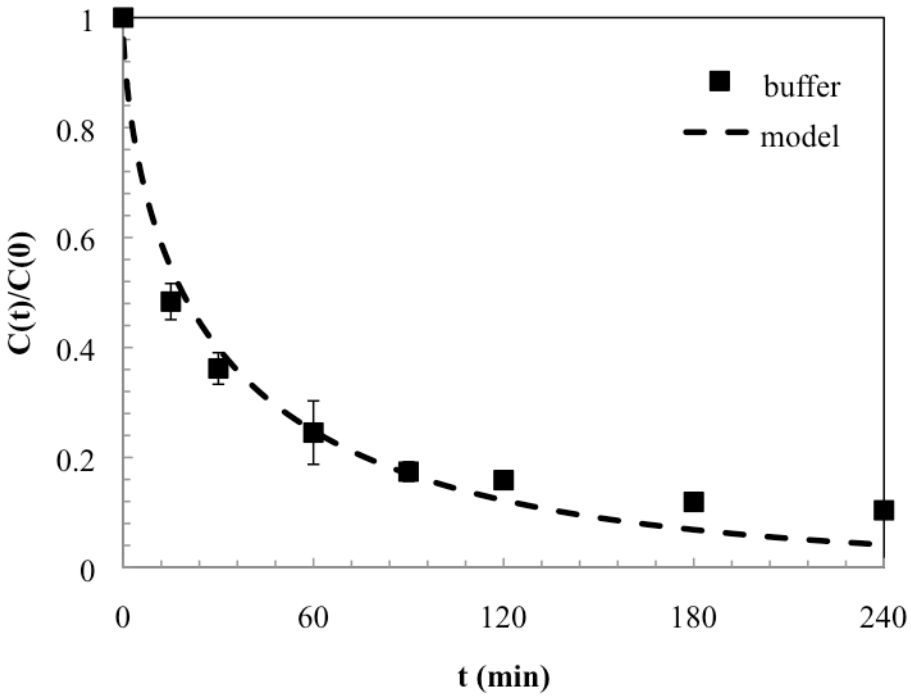


**Figure 8:** IL-6 capture data and model fits for buffer

Figure 9 shows the results of TNF capture in buffer. The average $\Gamma_i$ value obtained over those three trials was 7.16E-5 ± 4.4E-6 $cm^2 \cdot mL \cdot min^{-1} \cdot g^{-1}$. Total cytokine removal was more than 90% by the end of the four hour capture experiment, with more than 50% of the initial cytokine concentration depleted in the first 60 minutes of capture.

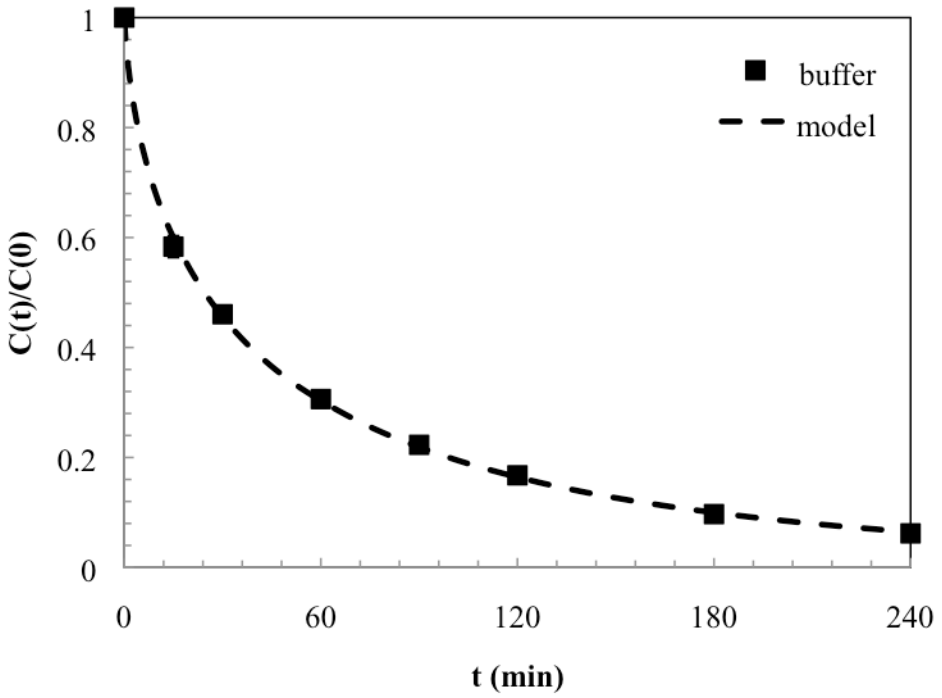


**Figure 9:** TNF capture data and model fits for buffer (error bars smaller than symbols)

For capture of IL-10 in buffer, results are shown in Figure 10, below. The average $\Gamma_i$ value obtained over those three trials was 5.65E-5 ± 6.8E-6 $cm^2 \cdot mL \cdot min^{-1} \cdot g^{-1}$. Total cytokine removal was 90% at the end of the four hour capture experiment, with more than 50% of the initial cytokine concentration depleted in the first 60 minutes of capture.

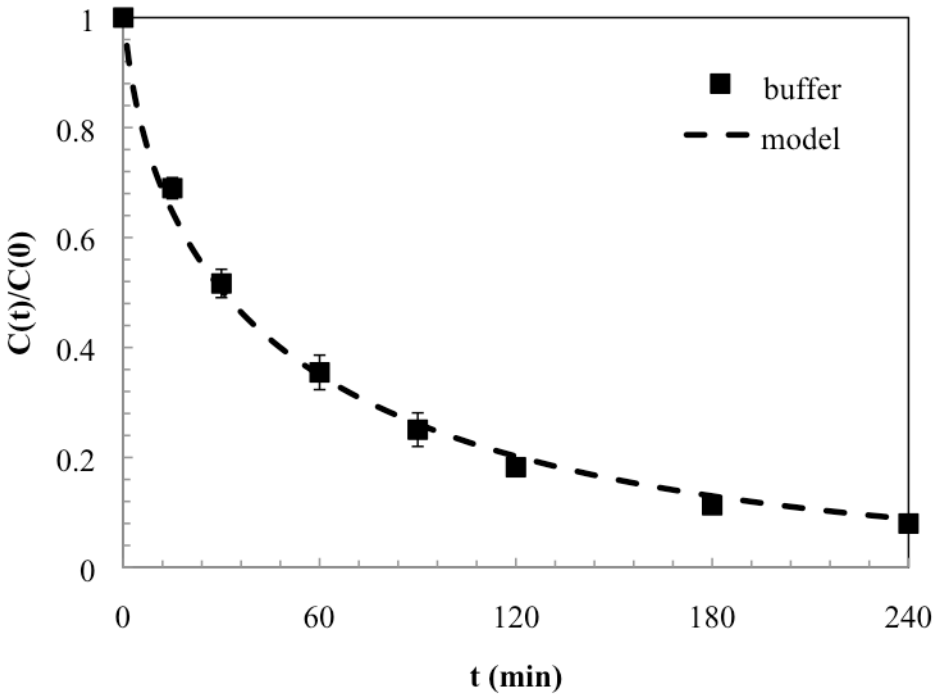


**Figure 10:** IL-10 capture data and model fits for buffer

A one-way ANOVA analysis of the three cytokines in buffer revealed that the mean $\Gamma_i$ values of each cytokines were not statistically different ($p=0.172$); total cytokine removal for all three capture experiments remained at or slightly above 90% and overall trends of capture were the same for all three cytokines in buffer.

### 2.3.2 Capture of test cytokines in serum

In this part of the study recombinent human cytokines were spiked into 8 mL aliquots of horse serum in order to add another degree of complexity to the suspension medium. This medium, unlike in plain buffer, includes receptors, growth factors, and other biologically active groups that may or may not have an effect on cpature and must be investigated. Horse serum, an

alternative for human sera, is less expensive to obtain and does not present the additional compelexity of specific soluble receptors for human cytokines. Data obtained from this set of experiments was statisically compared to data from capture in buffer to determine if the two suspensions produce the same results.

Figure 11 shows the results of IL-6 capture in horse serum. The average $\Gamma_i$ value obtained over those three trials was 1.05E-4 ± 2.4E-5 $cm^2 \cdot mL \cdot min^{-1} \cdot g^{-1}$ and was not significantly different compared to the $\Gamma_i$ values for IL-6 capture in buffer (1.00E-4 $cm^2 \cdot mL \cdot min^{-1} \cdot g^{-1}$, p=0.78). Total cytokine removal was 90% by the end of the four hour experiment, with more than 50% of the initial concentration depleted in the first 30 minutes. These capture kinetics were identical to those found in IL-6 capture in buffer, also given in Figure 11. As shown, the data are so closely related that it is difficult to differentiate between the two data sets.

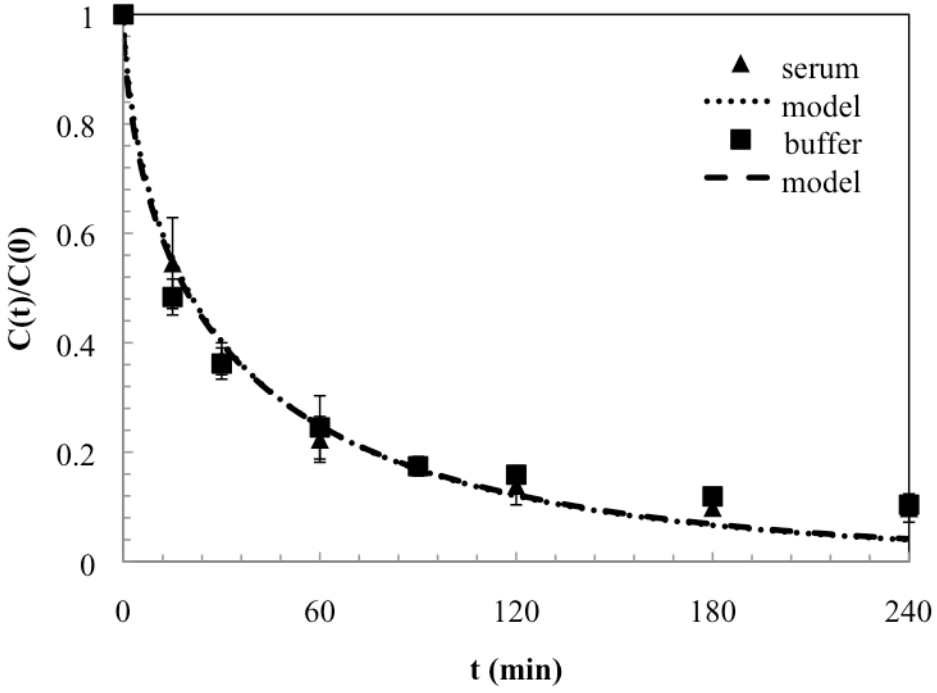


**Figure 11:** IL-6 capture data and model fits for serum and buffer

Results of TNF capture in serum are shown in Figure 12. The average $\Gamma_i$ value obtained over those three trials was 1.04E-5 ± 4.4E-6 $cm^2 \cdot mL \cdot min^{-1} \cdot g^{-1}$ and was significantly different from TNF capture in buffer (7.16E-5 $cm^2 \cdot mL \cdot min^{-1} \cdot g^{-1}$, $p<0.01$). Total cytokine removal was almost 65% by the end of the four hour experiment, with less than 40% of the initial concentration depleted in the first 60 minutes.

Our hypothesis for the decreased removal rate and total cytokine removal was due to the fact that the TNF molecule is biologically active in a trimeric form, which may be too large to diffuse efficiently into the pores when suspended in horse serum [47]. TNF, however, has been shown to dissociate into monomeric form in suspensions other than human serum, which may explain the significantly faster removal in simple buffer [48]. Additionally, the presence of TNF receptors, even if they are horse receptors, may have some impact on the removal rate of TNF in a serum suspension [49]. Investigation of this hypothesis is currently being done by other graduate students in our laboratory and is not within the scope of this thesis.

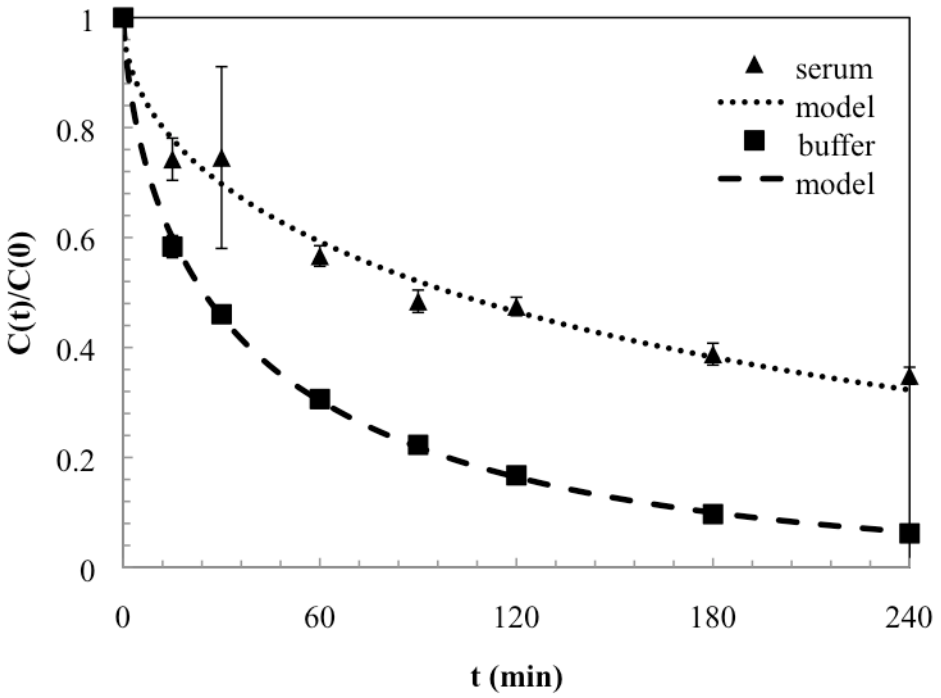


**Figure 12:** TNF capture data and model fits for serum and buffer

Finally, Figure 13 shows the results of IL-10 capture in serum. The average $\Gamma_i$ value obtained over those three trials was 4.12E-5 ± 2.3E-6 $cm^2 \cdot mL \cdot min^{-1} \cdot g^{-1}$. This value was not statistically different from the $\Gamma_i$ values of IL-10 capture in buffer (5.65E-4 $cm^2 \cdot mL \cdot min^{-1} \cdot g^{-1}$, p=0.17). Total cytokine removal was approximately 90%, similar to that found in buffer capture.

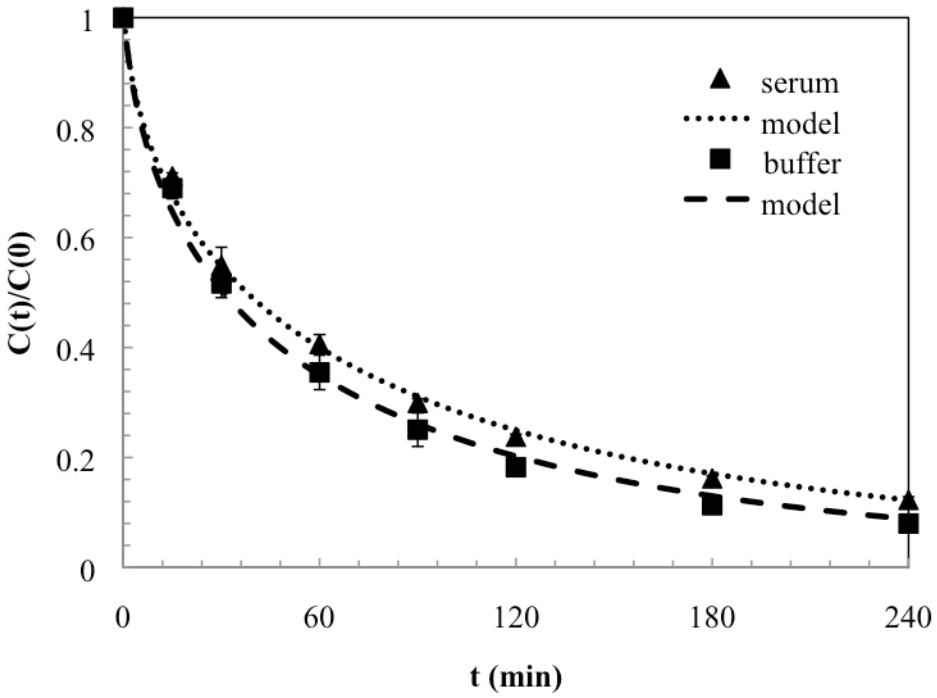


**Figure 13:** IL-10 capture data and model fits for serum and buffer

A one-way ANOVA analysis of the three cytokines in serum revealed that the mean $\Gamma_i$ values of each cytokines were statistically different ($p<0.01$); total cytokine capture for all three capture experiments varied significantly, with TNF having the lowest overall removal and IL-6 and IL-10 having similar total removal. Each of the three cytokines in buffer and serum, with their respective p values, are shown in Table 2, below.

**Table 2:** Gamma ($\Gamma_i$) values for IL-6, TNF, and IL-10 in buffer and serum

| | **Buffer** | **Serum** | **p value** |
|---|---|---|---|
| **IL-6** | 1.00E-4 | 1.05E-4 | p=0.78 |
| **TNF** | 7.16E-5 | 1.04E-5 | p<0.01 |
| **IL-10** | 5.65E-4 | 4.12E-4 | p=0.17 |

These results, as the first and simplest sets of baseline experiments for capture of cytokines in our laboratory, show that hemoadsorption in a simple buffer suspension and a simple serum suspension with CytoSorb polymer is able to remove significant amounts of IL-6, TNF, and IL-10. The results from capture in serum are consistent with general trends for *in vivo* studies done in rats by Kellum et al. [34, 41]. In these studies, significant levels of cytokines IL-6 and IL-10 were removed compared to sham circuit, which was absent a hemoadsorption column. Levels of TNF were not significantly altered. Due to the larger size of TNF and the possible interaction between recombinant human TNF and soluble TNF receptors, a reduced capture rate would be expected both *in vitro* and *in vivo*.

Further capture experiments in more complex suspensions are needed, however, for the development and validation our of in-house model as well as the systems model of sepsis currently being developed by our colleagues [43]. These systems models include complexities such as cytokine release and interactions of the cellular components of blood and are calibrated using capture data produced from our laboratory. Capture in more complex systems will be detailed later in Chapter 5.0 with experimentation in red blood cell suspensions. The work presented next, however, will detail the change in adsorption profiles during a change in the baseline polymer from one lot to the next followed by capture in polymer with a smaller diameter.

# 3.0 CHANGE IN CAPTURE DATA OVER MANUFACTURER LOT CHANGE

At one point in the characterization process of the CytoSorb$^{TM}$ polymer, depletion of our sample of polymer lot #101003 occurred. Cytosorbents, Inc., (Monmouth Junction, NJ) was able to manufacture and send two new cartridges of polymer, lot #070907/071007, which were to have the same characteristics of the previous lot, #101003 based on specifications used by the manufacturer during production. The average radius, however, a weighted average determined by the histogram provided by Cytosorbents, Inc. and done in-house as explained in section 2.1.3, revealed a smaller average radius. Characterization in serum and buffer was necessary, then, to ensure that the removal rate of cytokines with the new bead lots were statistically the same as the older lot of beads.

We first examined capture for IL-6, TNF, and IL-10 in buffer then expanded our work to include capture of a secondary group of cytokines: IL-1$\alpha$, IL-1 receptor antagonist (IL-1RA), high mobility group box 1 (HMG-B1), and IL-8. Details of these cytokines are included in section 3.2.2 along with capture profiles for buffer. We then repeated our work in horse serum, comparing capture rates between buffer and serum in the new lot as well as comparing capture rates between the new and old lots of beads to determine if differences in the polymer lots existed.

## 3.1 CAPTURE EXPERIMENTS

### 3.1.1 Materials and methods

In general, materials and methods for capture experiments in buffer and serum in the new lot of beads was done exactly as described in section 2.2.1. Fabricated CADs, however, were filled with CytoSorb$^{TM}$ polymer lot #070907/071007 from Cytosorbents, Inc. (Monmouth Junction, NJ).

### 3.1.2 Statistical analysis

To compare data sets for the two bead lots for each cytokines, the average $\Gamma_i$ value and standard deviation was calculated for each set of experiments, with n=3 unless otherwise stated. $\Gamma_i$ values were then compared using an independent t-test with $p < 0.05$ considered significant and indicating a difference in the mean $\Gamma_i$ values.

## 3.2 RESULTS AND DISCUSSION

### 3.2.1 Capture of test cytokines in buffer

Again, as the simplest form of suspension, recombinant cytokines were spiked into 8 mL of PBS with 5% BSA. Figure 14 shows the results of IL-6 capture for the new bead lot (#070907) in buffer compared to the old bead lot (#101003). The average $\Gamma_i$ value obtained over three trials

was 1.76E-4 ± 1.3E-5 $cm^2 \cdot mL \cdot min^{-1} \cdot g^{-1}$ which was statistically different from the $\Gamma_i$ value of IL-6 capture in buffer in the original polymer (1.0E-4 $cm^2 \cdot mL \cdot min^{-1} \cdot g^{-1}$, $p<0.01$). Total cytokine removal was approximately 95%, an increase of almost 5% compared to the previous lot of beads.

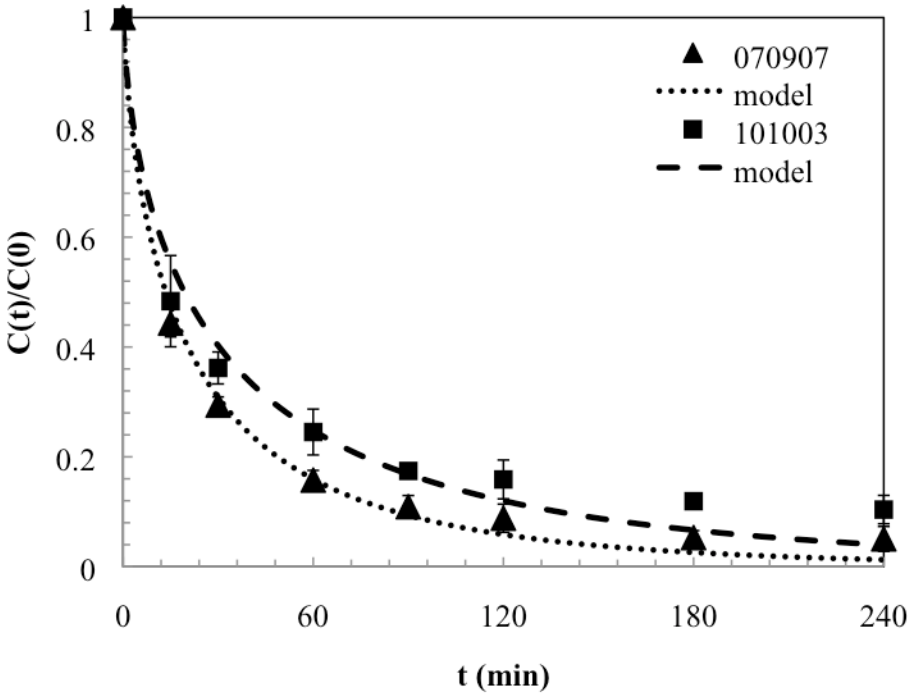


**Figure 14:** IL-6 capture data and model fits for both bead lots in buffer

The next cytokine tested in the new lot of beads was TNF with results shown in Figure 15, below. The average $\Gamma_i$ value obtained over three trials was 3.72E-5 ± 5.0E-6 $cm^2 \cdot mL \cdot min^{-1} \cdot g^{-1}$ which was statistically different from the $\Gamma_i$ value of TNF capture in the previous lot (7.15E-5 $cm^2 \cdot mL \cdot min^{-1} \cdot g^{-1}$, $p<0.01$). Total cytokine removal was approximately 89%, a decrease of 5% compared to the previous lot of beads. This decrease in capture rate and overall removal was surprising in light of IL-6 capture in the new bead lot, which showed faster removal.

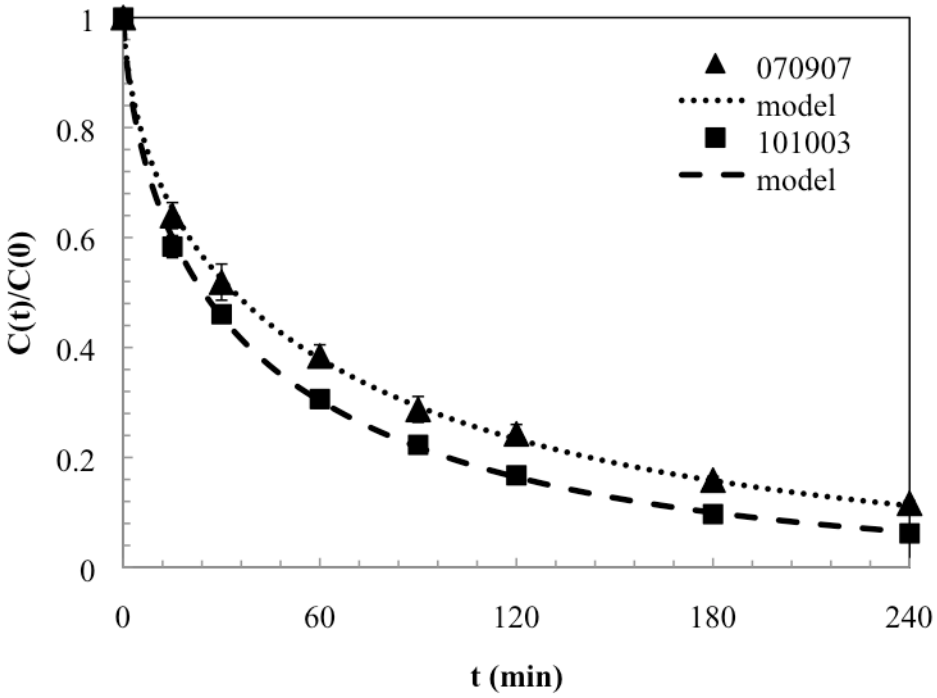


**Figure 15:** TNF capture data and model fits for both bead lots in buffer

IL-10 capture data in both lots of beads is found in Figure 16. Here, the average $\Gamma_i$ value obtained over three trials was 1.95E-5 ± 1.02E-6 $cm^2 \cdot mL \cdot min^{-1} \cdot g^{-1}$ which was statistically different from the $\Gamma_i$ value of IL-10 capture in the previous lot (7.15E-5 $cm^2 \cdot mL \cdot min^{-1} \cdot g^{-1}$, $p<0.05$). Total cytokine reduction was approximately 88%, a decrease of 5% compared to the previous lot of beads with over 94% removal. This decrease in capture rate and overall removal was the same trend as TNF in the new lot of beads, but different from IL-6 capture, which showed faster removal and greater overall removal.

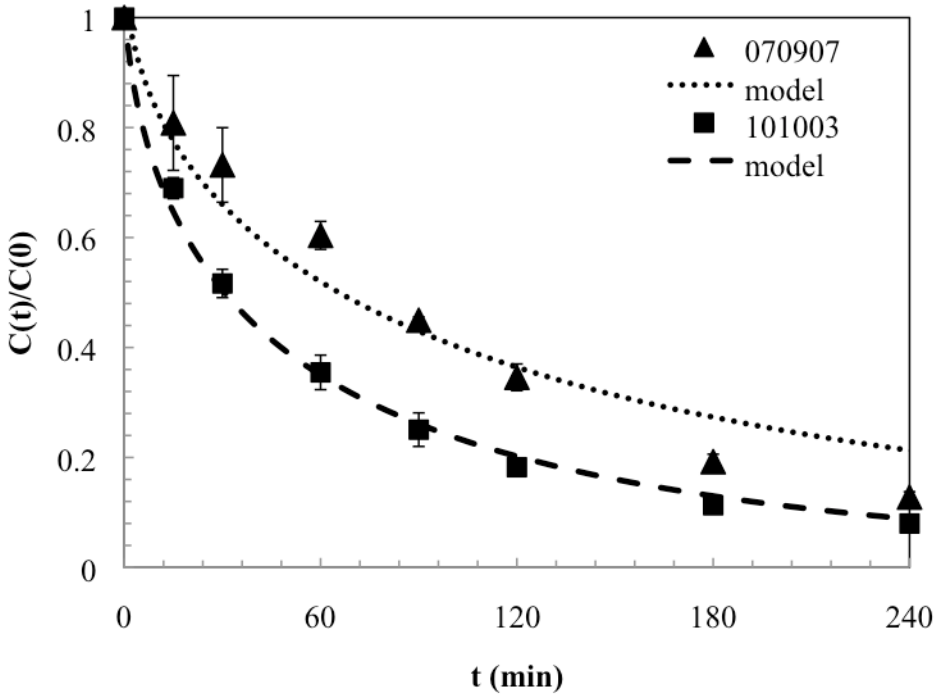


**Figure 16:** IL-10 capture data and model fits for both bead lots in buffer

In order to more easily compare the results of Chapter 2.0 and section 3.1, gamma values for capture in buffer for lots #101003 and #070907/071007 are found in Table 3, below. For capture in buffer, it is clear that the two bead lots are not statistically the same with p-values for each set of experiments less than 0.05. We hypothesized that differences in capture rates were attributed to possible differences in polymer lot characteristics, however, differences in capture were not consistent for all three cytokines with IL-6 removal increasing and TNF and IL-10 removal decreasing. Slight differences in pore size resulting in smaller average pore diameters would reduce the apparent surface area accessed by the cytokines and thereby reduce the effective diffusion coefficient, resulting in a reduced gamma value. Additionally, any alteration to the biocompatible coating, and therefore a change in the adsorption properties of the bead itself, may have conflicting results for capture. In order to fully account for these differences in future

experiments, the new lot of beads will now be considered the baseline polymer and all other capture experiments will be compared to this lot.

**Table 3:** Comparison of gamma ($\Gamma_i$) values for IL-6, TNF, and IL-10 in lot #101003 and #070907/071007 in buffer

| | **101003** | **070907/071007** | **p value** |
|---|---|---|---|
| **IL-6** | 1.00E-4 | 1.76E-4 | <0.01 |
| **TNF** | 7.16E-5 | 4.30E-5 | <0.001 |
| **IL-10** | 5.65E-4 | 1.86E-5 | <0.05 |

### 3.2.2 Capture of additional cytokines in buffer

As previously mentioned, sepsis is characterized by the release of multiple cytokines. In addition to the three main cytokines of interest in this thesis, removal kinetics of "secondary" cytokines such as IL-1α, IL-1 receptor antagonist (IL-1RA), HMG-B1, and IL-8 were also briefly studied and the results for capture of these cytokines in buffer are detailed below.

IL-1α is synthesized as a 31kDa precursor that is then cleaved into proteins of 17 kDa, secreted by activated monocytes, macrophages, lymphocytes, astrocutes, and endothelial cells in response to infection or inflammation. It induces fever, sleep, neutrophilia or neutropenia, and hypertension. In severe sepsis, the presence of TNF along with IL-1α has been shown to cause hypotension and shock and have a negative inotropic effect [16, 50]. Polymorphonuclear leukocytes are responsible for the production of IL-1 RA, a 17 kDa inhibitor of IL-1α. IL-1 RA binds to both forms of IL-1 (α and β) and blocks the binding of IL-1 to its receptor, blocking the inflammatory response both *in vitro* and *in vivo* [16].

Figure 17 shows IL-1α (left) and IL-1RA (right) capture data in both lots of beads. Here, the average $\Gamma_i$ value obtained over two trials was 1.25E-3 ± 8.78E-6 $cm^2 \cdot mL \cdot min^{-1} \cdot g^{-1}$, the largest $\Gamma_i$ value seen so far in capture results. Total cytokine reduction was approximately 100%, indicating complete removal of the circulating cytokine from the system before the first 60 minutes of recirculation were completed. Our hypothesis for such fast and complete removal is based upon both the size of IL-1α (17 kDa). A smaller cytokine such as IL-1α would more easily diffuse further into the pores of the CytoSorb polymer, increasing the apparent surface area of the beads and increasing the capture rate. Additionally, any relative differences in the structure or charge of one cytokine compared to another would change the relative affinity of that protein for the bead, $K_i$. These differences, then, would change the capture rate and $\Gamma_i$ value, which is based on individual cytokine affinities for a particular polymer.

For IL-1RA, the average $\Gamma_i$ value obtained over two trials was 2.67E-3 ± 9.2E-5 $cm^2 \cdot mL \cdot min^{-1} \cdot g^{-1}$. Total cytokine removal was approximately 100%, indicating complete removal of the circulating cytokine from the system before the first 30 minutes of recirculation were completed. Similarly to IL-1α, IL-1RA is a small cytokine (17 kDa) that presents a larger effective diffusion coefficient in our mathematical modeling, increasing the gamma value.

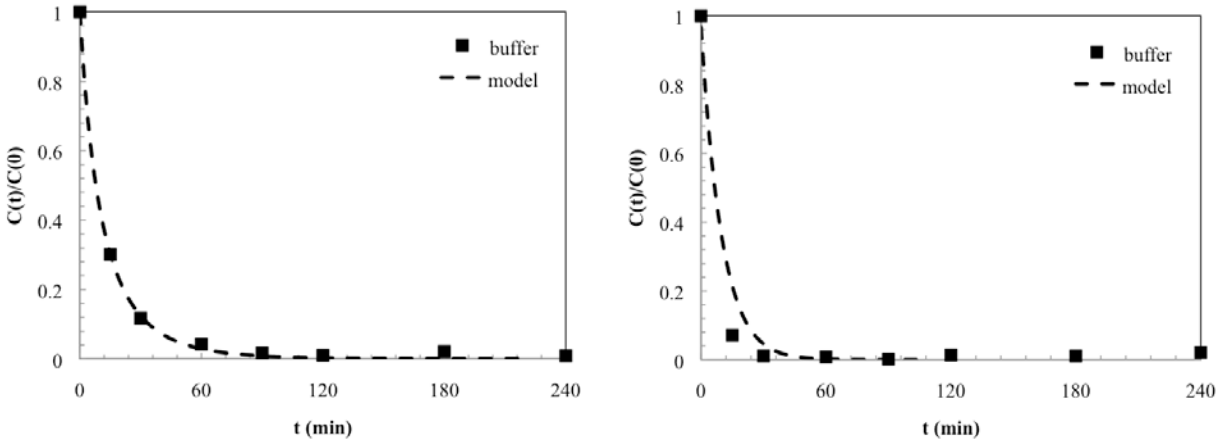


**Figure 17:** IL-1α (left) and IL-1RA (right) capture data and model fits for buffer

High mobility group-box 1 (HMG-B1) is a more recently discovered inflammatory cytokine produced in patients with sepsis and is secreted by macrophages. The timecourse of HMGB1 is different from that of other cytokines such as TNF since the rise in concentration occurs much later at 16 hours after LPS stimulation, compared to 1-1.5 hours for TNF [51].

Finally, IL-8 is a 10 kDa chemotatic and activating agent for neutrophils and T cells that is secreted by activated macrophages, monocytes, and Kupffer cells in response to infection. IL-8 also causes degranulation of neutrophils specific granules as well as induces expression of cell adhesion molecules and angiogenic [52]. Capture data for these four cytokines in the new bead lot for both buffer and serum are as follows.

Figure 18 shows HMG-B1 (left) and IL-8 (right) capture data in both lots of beads. For HMG-B1 (left), error bars indicate error associated with ELISA results for the one trial complete with the $\Gamma_i$ value of 9.32E-5 $cm^2 \cdot mL \cdot min^{-1} \cdot g^{-1}$. Total cytokine removal was approximately 90%. Only one trial of HMG-B1 capture was completed due to cost of the protein as well as the immunoassay kit (Shina-Test Co., LTD, Shanghai), a special order.

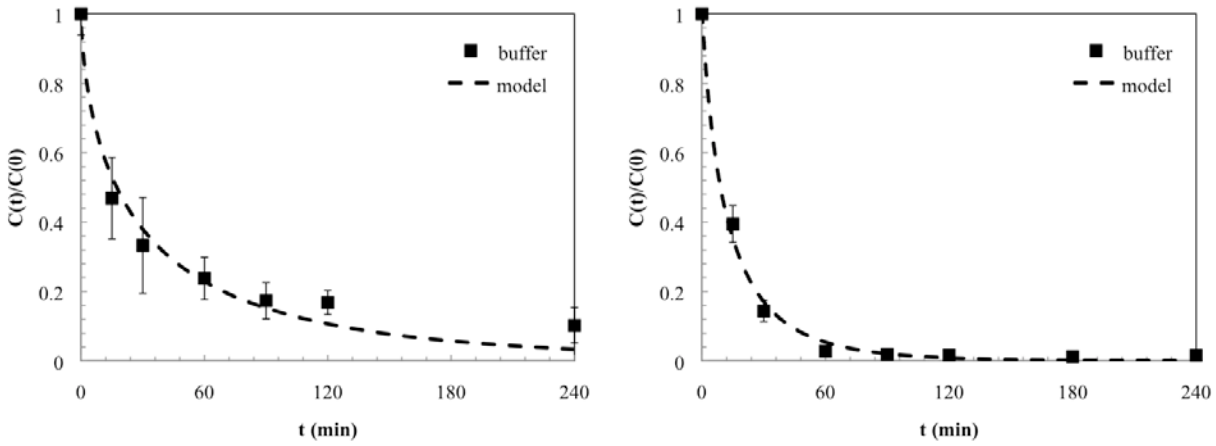


**Figure 18:** HMGB1 (left) and IL-8 (right) capture data and model fits for buffer

For IL-8, shown in the right panel of Figure 18 above, the average $\Gamma_i$ value obtained over two trials was 6.67E-4 ± 2.25E-5 $cm^2 \cdot mL \cdot min^{-1} \cdot g^{-1}$. Total cytokine reduction was approximately 100%, indicating complete removal of the circulating cytokine from the system before the first 120 minutes of recirculation were completed. Similarly to IL-1α, IL-8 is a small cytokine, however, at 10 kDa it is actually quite a bit smaller and removal was less than expected if molecular weight was the only consideration. Here, our hypothesis was that relative protein structure as well as relative protein affinity for the beads has some effect on capture rates and $\Gamma_i$ values. This hypothesis is supported by similar studies on IL-8 removal by adsorptive sorbents where differences in adsorption were not accounted for solely based on molecular weight and relative affinity of the chemokine was thought to contribute to the effect [53].

### 3.2.3 Capture of test cytokines in serum

Once again increasing the complexity of the suspension, seven cytokines were individually spiked into horse serum and recirculation experiments were completed. Figure 19 shows IL-6

capture data for both lots of beads in serum. The average $\Gamma_i$ value obtained over three trials was 5.08E-5 ± 4.2E-6 $cm^2 \cdot mL \cdot min^{-1} \cdot g^{-1}$. This value was statistically different from the $\Gamma_i$ value of IL-6 capture in serum for the old lot of beads (1.05E-4 $cm^2 \cdot mL \cdot min^{-1} \cdot g^{-1}$, $p<0.02$) and was also statistically different from the $\Gamma_i$ value of capture in buffer for the same lot (1.76E-4 $cm^2 \cdot mL \cdot min^{-1} \cdot g^{-1}$, $p<0.001$). Total cytokine removal was approximately 87%, a decrease of almost 5% compared to the previous lot of beads.

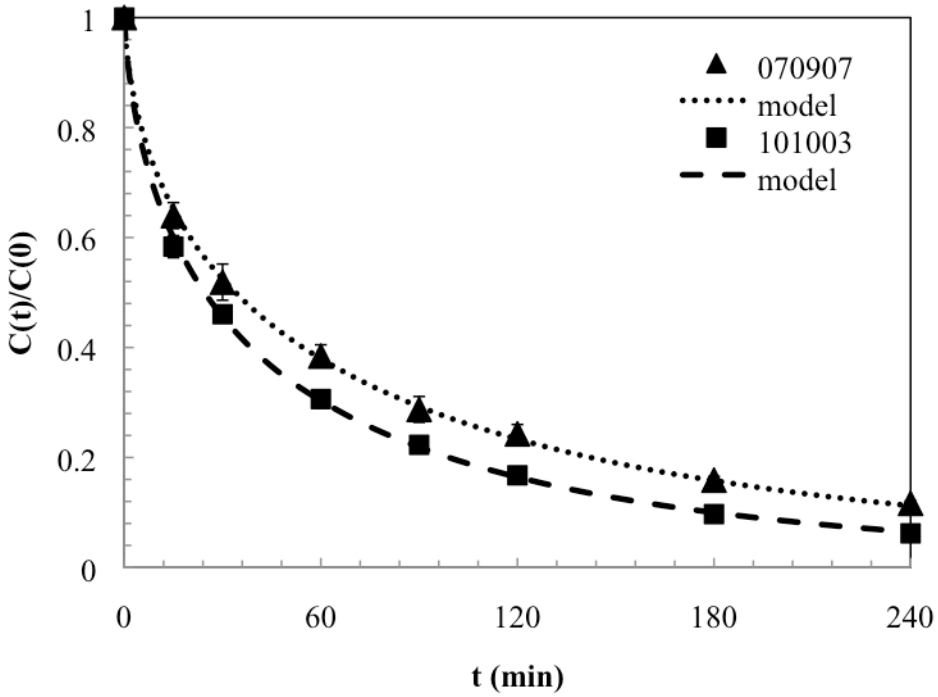


**Figure 19:** IL-6 capture data and model fits for both bead lots in serum

TNF capture results for both lots of beads in serum are shown in Figure 20. The average $\Gamma_i$ value obtained over three trials was 4.53E-6 ± 6.4E-7 $cm^2 \cdot mL \cdot min^{-1} \cdot g^{-1}$ and was statistically different from the $\Gamma_i$ value of TNF capture in the old lot of beads (1.04E-5 $cm^2 \cdot mL \cdot min^{-1} \cdot g^{-1}$, $p<0.01$). This value was also statistically different from the $\Gamma_i$ value of capture in buffer for the same lot

(3.72E-5 $cm^2 \cdot mL \cdot min^{-1} \cdot g^{-1}$, $p<0.001$). Total cytokine removal was approximately 55%, a decrease of more than 10% compared to the previous lot of beads.

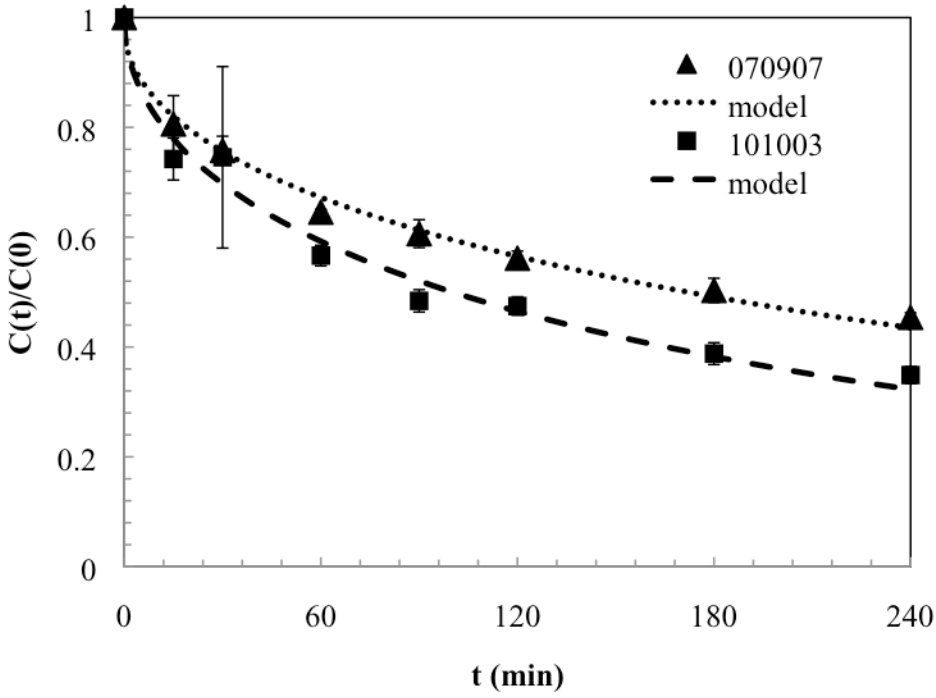


**Figure 20:** TNF capture data and model fits for both bead lots in serum

Figure 21 shows IL-10 capture data for both lots of beads in serum. The average $\Gamma_i$ value obtained over three trials was 2.25E-5 ± 2.0E-6 $cm^2 \cdot mL \cdot min^{-1} \cdot g^{-1}$. This value was statistically different from the $\Gamma_i$ value of TNF capture in the old lot of beads (1.04E-5 $cm^2 \cdot mL \cdot min^{-1} \cdot g^{-1}$, $p<0.01$) and was not statistically different from the $\Gamma_i$ value of capture in buffer for the same lot (1.96E-5 $cm^2 \cdot mL \cdot min^{-1} \cdot g^{-1}$, $p=0.10$). Total cytokine reduction was approximately 85%, a decrease of almost 5% compared to the previous lot of beads.

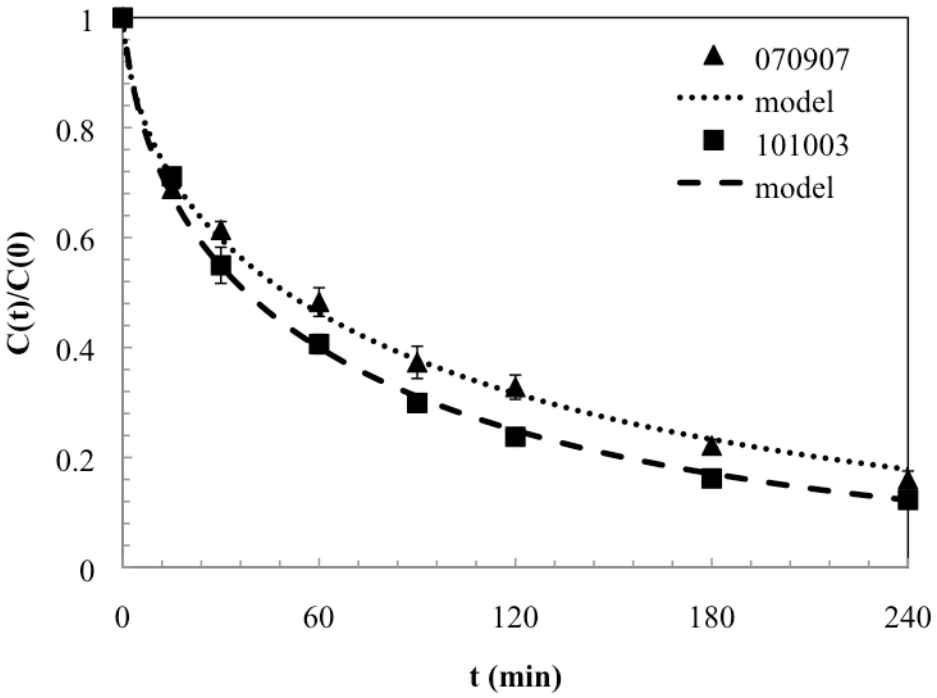


**Figure 21:** IL-10 capture data and model fits for both bead lots in serum

Summary of of $\Gamma_i$ values for lot #101003 and #070907/071007 is shown in Table 4 below. These results clearly indicate that there is a significant difference in capture rates between the two bead lots with p-values for each comparison less than 0.05. In contrast to capture in buffer, all three cytokine captures in serum were consistently slower in the new bead lot. Similarly to capture in buffer, we hypothesized that differences in capture rates were attributed to possible differences in polymer lot characteristics. For example, slight differences in pore size resulting in smaller average pore diameters would reduce the apparent surface area accessed by the cytokines and thereby reducing capture rates. Again, in order to fully account for these differences, the new lot of beads will now be considered the baseline polymer and all other capture experiments will be compared to this lot.

**Table 4:** Comparison of gamma ($\Gamma_i$) values for IL-6, TNF, and IL-10 in lot #101003 and #070907/071007 in serum

| | 101003 | 070907/071007 | p value |
|---|---|---|---|
| **IL-6** | 1.05E-4 | 5.08E-5 | <0.05 |
| **TNF** | 1.03E-5 | 4.52E-6 | <0.001 |
| **IL-10** | 4.12E-5 | 2.25E-5 | <0.001 |

### 3.2.4 Capture of additional cytokines in serum

For the secondary cytokine data, capture was completed for IL-1α, IL-1RA, HMG-B1, and IL-8 in serum for the new bead lot. Figure 22, below, shows capture data for IL-1α (left) and IL-1RA (right) in serum for both bead lots. The average $\Gamma_i$ value for IL-1α obtained over two trials was 3.58E-4 ± 1.8E-4 $cm^2 \cdot mL \cdot min^{-1} \cdot g^{-1}$. This value was statistically different from the $\Gamma_i$ value of IL-1α capture in buffer for the same lot of beads (1.25E-3 $cm^2 \cdot mL \cdot min^{-1} \cdot g^{-1}$, $p<0.05$). Total cytokine removal was approximately 90% over a four hour recirculation experiment, a decrease of almost 10% compared to capture in buffer, which showed 100% removal in the first 60 minutes.

For capture of IL-1RA in serum for both bead lots, the average $\Gamma_i$ value obtained over two trials was 8.49E-4 ± 2.9E-5 $cm^2 \cdot mL \cdot min^{-1} \cdot g^{-1}$. This value was statistically different from the $\Gamma_i$ value of IL-1RA capture in buffer for the same lot of beads (2.66E-3 $cm^2 \cdot mL \cdot min^{-1} \cdot g^{-1}$, $p<0.001$). Total cytokine removal was approximately 90% ninety minutes into the recirculation experiment. This reduction was not as fast as capture in buffer, which had complete removal in less than 30 minutes.

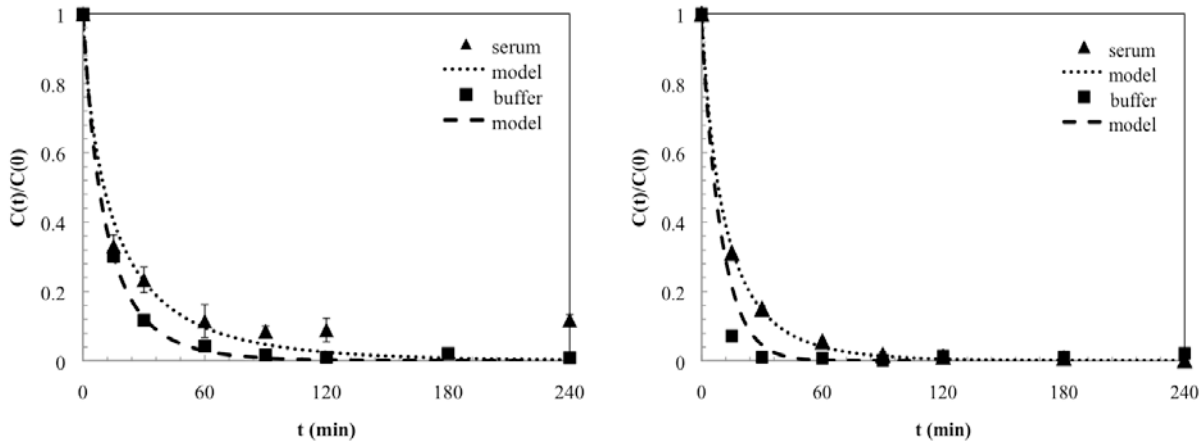


**Figure 22:** IL-1α (left) and IL-1RA (right) capture data and model fits for serum and buffer

Capture data for HMG-B1 (left) and IL-8 (right) in serum for both bead lots is shown in Figure 23. The $\Gamma_i$ value obtained for one trial of HMG-B1 capture was 1.57E-5 $cm^2 \cdot mL \cdot min^{-1} \cdot g^{-1}$, a value almost six times less than that for capture in buffer. Total cytokine removal was approximately 80% over the course of the four hour recirculation experiment, an increase of over 10% compared to capture in buffer.

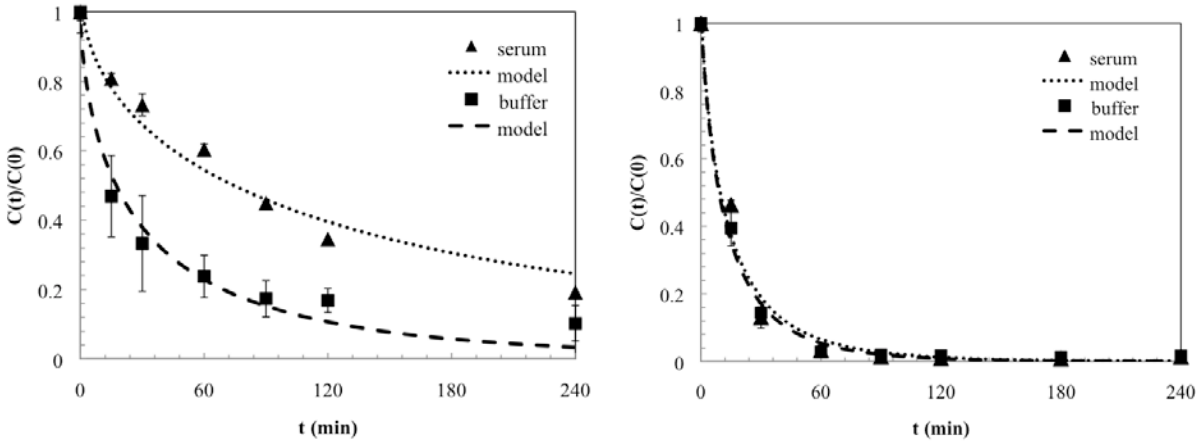


**Figure 23:** HMG-B1 (left) and IL-8 (right) capture data and model fits for serum and buffer

Finally, for the results of IL-8 capture in the new bead lot, the average $\Gamma_i$ value obtained over two trials was 5.41E-4 ± 9.4E-5 $cm^2 \cdot mL \cdot min^{-1} \cdot g^{-1}$. This value was not statistically different from the $\Gamma_i$ value of IL-8 capture in buffer for the same lot of beads (6.65E-4 $cm^2 \cdot mL \cdot min^{-1} \cdot g^{-1}$, p=0.55). Total cytokine reduction was increased to approximately 100%, indicating complete removal of the circulating cytokine from the system before the first 120 minutes of recirculation were completed. This result was the same as that in buffer.

In conclusion, for CytoSorb lot #070907/071007, differences in capture between buffer and serum are more complex that those found in the original polymer. There was, specifically, an increase in capture rate of IL-6 in buffer and decrease in capture rate for both TNF and IL-10 in buffer between the new and old lots while capture rates of all three cytokines decreased in serum. These differences, hypothesized to be the result of changes in manufacturing and polymer characteristics, will need to be taken into account for future experimentation and mathematical modeling. Baseline capture for the four additional cytokines (IL-1$\alpha$, IL-1RA, HMG-B1, and IL-8) will be advantageous since these new adsorption profiles will be useful in both the validation of our in-house model as well as calibration of systems model for sepsis.

# 4.0 SMALL BEAD POLYMER

In addition to larger diameter polymer, Cytosorbents, Inc., (Monmouth Junction, NJ) also provided polymer lots of smaller radii: WTY-076-44 (58.1 μm), WTY-076-135S (46.4 μm), and WTY-076-141S (42.09 μm). The smaller radius of a bead used in hemoadsorption presents a greater available surface area to cytokines in suspension, which in turn increases capture rates. This would be advantageous in a hemoadsorption device since increasing available surface area as well as capture rates could aid in reducing the length of time the device must be used clinically. Reducing the time used clinically would also reduce risks associated with prolong exposure such as activation of complement and the coagulation pathways which are major concerns in other purification techniques such as hemodialysis [54, 55]. A summary each of the bead lots used in this thesis can be found below in Table 5.

This chapter focuses on the characterization of the smaller diameter polymer. We hypothesize that small diameter polymer will result in significantly improved cytokine capture for all three of the main cytokines of interest. However, during biocompatibility experiments done by the Wagner laboratory, concern arose over the high rates of hemolysis with the smaller beads. The small beads, with greater surface area, are able to remove cytokines much faster; however, due to their small size, red blood cells are exposed to much higher shear stresses in devices filled with small beads [56]. High rates of hemolysis would be detrimental in clinical use, rendering the beads nonbiocompatible. For this reason, most devices that use sorbent such

as beads require a diameter of 100 μm or else a plasma filter must be used to separate the blood components to eliminate contact between red blood cells and polymer. In order to use the smaller diameter CytoSorb™ polymer, then, a re-design of the CAD is necessary to address these issues. This device, after the proper evaluative tests described in section 4.4, was characterized for IL-6, TNF, IL-10, IL-1α, and IL-1RA in serum. All of the data obtained in this chapter for the main cytokines of interest was then compared to baseline capture described in Chapter 3.0 using the larger diameter polymer and also compared to capture in the CAD with small diameter polymer.

**Table 5:** Summary of bead lots used in this study

| Lot # | Radius (μm) | Description |
|---|---|---|
| 101003 | 284.1 | Previous baseline lot |
| 070907 | 266.58 | Baseline lot |
| WTY-076-44 | 58.1 | Small bead |
| WTY-076-135S | 46.4 | Small bead |
| WTY-076-141S | 42.09 | Small bead |

## 4.1 reCAD DESIGN AND FABRICATION

### 4.1.1 Design

In order to reduce the shear stress in the device we re-engineered the CAD. Using the Ergun equation for fluid flow in a packed bed

$$\Delta P = 150 \frac{L\mu V_s (1-\varepsilon)^2}{D_p{}^2 \varepsilon^3} \quad \textbf{(4)}$$

we calculated the theoretical pressure drop in a packed bed where $\Delta P$ is the pressure drop, $L$ is the length of the bed, μ is the viscosity of the solution, $V_s$ is the superficial velocity, $D_p$ is the diameter of the resin, and ε is the void fraction of the bed. Using this pressure drop we were able to calculate the theoretical shear stress as:

$$\tau = \frac{\Delta P A_\varepsilon}{S_p} \quad \textbf{(5)}$$

where τ is the shear stress, Aε is the area of void space in the column, and $S_p$ is the surface area of the particles [57]. With these equations, we then modified existing parameters for bed length and diameter of the column to obtain a shear stress below the hemolysis threshold. Figure 24, a shear stress versus time plot [57], shows the results of plotting the theoretical data for large and small beads in the CAD as well as small beads in the reCAD and experimental data for the reCAD. The lines indicate cell trauma limits induced by shear, the material, and hemolysis. The ideal device would induce shear stresses below the hemolysis line (small black dash). From the

plot below, small beads in the CAD produce shear above the hemolysis line (teal); however, re-engineering the device to modify the dimensions of the packed bed reduces the shear stress over exposure time to a more acceptable level (pink).

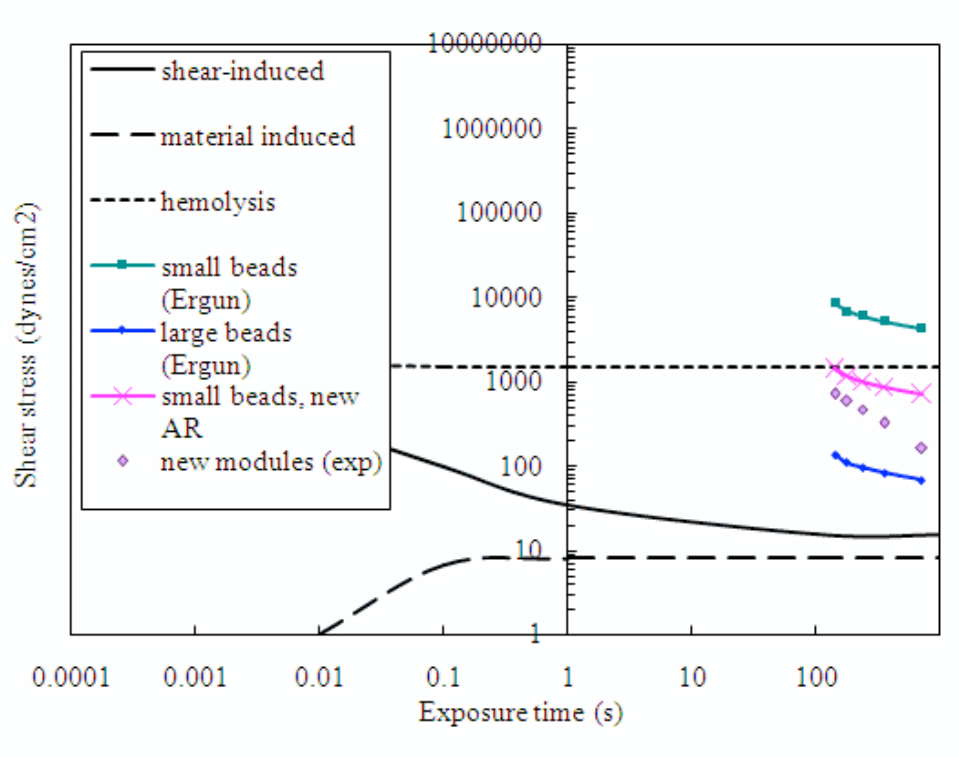


**Figure 24:** Plot of shear stress versus exposure time to determine hemolytic tendencies of our devices [57]

Therefore, to reduce shear, we designed a device that had a shorter bead bed length and wider bed width, as seen in Figure 25. The dimensions of packed bead bed in the re-engineered CAD, or reCAD, are 1/4" in length and 1" wide, which theoretically allows flow in the device to be within an acceptable range for shear stress. Table 6 shows a comparison of design parameters for both the CAD and reCAD.

**Figure 25:** reCAD

**Table 6:** Comparison of design parameters for CAD and reCAD

| | **CAD** | **reCAD** |
|---|---|---|
| Bead length | 1 inch | 0.25 inch |
| Bed width | 0.31 inch | 1 inch |
| Mass of beads | 1.49 g | 2.4 g |

### 4.1.2 Fabrication

Fabrication of the reCAD required machining and assembly by the laboratory fabricator, Mr. Brian Frankowski. The clear end of the reCAD is a 1.13" long section of the end of a BD 30 mL Luer-Lok disposable syringe, machined to the correct dimensions. The opaque end of the reCAD is machined Delrin with a female luer-to-thread secured with adhesive. To keep the beads packed within the device, a 13/16" in diameter 36 μm polyurethane mesh (Small Parts, Inc., Miramar, FL) disc is glued into the clear end cap suing a small amount of clear RTV silicone adhesive sealant (Permatex, Solon, OH). A 9/16" in diameter 36 μm polyurethane mesh (Small Parts, Inc., Miramar, FL) disc is then glued to the inner side of the Delrin end cap using

the same adhesive. Once completely dried, the CAD is assembled as shown in Figure 26, below, with caps screwed onto the ends of the device.

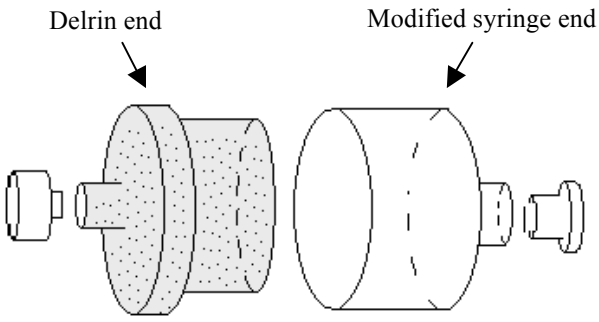


**Figure 26:** Schematic of reCAD

To ensure repeatability, devices are weighed before and after packing. The mass value is then compared to a set average mass established in-house, plus or minus one standard deviation, of 2.4 g ± 0.12 g (2.28 g – 2.52 g). This is to ensure that all of the cartridges are packed to the same weight specification for repeatability.

## 4.2 EVALUATIVE TESTING

After initial testing with the reCAD, especially biocompatibility tests done by our colleagues in another lab, it became apparent that settling might become an issue in the device. Settling, caused by nonbuyout beads responding to the pull of gravity, would likely cause shunting in the device and nonideal flow through the bead bed. If shunting were to occur, apparent surface area for cytokine adsorption would be limited thereby reducing capture rates and creating an inefficient device. Due to these concerns, then, the proper orientation for use needed to be

determined for the reCAD. To do this, both pressure drop testing and flow visualization were completed on several devices. Pressure drop testing was used to determine if shunting was occurring; however, a negligible drop across the reCAD (similar to results with the original CAD), made this test ineffective. Therefore, flow visualization using a dye was used to determine flow patterns in several orientations of the reCAD.

### 4.2.1 Flow visualization

Flow visualization was used as the most basic method to determine flow patterns in the newly engineered reCAD. Three sets of flow visualization experiments were completed. In the first, the reCAD was placed in a horizontal position with the opaque end cap as the inlet. The second study also had the device placed horizontally, but with the clear end as the inlet. Finally, the reCAD was oriented vertically with the clear end on the bottom as the inlet.

To do these experiments, a freshly made reCAD was attached to 2 5" pieces of 3/32" ID Tygon tubing (OD 5/32") with a male and female 3/32" to barb leur. The device was clamped and placed in the desired orienation using a three-prong clamp and ring stand. A syringe pump with a 50 mL BD syringe was attached to a three-way stopcock that was in turn connected to the tubing leading to the reCAD. The stopcock was used as a way to introduce a bolus of dye into the stream of clear distilled water. To do this, a small volume of distilled water was dyed using Evens Blue (Sigma) and taken up in a 5 mL BD syringe. Once the reCAD was completely primed, the pump was turned off, the syringe was loaded into the stopcock, and the dye injected. The syringe pump was then quickly turned back on and the flow pattern of the dye was visualized and documented by digital camera.

The result of the first test is shown in Figure 27, below. In this test, the opaque end, with the smaller inlet entrance (compared to the clear end) was the inlet and the device was placed horizontally. From the picture, the area of blue appearing along the bottom of the device is easily identifiable. This flow represents a nonideal pattern since it is shows perfusion through less than 50% of the available area. Similarly, the second test, with the clear end as the inlet, had similar flow pattern through the device, with the blue dye flowing only through the bed along the bottom of the device. We hypothesized that since the packed bed is in reality in slurry form, the nonbuoyant beads settled to the bottom of the device and affect the flow through the device. In order to correct this, the final set of experiments involved reorienting the device to a vertical position.

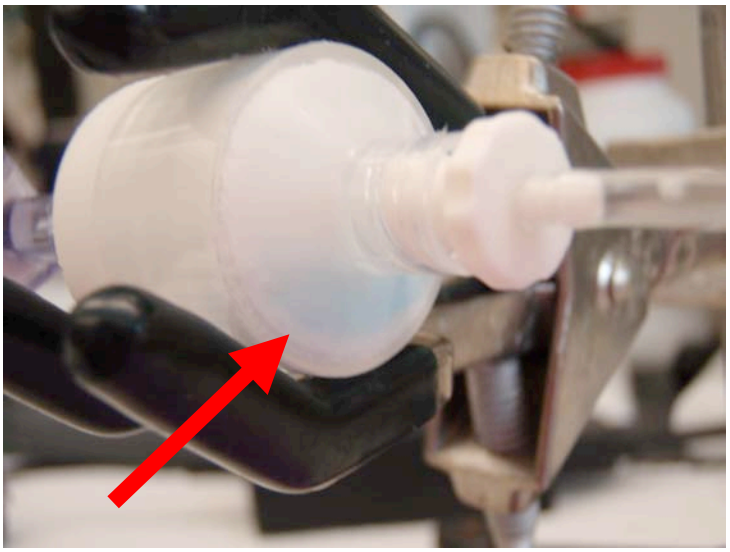

**Figure 27:** Flow visualization test results for horizontal orientation. Note the area of dye at the bottom of the device due to settling, a nonideal flow pattern (red arrow).

The third set of tests with the reCAD in the vertical position with the clear end as the inlet on the bottom yielded the best results but with a slight modification. As shown in the upper panel of Figure 28, the vertically oriented reCAD continued to show nonideal flow in that only half the

device had dye perfusing through it. We hypothesized that since this device was resting on its side prior to testing, the beads had enough time to settle. A series of flow visualization experiments testing this hypothesis found it to be true. The final experiment, results of which are shown in the lower panel of Figure 28, involved keeping the device in an upright position prior to testing to ensure an evenly distributed bead bed. The flow in this device was evenly distributed as indicated by the blue dye. In order to obtain the best possible flow, the last recommendation made included perfusing the device with the clear end as the inlet, since this end was fabricated with a more gradual and wider entrance opening for fluid flow.

**Figure 28:** Flow visualization test results for horizontal orientation. First reCAD (upper panel) was resting horizontally before testing (red arrow indicates nonideal flow pattern) while second reCAD (lower panel) was placed in an upright position has more evenly distributed flow.

## 4.3 reCAD CAPTURE EXPERIMENTS

### 4.3.1 Materials and methods

In general, materials and methods for capture experiments serum with the small bead polymer in the newly engineered reCAD were done exactly as described in section 2.2.1 except reCADs were placed in a vertical orientation with the clear end as the bottom. Fabricated reCADs were filled with CytoSorb$^{TM}$ polymer lot WTY-076-44 (58.1 μm), WTY-076-135S (46.4 μm), or WTY-076-141S (42.09 μm) provided by Cytosorbents, Inc. (Monmouth Junction, NJ).

### 4.3.2 Statistical analysis

To compare data sets for the two bead lots for each cytokines, the average $\Gamma_i$ value and standard deviation was calculated for each set of experiments, with n=3 unless otherwise stated. $\Gamma_i$ values were then compared using an independent t-test with $p < 0.05$ considered significant and indicating a difference in the mean $\Gamma_i$ values.

## 4.4 RESULTS AND DISCUSSION

### 4.4.1 Capture of test cytokines in serum

Results of IL-6 capture in the reCAD using the small bead polymer are shown in Figure 29. The average $\Gamma_i$ value obtained over three trials was 9.08E-6 ± 6.5E-6 $cm^2 \cdot mL \cdot min^{-1} \cdot g^{-1}$. This value

was statistically different from the $\Gamma_i$ value of IL-6 capture in what we refer to as the baseline lot, lot #070907, with a larger radius of 266.58 μm (5.08E-5 $cm^2 \cdot mL \cdot min^{-1} \cdot g^{-1}$, $p<0.001$). Total cytokine removal using the small bead lot was more than 90%, the same as that in the larger polymer over the entire four hour experiment. Unfortunately, the fit of the model for the smaller polymer is poor for timepoints beyond 60 minutes. This deviation occurred after 90% of the cytokine was removed; however, $\Gamma_i$ values were not statistically the same between small bead and baseline polymer. A change to the current model could be implemented to correct for the poor model fits seen in IL-6 capture as well as IL-10 capture, detailed later in this section. A properly fit model would then produce the expected $\Gamma_i$ value, one that is statistically the same as the baseline polymer.

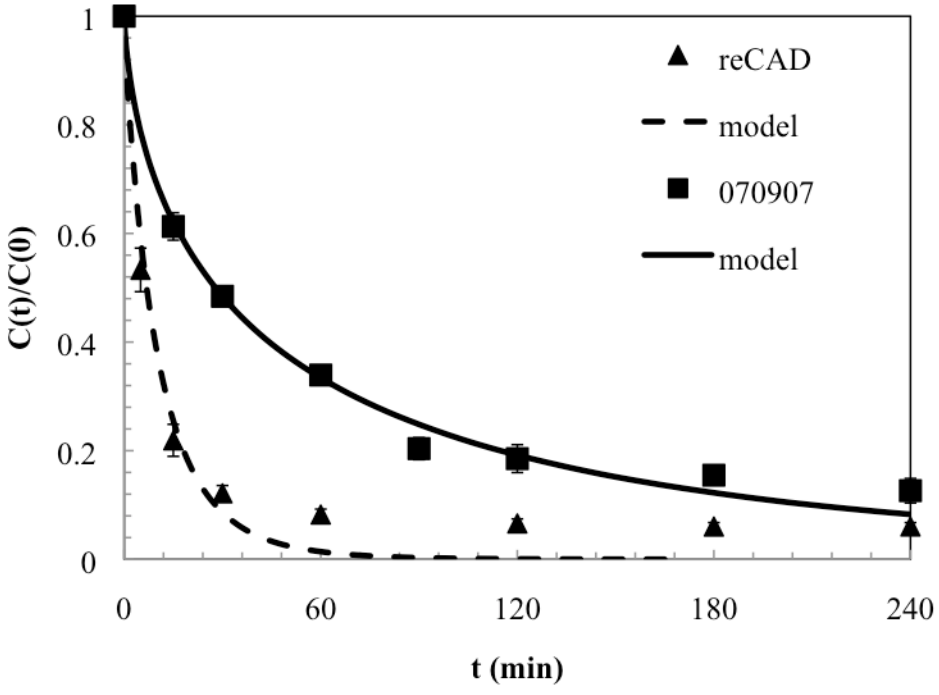


**Figure 29:** IL-6 capture data and model fits for serum

As a first step towards modifying the model and correcting the fits, a modification was made to the current model to include another fitting parameter, $C_{inf}$, or concentration at infinity, so that later timepoints fit to the model more suitably. Incorporation of this parameter into the MATLAB™ integration and fitting programs is shown in Appendix A.2 and

the results for IL-6 are shown in Figure 30, below. The new model fit produced a $\Gamma_i$ value of 3.40E-5 ± 6.7E-6 $cm^2 \cdot mL \cdot min^{-1} \cdot g^{-1}$ ($R^2$ = 0.99) which was not significantly different from baseline capture (5.08E-5 $cm^2 \cdot mL \cdot min^{-1} \cdot g^{-1}$, p=0.077). These results indicate that the modified model is able to properly fit the experimental data and produce an expected $\Gamma_i$ value. This modified model will be used to fit other capture data that deviates from the original model to a specified extent. Deviations will be quantified using $R^2$, with any $R^2$ values less than 0.95 resulting in the use of the modified model. This $R^2$ value was determined empirically by comparing results of several capture experiments fit to the original model and the modified model.

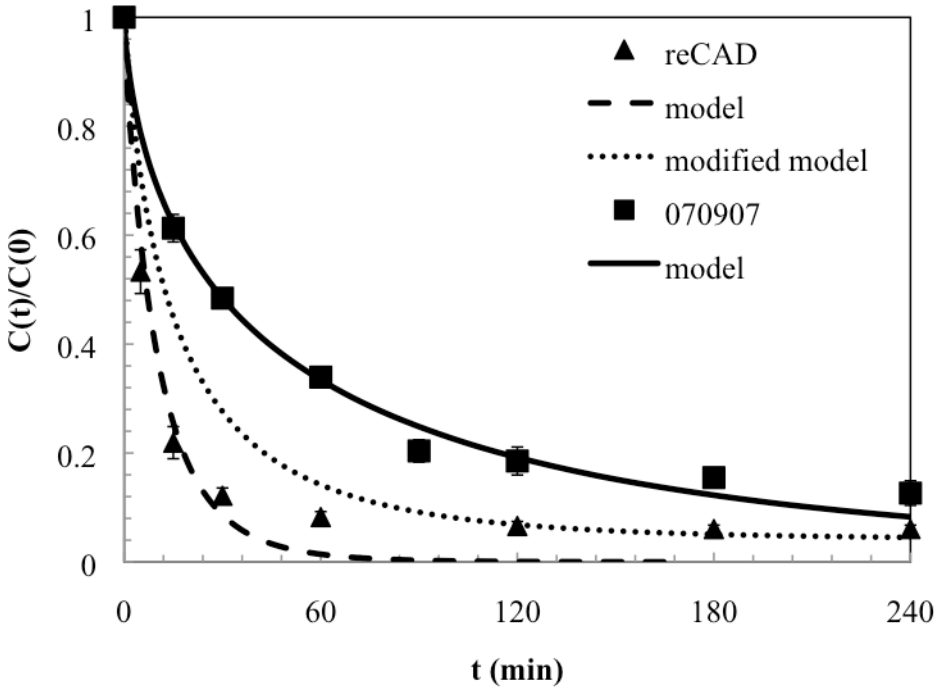


**Figure 30:** Modified model fit for IL-6 capture with small bead polymer

For TNF capture in the reCAD, shown in Figure 31, the average $\Gamma_i$ value obtained over three trials was 6.47E-6 ± 4.7E-6 $cm^2 \cdot mL \cdot min^{-1} \cdot g^{-1}$. This value was not statistically different from the $\Gamma_i$ value of TNF capture in the larger polymer, lot #070907 (4.528E-6 $cm^2 \cdot mL \cdot min^{-1} \cdot g^{-1}$, p=0.513). Total cytokine reduction using the small bead lot in the reCAD was approximately 94%. This value was significantly improved over that of the baseline polymer with only 55% total removal. The increase in removal was attributed to increased apparent surface area available to the TNF molecules for adsorption. Unlike IL-6, model fits for TNF do not deviate far from the experimental data with $R^2$ values greater than 0,98; therefore, TNF data was not fit to the modified model.

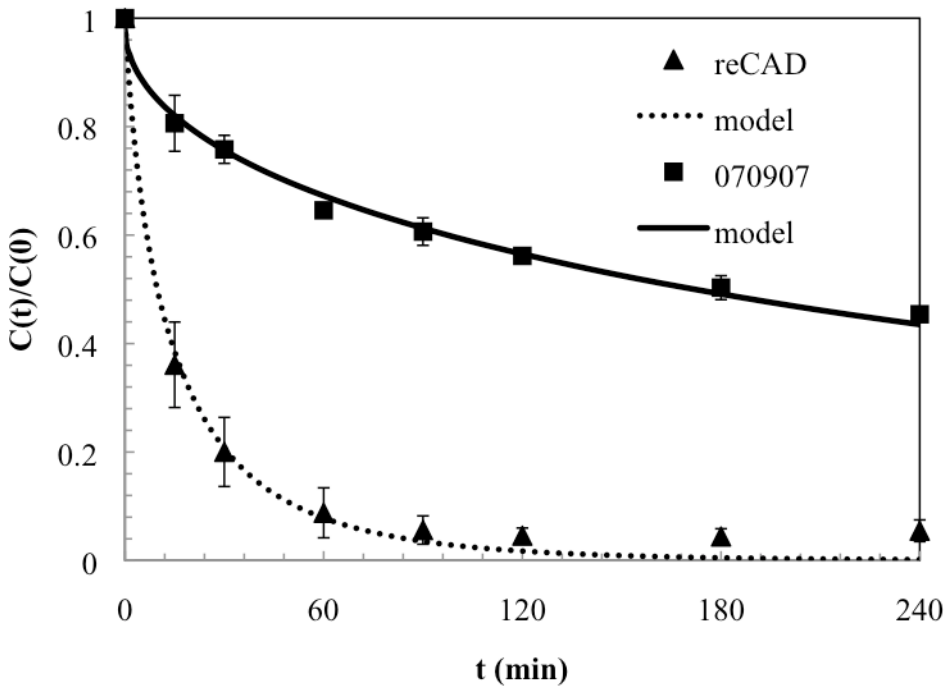


**Figure 31:** TNF capture data and model fits for serum

For IL-10 capture in the reCAD, shown in Figure 32, the modified model gave a $\Gamma_i$ value of 1.38E-4 ± 1.6E-4 $cm^2 \cdot mL \cdot min^{-1} \cdot g^{-1}$. This value was also not statistically different from the $\Gamma_i$ value of IL-10 capture in lot #070907 (2.25E-5 $cm^2 \cdot mL \cdot min^{-1} \cdot g^{-1}$, p=0.369). Total cytokine reduction using the small bead lot in the reCAD was approximately 97%, an almost 10% increase in removal compared to the larger diameter bead lot.

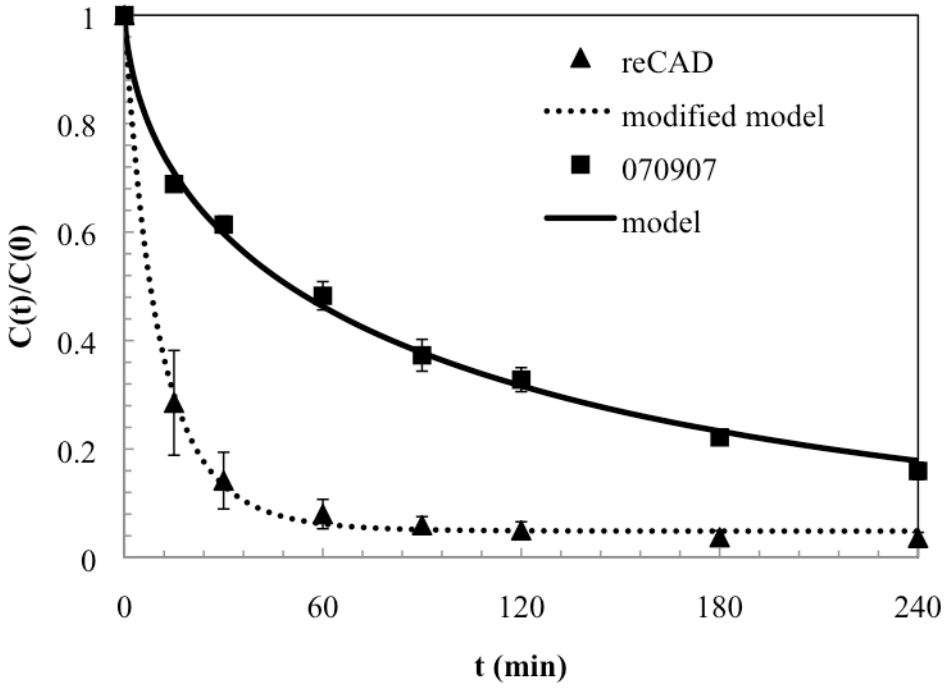


**Figure 32:** IL-10 capture data and model fits for serum

IL-1α (left) and IL-1RA (right) captures in the reCAD are shown in Figure 33, below. The average $\Gamma_i$ value for IL-1α over three trials could not be obtained using our mathematical model and it was concluded that the resolution within the first three timepoints was not great enough for MATLAB to run the program correctly. Total cytokine reduction using the small bead lot in the reCAD was 100% within the first 60 minutes of the experiment compared to 90% over the course of the experiment with the larger diameter polymer in the CAD. Average IL-1RA $\Gamma_i$ value for three trials was 8.03E-6 ± 7.9E-5 $cm^2 \cdot mL \cdot min^{-1} \cdot g^{-1}$. This value was statistically different from the $\Gamma_i$ value of IL-1RA capture in lot #070907 (8.49E-4 $cm^2 \cdot mL \cdot min^{-1} \cdot g^{-1}$, $p<0.001$). Total IL-1RA removal was 100% within the first ninety minutes of the capture experiment, the same as the baseline polymer in the CAD. Our hypothesis for such fast and complete removal is based upon both the size of IL-1α and IL-1RA (17 kDa). A smaller

cytokine such as IL-1α or IL-1RA would more easily diffuse further into the pores of the smaller CytoSorb polymer, further increasing the apparent surface area of the beads and increasing the capture rate over that of the larger polymer.

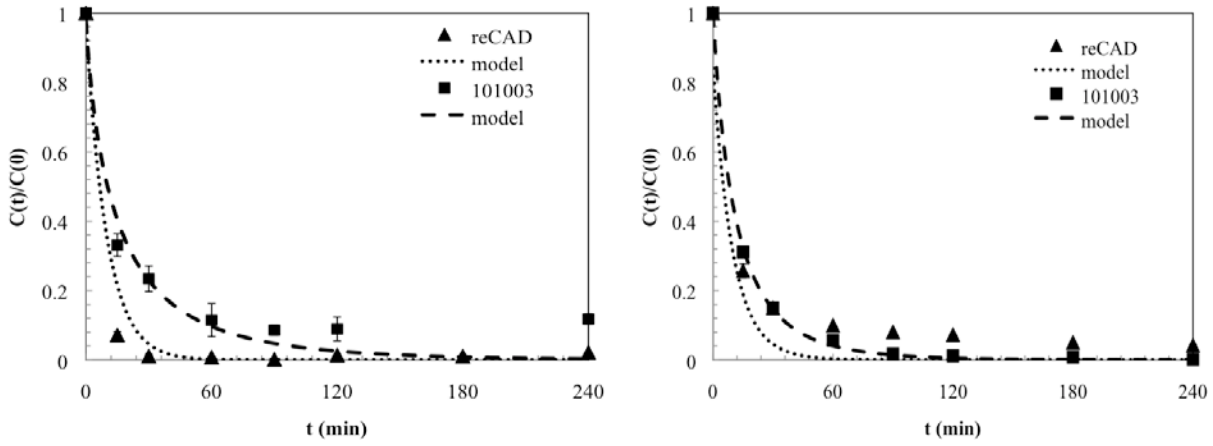


**Figure 33:** IL-1α (left) and IL-1RA (right) capture data and model fits for serum

In conclusion, we were able to engineer and develop a device for use with small diameter polymer that has reduced shear stress compared to our original CAD. Furthermore, capture of IL-6, TNF, and IL-10 in lots of smaller diameter polymer in the newly re-engineered CAD, or reCAD, results in significantly increased total removal as well as significantly decreased times to total removal compared to the baseline polymer in the CAD. Baseline capture for the two additional cytokines (IL-1α and IL-1RA) were beneficial given that these new adsorption profiles will be useful in the calibration of both our in-house model as well as the systems model for sepsis for the reCAD.

The introduction of the modified model was also advantageous in this part of the study, producing model fits with higher $R^2$ values and producing $\Gamma_i$ values that were statistically the same as capture in the CAD, as summarized in Table 7, below.

**Table 7:** Gamma ($\Gamma_i$) values for IL-6, TNF, and IL-10 capture using small diameter polymer in the reCAD

| | CAD | Small bead reCAD | p value | Modified code | p value |
|---|---|---|---|---|---|
| **IL-6** | 5.08E-5 | 9.08E-6 | <0.001 | 3.40E-5 | =0.310 |
| **TNF** | 4.52E-6 | 6.47E-6 | =0.513 | - | - |
| **IL-10** | 2.25E-5 | 1.59E-5 | =0.483 | 1.38E-4 | =0.369 |

## 4.5 CAD CAPTURE EXPERIMENTS

In order to ensure that flow within the reCAD was ideal and uniform, testing of the small polymer in the original CAD was completed for IL-6, TNF, and IL-10. Using these results, we were able to determine that the capture rates using the CAD and reCAD were statistically the same, indicating that flow within the reCAD was sufficient. The results of this work are presented in the following sections.

### 4.5.1 Materials and methods

In general, materials and methods for fabrication and capture experiments in serum only with the small bead polymer were done exactly as described in sections 2.1.2 and 2.2.1. Fabricated CADs, however, were filled with CytoSorb™ polymer lot WTY-076-44 (58.1 μm), WTY-076-

135S (46.4 μm), or WTY-076-141S (42.09 μm) provided by Cytosorbents, Inc. (Monmouth Junction, NJ). These smaller diameter beads required the use of a finer mesh screen for the filters, a 36 μm polyurethane mesh (Small Parts, Inc., Miramar, FL), instead of the larger 250 μm polyurethane mesh (Small Parts, Inc., Miramar, FL).

### 4.5.2 Statistical analysis

To compare data sets for the two bead lots for each cytokines, the average $\Gamma_i$ value and standard deviation was calculated for each set of experiments, with n=3 unless otherwise stated. $\Gamma_i$ values were then compared using an independent t-test with $p < 0.05$ considered significant and indicating a difference in the mean $\Gamma_i$ values.

## 4.6 RESULTS AND DISCUSSION

### 4.6.1 Capture of test cytokines in serum

Results of IL-6 in the small bead polymer are shown in Figure 34. The modified model fit produced a $\Gamma_i$ value of 2.60E-4 ± 2.5E-4 $cm^2 \cdot mL \cdot min^{-1} \cdot g^{-1}$ which was not significantly different from baseline capture (5.08E-5 $cm^2 \cdot mL \cdot min^{-1} \cdot g^{-1}$, p=0.225) and was not statistically different from small bead polymer in the reCAD (9.08E-6 $cm^2 \cdot mL \cdot min^{-1} \cdot g^{-1}$, p=0.490). Total cytokine removal using the small bead lot was more than 90%, the same as that in the smaller polymer in the reCAD over the entire four hour experiment.

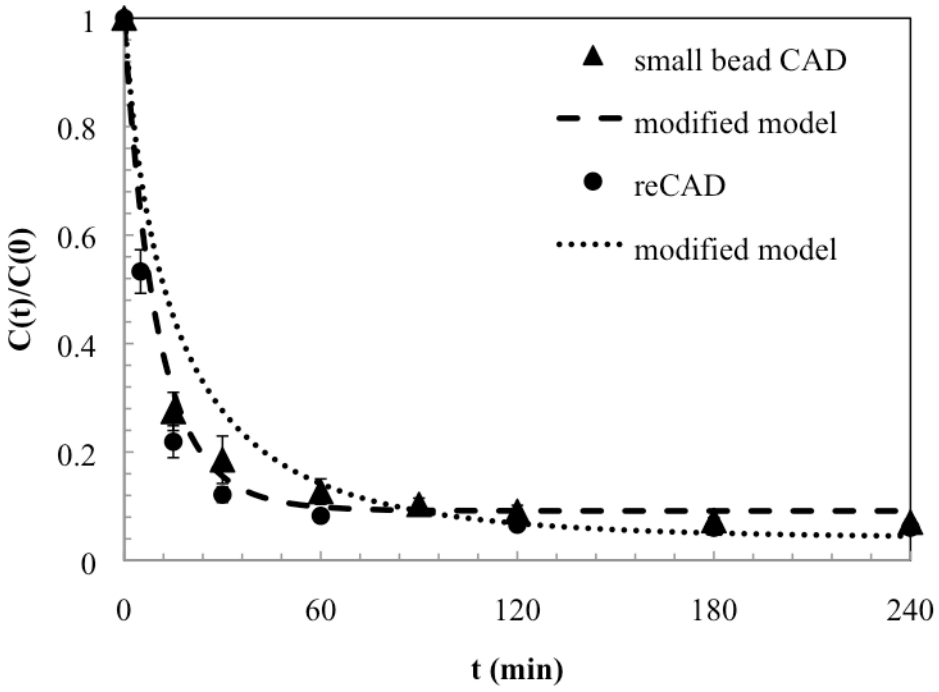


**Figure 34:** IL-6 capture data and model fits for serum

Results of TNF in the small bead polymer are shown in Figure 35. The average $\Gamma_i$ value obtained over three trials was 4.77E-6 ± 1.0E-6 $cm^2 \cdot mL \cdot min^{-1} \cdot g^{-1}$. This value was not statistically different from the $\Gamma_i$ value of TNF capture in the larger polymer, lot #070907 (4.53E-6 $cm^2 \cdot mL \cdot min^{-1} \cdot g^{-1}$, p=0.749) and was not statistically different from capture with the small bead in the reCAD (6.47E-6 $cm^2 \cdot mL \cdot min^{-1} \cdot g^{-1}$, p=0.570). Total cytokine removal using the small bead lot was increased to more than 90%, which is a significant increase compared to a 55% total removal in the larger diameter beads yet was the same as removal in the reCAD. This increase in removal was attributed to increased apparent surface area available to the TNF molecules for adsorption. Unlike IL-6, model fits for TNF do not deviate far from the experimental data; therefore, TNF data was not fit to the modified model.

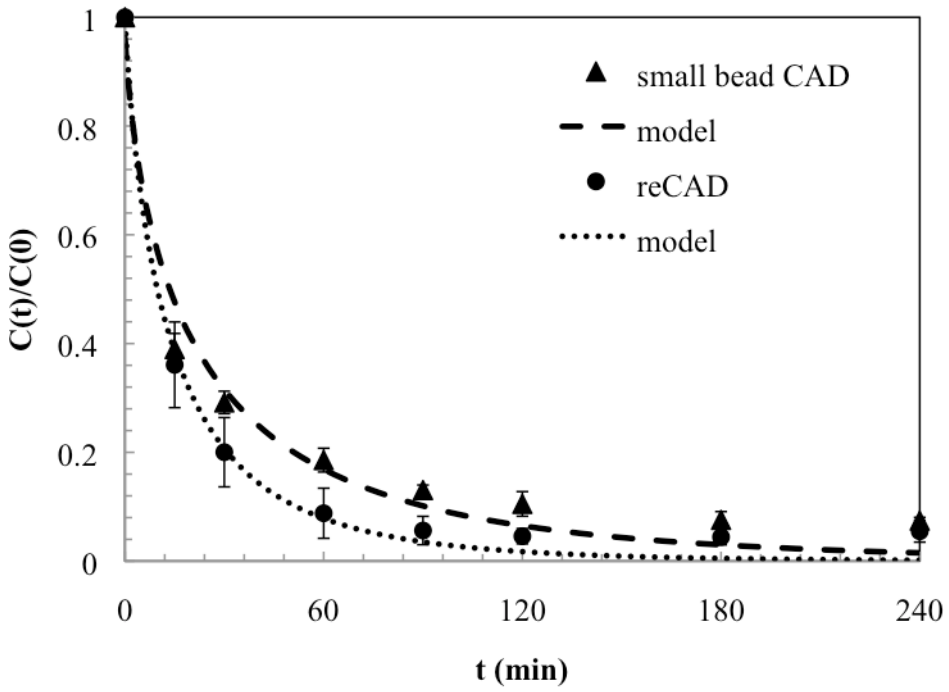


**Figure 35:** TNF capture data and model fits for serum

Results of IL-10 in the small bead polymer are shown in Figure 36. Producing a better fit, the modified model gave a $\Gamma_i$ value of 3.39E-5 ± 1.1E-5 $cm^2 \cdot mL \cdot min^{-1} \cdot g^{-1}$. This value was not statistically different from the $\Gamma_i$ value of IL-10 capture in lot #070907 (2.25E-5 $cm^2 \cdot mL \cdot min^{-1} \cdot g^{-1}$, p=0.159) and was not statistically different from small bead polymer in the reCAD (1.38E-5 $cm^2 \cdot mL \cdot min^{-1} \cdot g^{-1}$, p=0.435). Total cytokine removal using the small bead lot was approximately 94%, an almost 10% increase in removal compared to the larger diameter bead lot and the same as in the reCAD.

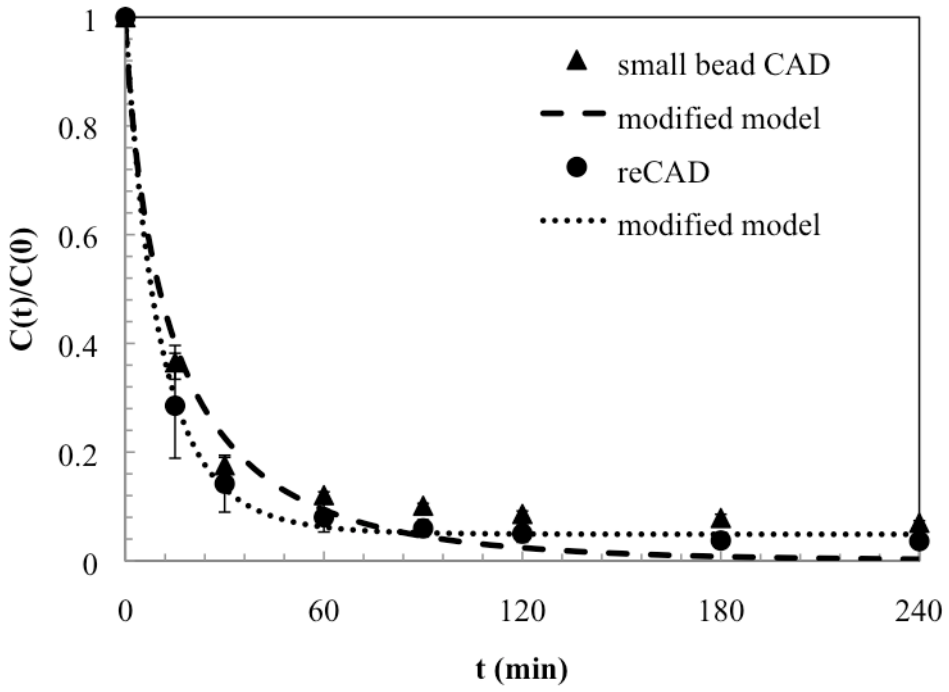


**Figure 36:** IL-10 capture data and model fits for serum

In conclusion, capture of IL-6, TNF, and IL-10 in lots of smaller diameter polymer in both the CAD and reCAD results in significantly increased total removal as well as significantly decreased times to total removal. Since the gamma values for capture using the small polymer were statistically the same, the flow within the reCAD is assumed to be ideal and uniform. Therefore, the recommendations established from flow visualization in section 4.2.1 are validated and should be followed when testing using the reCAD.

# 5.0 CAPTURE IN RED BLOOD CELL SUSPENSIONS

The previous chapters in this work are beneficial for the development and optimization of a new sorbent material by establishing baseline capture rates for main cytokines of interest in the simplest buffer suspensions. Although extremely useful in our preliminary work, capture profiles of the cytokines of interest must also be done in more complex suspensions such as whole blood. This work will be important not only for our understanding of capture profiles in whole blood, for which the device will ultimately be used, but also for the calibration and optimization of the systems model of sepsis being developed by our colleagues. In this chapter, we wanted to test whether the presence of red blood cells, plasma components, and white blood cells would have an effect on capture. These final sets of experiments involve cytokines spiked into several different red blood cell suspensions. We first hypothesized that the presence of red blood cells in a buffer suspension would not have any effect on capture rates when compared to baseline capture in buffer. Furthermore, we hypothesized that the presence of plasma and serum components such as cytokine receptors, complement component, and growth factors would have no effect on capture rates when compared to baseline capture in serum. Finally, we hypothesized that capture of cytokine in healthy human whole blood would not be changed when compared to baseline capture in human plasma. To test these hypotheses, we first resuspended washed human red blood cells obtained from healthy volunteers in buffer spiked with the cytokine of interest. Next, we performed a set of capture experiments for red blood cells resuspended in fresh human

plasma spiked with cytokines. Finally, we completed our testing with capture of human whole blood spiked with cytokines. All of these data sets were completed for the three main cytokines of interest: IL-6, TNF, and IL-10. Additional controls were also performed and will be discussed in the appropriate sections.

Collection data in red blood cell suspensions becomes important not only for the validation of our mathematical model, but also to investigate any possible interactions the presence of red blood cells, white blood cells, and plasma components may have on capture rates. Although these additional complexities are not accounted for in our in-house mathematical model, our colleagues developing a systems model of sepsis and treatment with our device would benefit from such data for calibration.

## 5.1 CAPTURE EXPERIMENTS

### 5.1.1 Materials and methods

In general, recirculation experiments in red blood cell suspensions were done as follows. With approval of the University of Pittsburgh Institutional Review Board (IRB), 100 mL of fresh human whole blood was obtained from healthy, consenting volunteers and collected into heparinated tubes. The blood was then centrifuged and the plasma pipetted and discarded or collected depending upon the experiment performed. Fresh PBS (pH 7.4) was added to the tubes in a 3:1 ratio to red blood cells. Cells were gently mixed to resuspend them and then centrifuged. Two more washing steps were then completed.

Once the red blood cells were washed, the suspension of choice (buffer or human plasma) was prepared and spiked with the cytokine of interest for a final concentration of 1000-5000 pg/mL. For each reservoir, 9 mL of spiked buffer or plasma was added to 6 mL of red blood cells and gently mixed. The suspension was then placed on a stir plate and mixed well before the start of the experiment.

A fabricated CAD was then filled with CytoSorb$^{TM}$ polymer lot #070907 from Cytosorbents, Inc. (Monmouth Junction, NJ). The mass of the device before and after filling was measured and recorded in order to ensure repeatability between trials, as described in section 2.1.2. To connect the CAD to tubing, a female 3/32" leur lock with a 5" piece of 3/32" ID (5/32" OD) Tygon tubing and a male 3/32" leur lock with a 5" piece of 3/32" ID (5/32" OD) Tygon tubing were connected to the appropriate ends of the CAD. This was then connected to a 3/32" fitting for a low-flow peristaltic pump (Fisher Scientific, Waltham, MA) and the other end of the fitting was connected to a 10" piece of 3/32" ID (5/32" OD) Tygon tubing, see Figure 37, below, for an actual experimental set-up.

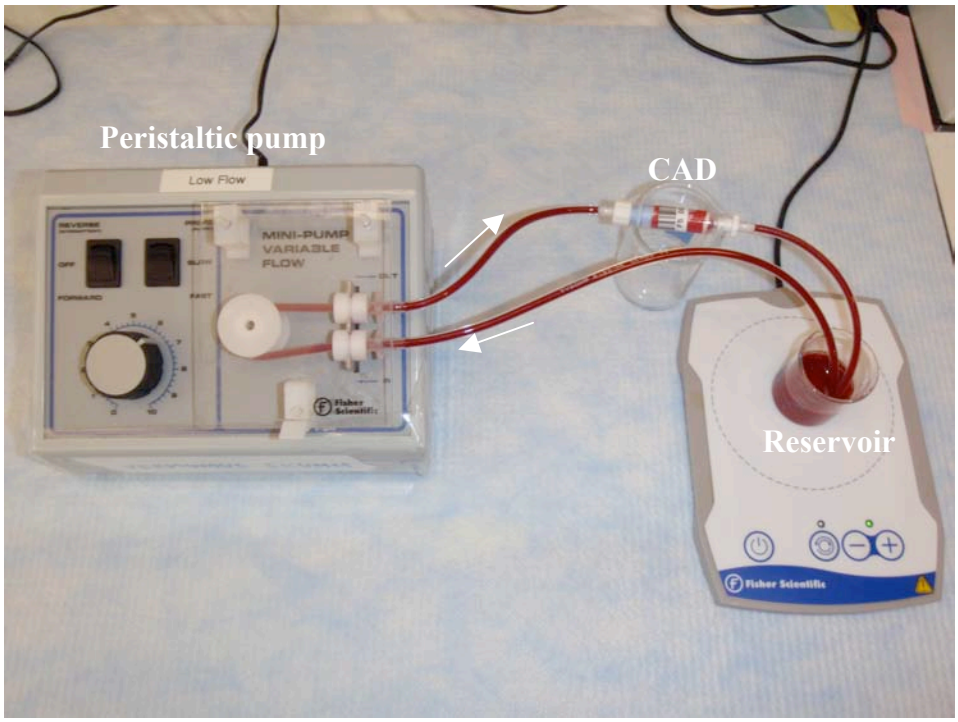


**Figure 37:** Experimental set-up of red blood cell suspension recirculation through a CAD

Once the tubing was fitted into the pump, the inlet end was placed in a beaker containing approximately 20 mL of PBS (pH 7.4) and the tubing and CAD were primed for at least 30 minutes. During this time, the pump was calibrated to the appropriate flow rate of 1.33 mL/min, unless otherwise stated. Note the increased flow rate due to scaling up by hematocrit (40%). In order for these experiments to be compared to those of the previous chapters, the flow rate and reservoir volume were scaled by hematocrit so that "plasma" flow rate, $Q_p$, and "plasma" reservoir volume, $V_p$, remained 0.8 mL/min and 8 mL, respectively. This is because cytokines are present only in the plasma phase, therefore $Q_p$ and $V_p$ must be uniform. $Q_p$ and $V_p$ are defined as:

$$Q_p = (1\text{-}HCT)Q \qquad \textbf{(6)}$$

where HCT is % hematocirt and Q is the total flow rate and

$$V_p = (1\text{-}HCT)V \quad \textbf{(7)}$$

where HCT is % hematocirt and V is the total reservoir volume.

Once the tubing and CAD were fully primed with PBS, the inlet end of the tubing was removed from the reservoir to create approximately a 3" bubble of air in the tubing. The tubing inlet was then placed in the reservoir containing the suspension of interest. The experiment began when the first drop of the suspension entered the reservoir from the outlet end of the tubing. Sampling was done by pipetting 500 μL volumes from the reservoir and transferring to a labeled eppendorf tube for time points: 0 (baseline, before recirculation begins), 15, 30, 60, 90, 120, 180, and 240 minutes for all capture experiments. Samples were then centrifuged and the supernatant frozen at -80$^{o}$C until they could be assayed. All samples were assayed using a solid phase sandwich Enzyme Linked Immunosorbent Assay (ELISA) purchased commercially, according to the instructions from the manufacturer (Invitrogen, Camarillo, CA).

During experimentation with whole blood in section 5.4.1, decreased capture rates observed were hypothesized to be the result of either the production of cytokines and/or the activation of white blood cells. The activation of white blood cells and platelets may be caused by the circuit itself, since the reservoir is open to air and not temperature controlled, i.e. kept at room temperature and not 37$^{o}$C. For the experimental set-up using a blood bag in section 5.4.1 that addresses the concerns of temperature and open-loop, materials and methods are as follows. Whole blood was obtained and spiked as described previously. The recirculation loop was

prepared by connecting the fabricated CAD to a female 3/32" leur lock with a 2" piece of 3/32" ID (5/32" OD) Tygon tubing to the inlet side and a three-way stopcock on the outlet side. The short piece of tubing was then connected to a 3/32" fitting for a low-flow peristaltic pump (Fisher Scientific, Waltham, MA) and the other port of the stopcock was connected to the tubing attached to a blood bag spike, cut to approximately 2". The other end of the pump fitting was connected to a 4" piece of 3/32" ID (5/32" OD) Tygon tubing which was in turn attached to a three-way stopcock and then the tubing attached to the blood bag, a Cyrostore CS 25q 25 mL bag from OriGen Biomedical (Austin, TX). The top of the blood bag was folded over and clamped off with small binder clips to keep the blood in the main part of the bag. See Figure 38, below, for a schematic of the experimental set-up.

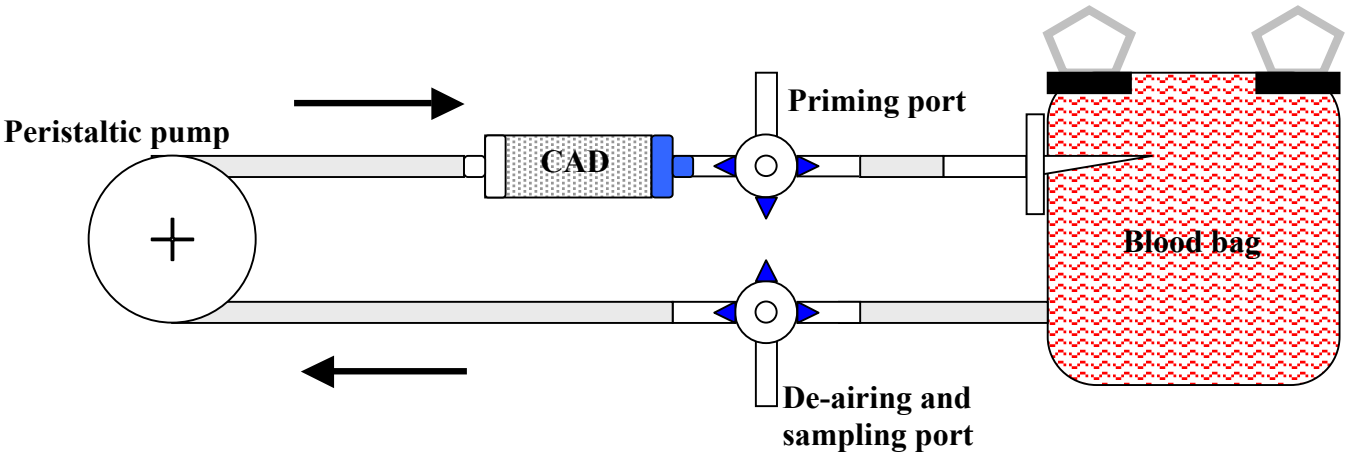


**Figure 38:** Schematic of a closed-loop capture experiment set-up

To prime and de-air the loop, all tubing and parts were connected and removed from the pump head. With a syringe, 15-20 mL of PBS (pH 7.4) was added to the loop from the stopcock connected to the CAD (priming port). The loop was then re-connected to the pump head and

allowed to recirculate for 30 minutes. After 30 minutes, the loop was drained. With a syringe, 15 mL of spiked whole blood was slowly introduced into the loop by the priming port (other stopcock closed towards blood bag to prevent blood from spilling) ensuring that no bubbles were introduced into the blood bag. To de-air any bubbles that did form, the stopcock connected to the CAD was closed and a syringe attached to the de-airing port in the other stopcock to pull the air from the blood bag. When all bubbles were removed, the tubing was reconnected and connected to the pump head. The blood bag was placed inside an ISOTEMP 2025 water bath (Fisher Scientific, Pittsburgh, PA) to maintain blood temperature at 37$^{o}$C. Additionally, the bag was hand mixed every 15 minutes to ensure proper mixing. The experiment began as soon as the pump was turned on.

Sampling was done by transferring 500 μL volumes from the sampling port located in the stopcock after the blood bag in the loop and transferring to a labeled eppendorf tube for time points: 0 (baseline, before recirculation begins), 15, 30, 60, 90, 120, 180, and 240 minutes for all capture experiments. To sample effectively from the blood bag (reservoir), a small volume was drawn out of the loop first, then the sample taken, then the small volume was reintroduced. Samples were then centrifuged and the supernatant frozen at -80$^{o}$C until they could be assayed. All samples were assayed using a solid phase sandwich Enzyme Linked Immunosorbent Assay (ELISA) purchased commercially, according to the instructions from the manufacturer (Invitrogen, Camarillo, CA).

### 5.1.2 Statistical analysis

To compare data sets for different cytokines or different suspensions, the average $\Gamma_i$ value and standard deviation was calculated for each set of experiments, with n=3 unless otherwise stated.

$\Gamma_i$ values were then compared using an independent t-test with $p < 0.05$ considered significant and indicating a difference in the mean $\Gamma_i$ values.

## 5.2 CAPTURE OF CYTOKINES OF INTEREST IN RED BLOOD CELLS RESUSPENDED IN BUFFER

### 5.2.1 Capture of IL-6 in RBC resuspended in buffer

As a first set of experiments, we wanted to simplify capture in blood as much as possible and determined that red blood cells resuspended in buffer would achieve such a goal. We hypothesized that the presence of red blood cells would have no effect on capture rates and as shown in Figure 39, our hypothesis proved to be correct. For IL-6 capture in red blood cells resuspended in buffer, the average $\Gamma_i$ value obtained over three trials was 1.56E-4 ± 4.4E-5 $cm^2 \cdot mL \cdot min^{-1} \cdot g^{-1}$. This value was not statistically different from the $\Gamma_i$ value of IL-6 capture in buffer (1.76E-4 $cm^2 \cdot mL \cdot min^{-1} \cdot g^{-1}$, p=0.505). Total cytokine removal and overall trend of capture was exactly as seen in IL-6 capture in only buffer.

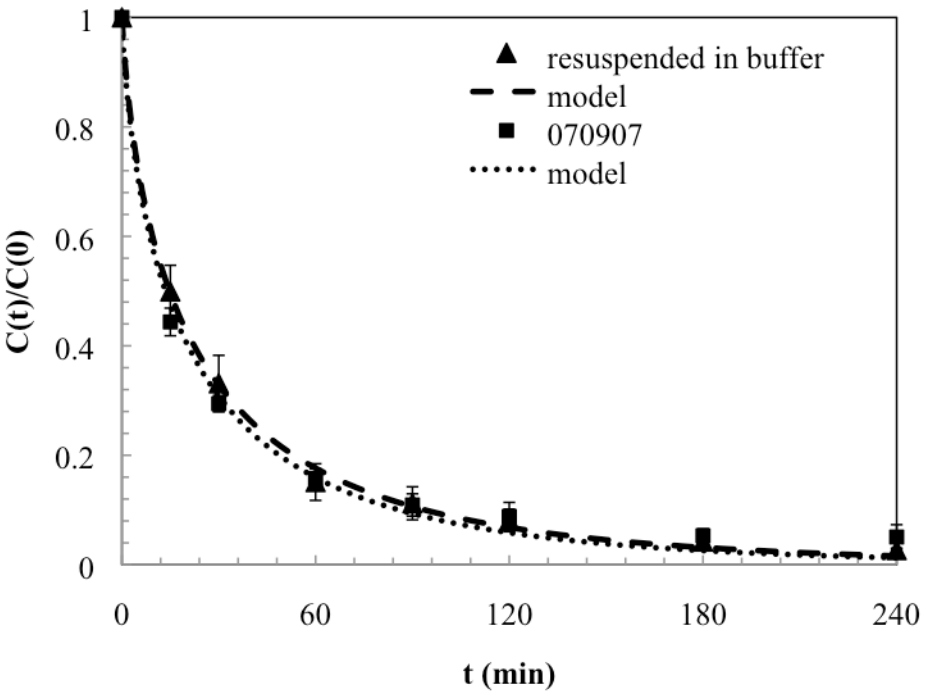


**Figure 39:** IL-6 capture in red blood cells resuspended in buffer

To ensure that no interaction between the red blood cells (or lysate) and IL-6 was taking place, two additional controls were also performed. In the first, IL-6 was spiked into buffer that contained lysed red blood cells. For this experiment, approximately 13 mL of washed red blood cells resuspended in buffer (40% HCT) were mechanically lysed with small metal ball bearings and then centrifuged. The supernatant was removed and placed into beakers for a typical recirculation experiment. Results of this experiment are shown in Figure 40 (left). The average $\Gamma_i$ value obtained over two trials was 1.43E-4 ± 2.4E-5 $cm^2 \cdot mL \cdot min^{-1} \cdot g^{-1}$. This value was not statistically different from the $\Gamma_i$ value of IL-6 capture in buffer (1.76E-4 $cm^2 \cdot mL \cdot min^{-1} \cdot g^{-1}$, p=0.268). In the second experiment, red blood cells were incubated with spiked buffer for one hour on a rocker. After the incubation, the suspension was centrifuged and the supernautant removed and used in a typical recirculation experiment. Results of this experiment are shown in

Figure 40 (right). The average $\Gamma_i$ value obtained over two trials was 1.23E-4 ± 3.5E-7 $cm^2 \cdot mL \cdot min^{-1} \cdot g^{-1}$. This value was not statistically different from the $\Gamma_i$ value of IL-6 capture in buffer (1.76E-4 $cm^2 \cdot mL \cdot min^{-1} \cdot g^{-1}$, p=0.144). From these controls, it is clear that there is no interaction between the red blood cells and the cytokine.

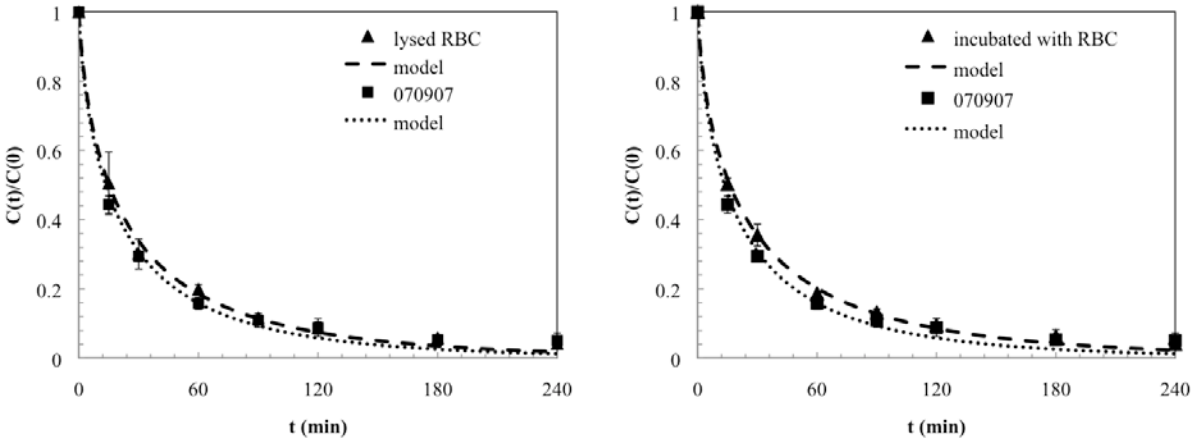


**Figure 40:** Lysed red blood cell capture (left) and buffer incubated in red blood cell capture (right) controls for red blood cell suspension capture

The next set of experiments included modifying the resevior volume and flow rate to test wheather the model was able to predict a change in $\Gamma_i$ value associated with not scaling the experiment to hematocrit, i.e. having a slower flow rate and reduced reservoir volume. From past validation experiments [46], the model was able to accurately predict changes in flow rate and reservoir volume and we hypothesized that the model would perform the same with this experiment. As shown in Figure 41, not scaling the red blood cell experiment does have an effect on overall capture trends, causing faster removal. We hypothesize that this effect is most likely due to the decreased reservoir volume, with decreased flow rate having a lesser effect. The average $\Gamma_i$ value obtained over three trials was 4.85E-4 ± 1.8E-4 $cm^2 \cdot mL \cdot min^{-1} \cdot g^{-1}$. This value was not statistically different from the $\Gamma_i$ value of IL-6 capture in buffer (1.76E-4

$cm^2 \cdot mL \cdot min^{-1} \cdot g^{-1}$, p=0.101). Therefore, the model was able to predict changes in the model regardless of scaling to hematocrit.

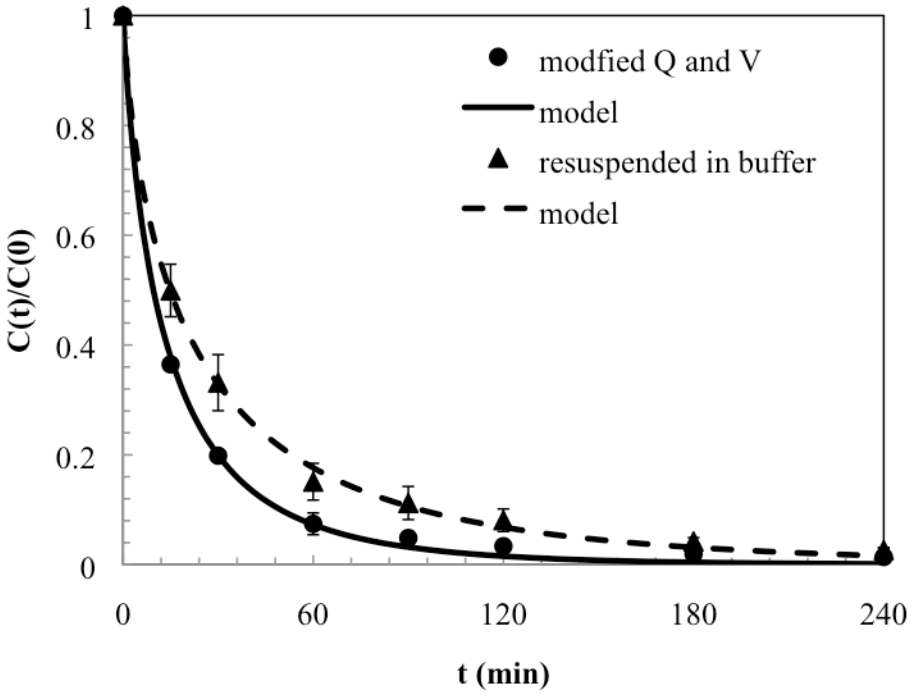


**Figure 41:** IL-6 capture with modified flow rate and reservoir volume to test model validation

### 5.2.2 Capture of TNF in RBC resuspended in buffer

Similarly to capture with IL-6, as a first set of experiments, we wanted to simplify capture in blood as much as possible and began experimentation with TNF in red blood cells resuspended in buffer. We hypothesized that the presence of red blood cells would again have no effect on capture rates and as shown in Figure 42, our hypothesis proved to be correct. For TNF capture in red blood cells resuspended in buffer, the average $\Gamma_i$ value obtained over three trials was 2.38E-5 ± 2.5E-6 $cm^2 \cdot mL \cdot min^{-1} \cdot g^{-1}$. This value was not statistically different from the $\Gamma_i$ value of TNF

capture in buffer (3.72E-5 $cm^2 \cdot mL \cdot min^{-1} \cdot g^{-1}$, p=0.810). Total cytokine removal and overall trend of capture was exactly as seen in TNF capture in only buffer. These results indicate that the presence of red blood cells alone have no effect on capture of TNF in buffer.

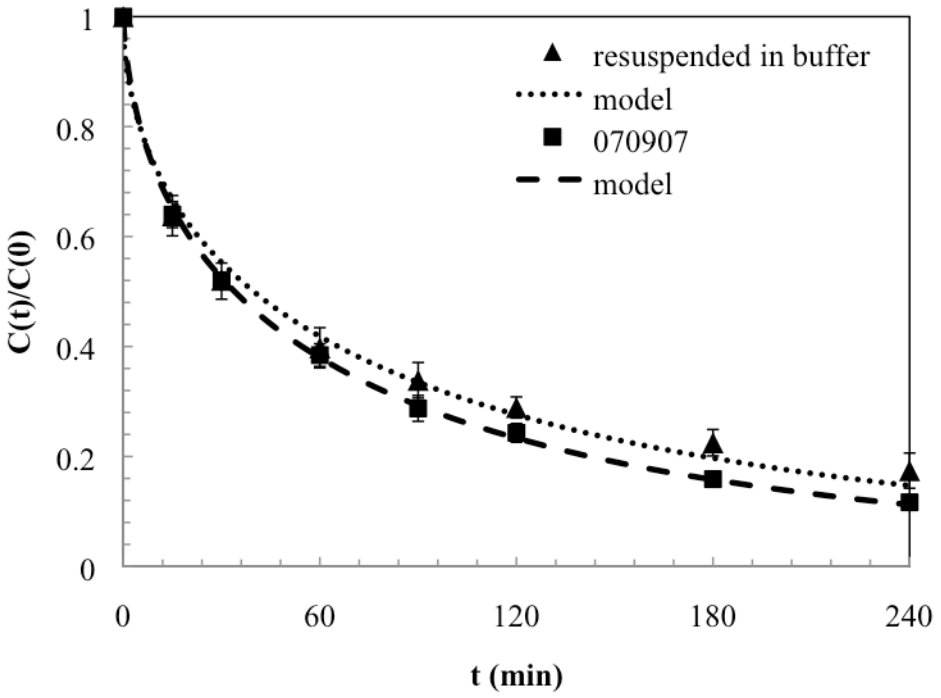


**Figure 42:** TNF capture in red blood cells resuspended in buffer

### 5.2.3 Capture of IL-10 in RBC resuspended in buffer

To round out our set of experiments of resuspended red blood cells, we finish this section with capture of IL-10 in each of the three previously discussed suspensions. For IL-10 capture in red blood cells resuspended in buffer, shown in Figure 43, the average $\Gamma_i$ value obtained over three trials was 1.66E-5 ± 3.0E-6 $cm^2 \cdot mL \cdot min^{-1} \cdot g^{-1}$. This value was not statistically different from the

$\Gamma_i$ value of IL-10 capture in buffer (5.64E-5 $cm^2 \cdot mL \cdot min^{-1} \cdot g^{-1}$, p=0.187). Total cytokine removal and overall trend of capture was exactly as seen in IL-10 capture in buffer only.

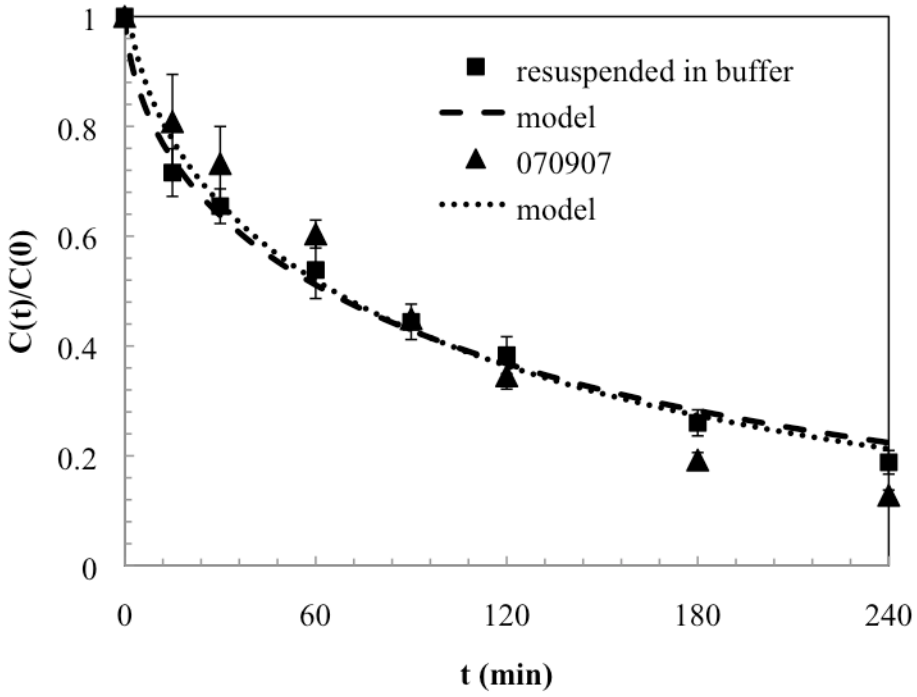


**Figure 43:** IL-10 capture in red blood cells resuspended in buffer

In conclusion, capture of IL-6 in red blood cell suspensions of buffer, as well as controls, were as expected, proving that the presence of red blood cells was not significant and had no interaction with the beads or IL-6. Additional experiments in this section included proved that the model was valid for capture experiments that were not scaled to hematocrit. Capture of TNF and IL-10 in red blood cell suspensions of buffer were both also as expected, proving that the presence of red blood cells was not significant and had no interaction with the beads or TNF or IL-10.

## 5.3 CAPTURE OF CYTOKINES OF INTEREST IN RED BLOOD CELLS RESUSPENDED IN HUMAN PLASMA

### 5.3.1 Capture of IL-6 in RBC resuspended in plasma

Our second set of experiments included recirculation of IL-6 in human plasma (compared to horse serum) as well as human red blood cells resuspended in human plasma. Here, we wanted to add another degree of complexity over simple buffer experiments and test whether the presence of human plasma would affect capture similarly to horse serum. We hypothesized that the presence of red blood cells would again have no effect on capture rates between capture in horse serum, capture in plasma only, and capture in red blood cells resuspended in plasma. However, there would be a difference between capture in plasma-based suspensions and those in only buffer. This reduction in capture rates from buffer to serum would most likely be due to the presence of additional components found in serum and plasma suspensions such as cytokine receptors, additional larger proteins, complements, etc.

For these capture experiments, shown in Figure 44, the average $\Gamma_i$ value obtained over two trials of IL-6 capture in human plasma was 6.90E-5 ± 4.0E-5 $cm^2 \cdot mL \cdot min^{-1} \cdot g^{-1}$. This value was not statistically different from the $\Gamma_i$ value of IL-6 capture in horse serum (5.08E-5 $cm^2 \cdot mL \cdot min^{-1} \cdot g^{-1}$, $p=0.672$) and was statistically different from capture in red blood cells resuspended in buffer (1.56E-5 $cm^2 \cdot mL \cdot min^{-1} \cdot g^{-1}$, $p<0.01$). For IL-6 capture in red blood cells resuspended in plasma, the average $\Gamma_i$ value obtained over three trials was 3.79E-5 ± 7.1E-6 $cm^2 \cdot mL \cdot min^{-1} \cdot g^{-1}$. This value was not statistically different from the $\Gamma_i$ value of IL-6 capture in serum (5.80E-5 $cm^2 \cdot mL \cdot min^{-1} \cdot g^{-1}$, $p=0.060$). Total removal of IL-6 in red blood cells

resuspended in plasma was decreased 5% to 93% removal compared to red blood cells resuspended in buffer with 97% removal.

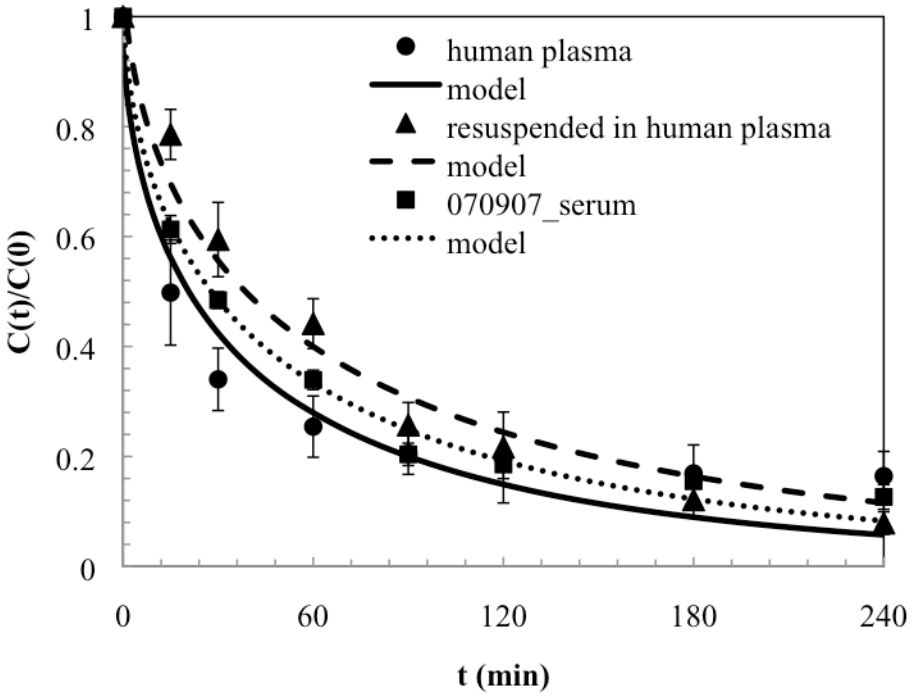


**Figure 44:** IL-6 capture in human plasma and red blood cells resuspended in human plasma

### 5.3.2 Capture of TNF in RBC resuspended in plasma

Our second set of experiments included recirculation of TNF in human plasma (compared to horse serum) as well as human red blood cells resuspended in human plasma. We again hypothesized that the presence of red blood cells would again have no effect on capture rates between capture in horse serum, capture in plasma only, and capture in red blood cells resuspended in plasma. However, there would be a difference between capture in plasma-based suspensions and those in only buffer.

For these capture experiments, shown in Figure 45, the average $\Gamma_i$ value obtained over two trials of TNF capture in human plasma was 7.69E-6 ± 1.7E-6 $cm^2 \cdot mL \cdot min^{-1} \cdot g^{-1}$ and was not statistically different from the $\Gamma_i$ value of TNF capture in horse serum (4.53E-6 $cm^2 \cdot mL \cdot min^{-1} \cdot g^{-1}$, p=0.530) and was statistically different from capture in red blood cells resuspended in buffer (2.38E-5 $cm^2 \cdot mL \cdot min^{-1} \cdot g^{-1}$, $p<0.05$). For TNF capture in red blood cells resuspended in plasma, the average $\Gamma_i$ value obtained over three trials was 4.90E-5 ± 4.9E-7 $cm^2 \cdot mL \cdot min^{-1} \cdot g^{-1}$. This value was not statistically different from the $\Gamma_i$ value of TNF capture in serum (4.52E-6 $cm^2 \cdot mL \cdot min^{-1} \cdot g^{-1}$, p=0.501). Total reduction of TNF spiked in whole blood was decreased more than 25% to 56% total removal compared to red blood cells resuspended in buffer with more than 80% removal.

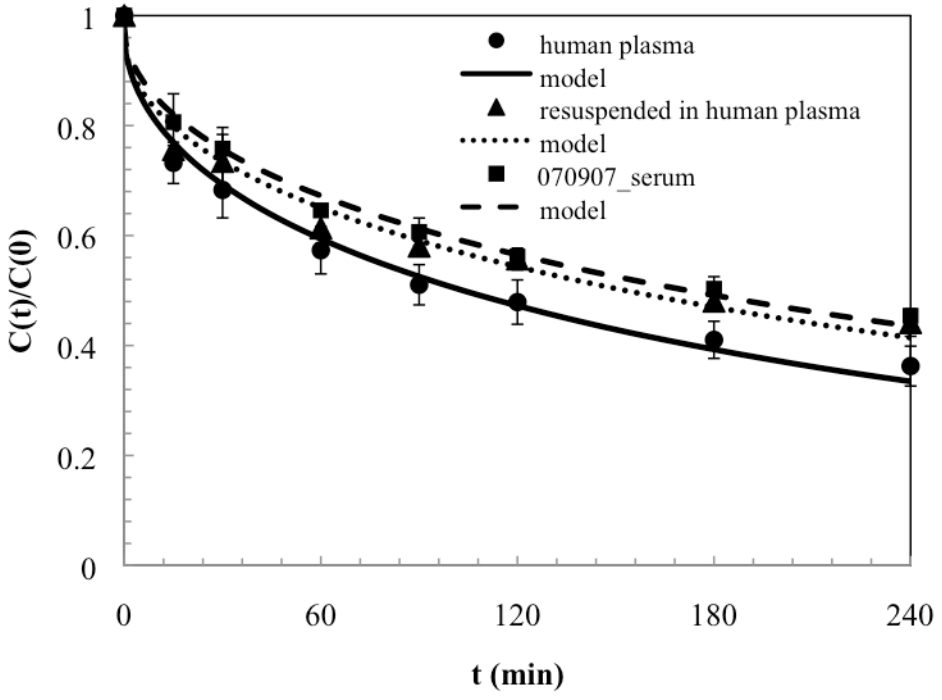


**Figure 45:** TNF capture in human plasma and red blood cells resuspended in human plasma

### 5.3.3 Capture of IL-10 in RBC resuspended in plasma

For IL-10 capture experiments in plasma and red blood cells resuspended in plasma, shown in Figure 46, the average $\Gamma_i$ value obtained over two trials of IL-10 capture in human plasma was 1.96E-5 ± 6.9E-6 $cm^2 \cdot mL \cdot min^{-1} \cdot g^{-1}$. This value was not statistically different from the $\Gamma_i$ value of IL-10 capture in horse serum (4.12E-5 $cm^2 \cdot mL \cdot min^{-1} \cdot g^{-1}$, p=0.577) and was not statistically different from capture in red blood cells resuspended in buffer (1.66E-5 $cm^2 \cdot mL \cdot min^{-1} \cdot g^{-1}$, p=0.691). For IL-10 capture in red blood cells resuspended in plasma, the average $\Gamma_i$ value obtained over three trials was 2.48E-5 ± 5.7E-7 $cm^2 \cdot mL \cdot min^{-1} \cdot g^{-1}$. This value was not statistically different from the $\Gamma_i$ value of IL-10 capture in serum (4.12E-5 $cm^2 \cdot mL \cdot min^{-1} \cdot g^{-1}$, p=0.456). Total cytokine removal and overall trend of capture was exactly as seen in all previous IL-10 captures. These results indicate that there is no statistical difference in capture rates for IL-10 in buffer or any of the red blood cell suspensions.

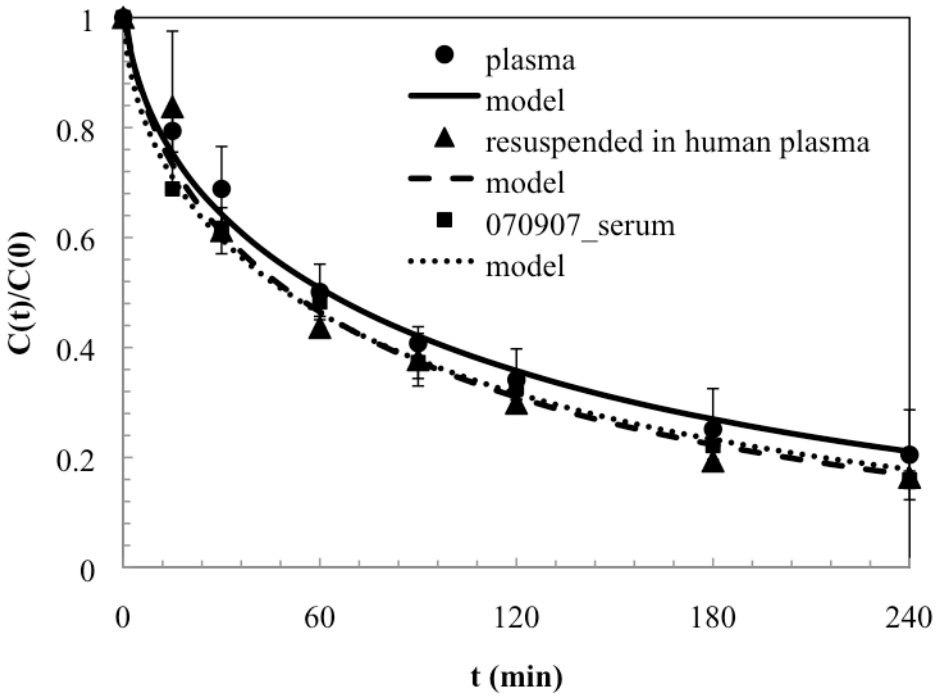


**Figure 46:** IL-10 capture in human plasma and red blood cells resuspended in human plasma

In conclusion, capture of IL-6 in red blood cell suspensions of plasma prove that the presence of red blood cells was not significant and had no interaction with the beads or IL-6. Capture of TNF and IL-10 in red blood cell suspensions of plasma were again as expected, proving that the presence of red blood cells was not significant and had no interaction with the TNF of IL-10.

## 5.4 CAPTURE OF CYTOKINES OF INTEREST HEALTHY HUMAN WHOLE BLOOD

### 5.4.1 Capture of IL-6 in whole blood

As a final set of experiments, we chose to spike IL-6 directly into 40% HCT healthy human whole blood and perform recirculation. In this set of experiments, additional complexities inherent in whole blood suspensions such as the presence of white blood cells were hypothesized to possibly cause issues in capture rates. . White blood cells make up approximately 1% of the total volume of whole blood in a healthy adult and consist of monocytes, neutrophils, basophils, and eosinophils. These cells are crucial for the body's immune response and many are responsible for the production of cytokines and chemokines involved in sepsis and septic shock. For example, activated monocytes produce IL-6 and activated macrophages produced IL-10 and TNF.

For these capture experiments, shown in Figure 47, the average $\Gamma_i$ value obtained over three trials of IL-6 capture was 1.21E-5 ± 1.1E-6 $cm^2 \cdot mL \cdot min^{-1} \cdot g^{-1}$. This value was statistically different from the $\Gamma_i$ value of previous IL-6 capture in red blood cells resuspended in plasma (3.80E-5 $cm^2 \cdot mL \cdot min^{-1} \cdot g^{-1}$, $p<0.001$). Total reduction of IL-6 spiked into whole blood was decreased more than 20% to only 70% removal compared to red blood cells resuspended in plasma with 93% total removal.

These results suggest the presence of some underlying mechanism that results in modified capture rates. We hypothesized that the reduction in capture of IL-6 was possibly due to one of two mechanisms: the production of cytokines by activated white blood cells present in the whole blood suspension or the adsorption of activated white blood cells and activated

platelets to the surface of the beads and subsequent production of cytokines. The activation of white blood cells and platelets may be caused by the circuit and/or interaction with the beads.

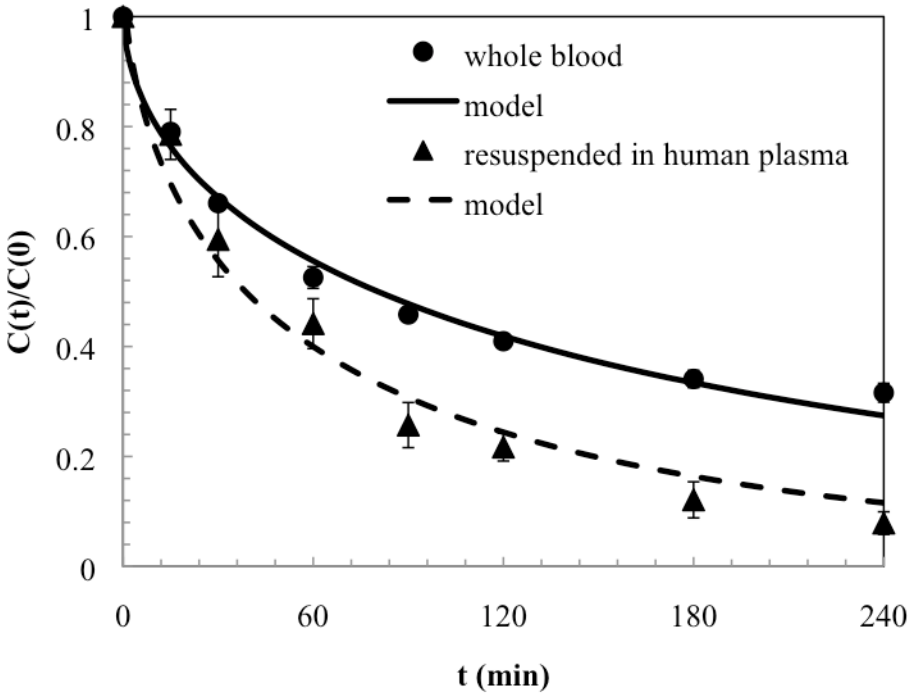


**Figure 47:** IL-6 capture in whole human blood compared to capture of red blood cells resuspended in human plasma

In order to test these hypotheses, two experiments were completed. In the first, a sham experiment (circuit without a CAD) was completed to test whether whtie blood cells were prodcuing cytokines that would reduce overall capture rates. The results of this experiment (not shown) indicate that cytokines are not being produced as concentration of IL-6 remained at or within 1% of the initial concentration. The second experiment involved closing the loop to air and keeping it temperature controlled, as described in section 5.1.1, in order to reduce possible activation of white blood cells and platelets. The results of this experiment are shown in Figure

48. The $\Gamma_i$ value obtained over one trial was 1.55E-5 $cm^2 \cdot mL \cdot min^{-1} \cdot g^{-1}$, an order or magnitude less than the $\Gamma_i$ value for IL-6 capture in red blood cells resuspended in buffer. Overall trend of capture was statistically the same to that of IL-6 spiked in whole blood. These results show that closing the loop and keeping it temperature controlled have little effect on capture rates. However, results of SEM images from our colleagues in the Kellum Laboratory indicate that white blood cells are adsorbing onto the surface of the beads in significant numbers. Figure 49 shows the results of the SEM images, with the whole blood perfused beads showing significant platelet and leukocyte adsorption compared to the control with no blood flow. The significant number of white blood cells adsorbed onto the surface of the beads also results in higher amounts of activation of the white blood cells as determined by flow cytometry analysis by our colleagues. An increase in white blood cell activation due to the presence of the novel sorbet polymer could in turn produce significant amounts of cytokines, affecting capture rates seen *in vitro*. Further investigation into this issue will be completed in the future.

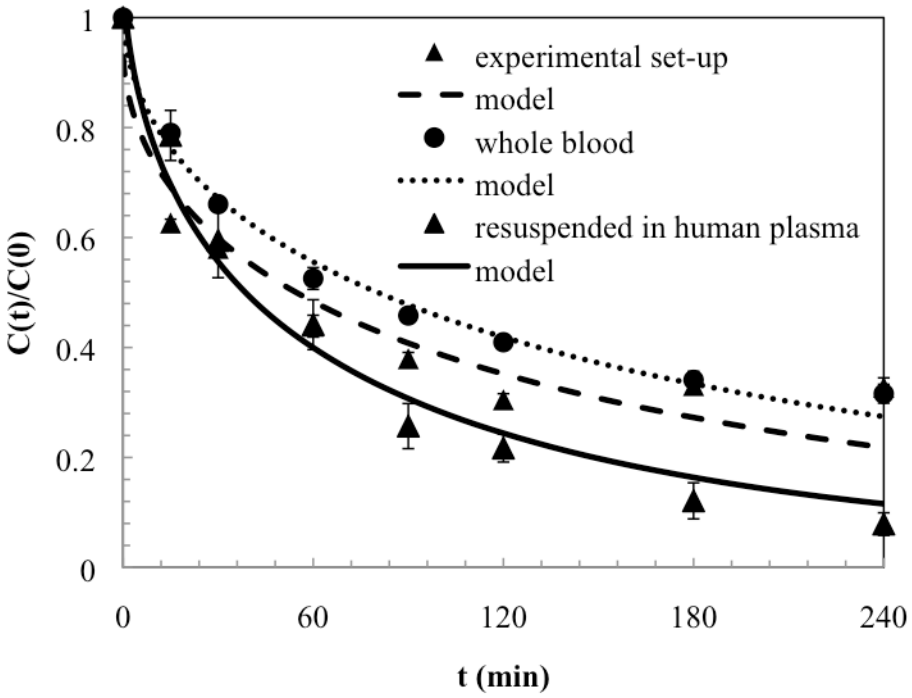


**Figure 48:** IL-6 capture in a modified experimental set up compared to capture in whole blood and capture in red blood cells resuspended in human plasma

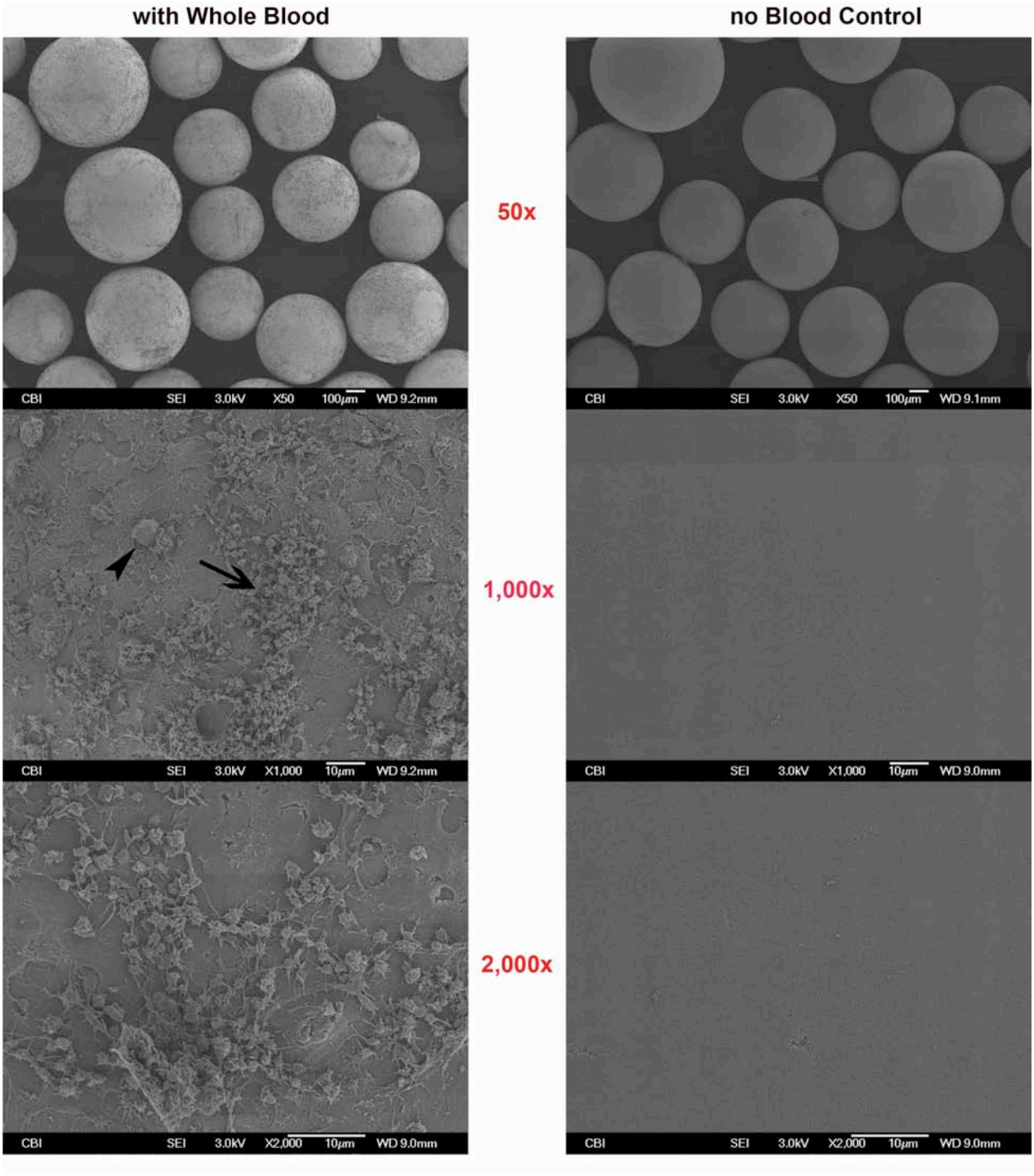


**Figure 49:** SEM images of the CytoSorb beads perfused with whole blood or no blood, as down by our colleagues in the Kellum Laboratory. A significant number of white blood cells are shown as adsorbed to the surface of the whole blood perfused bead.

### 5.4.2 Capture of TNF in whole blood

As a final set of experiments, we chose to spike TNF directly into 40% HCT healthy human whole blood and perform recirculation. For these capture experiments, shown in Figure 50, the average $\Gamma_i$ value obtained over three trials was 4.32E-6 ± 5.5E-7 $cm^2 \cdot mL \cdot min^{-1} \cdot g^{-1}$. This value was not statistically different from the $\Gamma_i$ value of previous TNF capture in red blood cells resuspended in plasma (4.90E-6 $cm^2 \cdot mL \cdot min^{-1} \cdot g^{-1}$, p=0.117). Total reduction of TNF in red blood cells resuspended in plasma was decreased 10% to 46% removal compared to red blood cells resuspended in plasma with 56% total removal. Unlike removal of IL-6, these results suggest that there is no effect of the presence of white blood cells on capture of TNF.

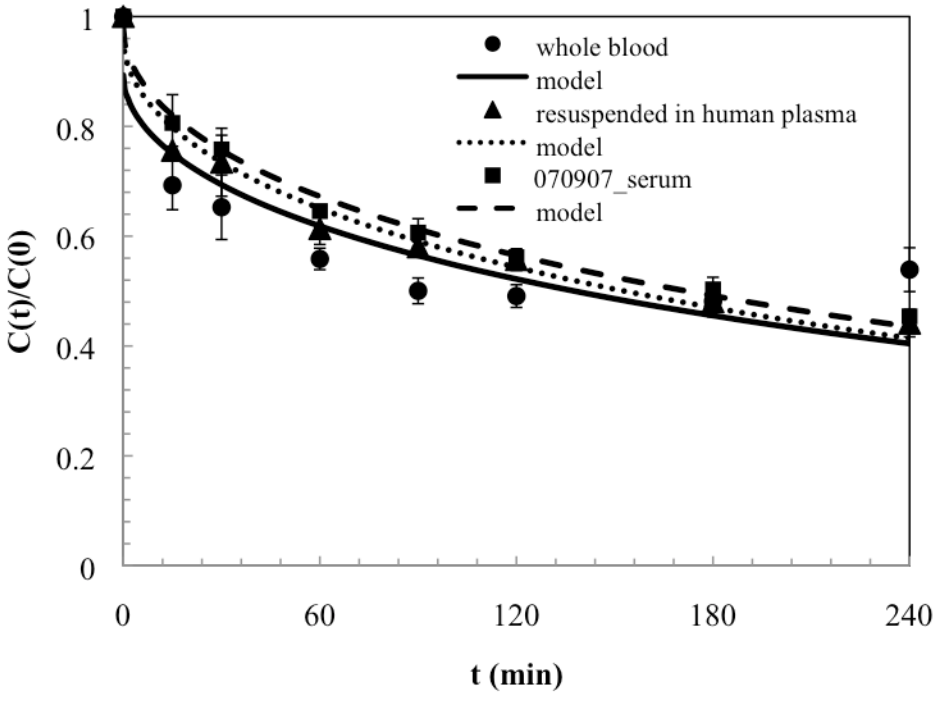


**Figure 50:** TNF capture in whole human blood compared to capture of red blood cells resuspended in human plasma

### 5.4.3 Capture of IL-10 in whole blood

For the final set of experiments in whole blood, shown in Figure 51, the average $\Gamma_i$ value obtained over three trials of IL-10 capture was 6.27E-6 ± 1.2E-6 $cm^2 \cdot mL \cdot min^{-1} \cdot g^{-1}$. This value was statistically different from the $\Gamma_i$ value of previous IL-10 capture in red blood cells resuspended in plasma (2.48E-5 $cm^2 \cdot mL \cdot min^{-1} \cdot g^{-1}$, $p<0.01$). Total reduction of IL-10 spiked in whole blood was decreased nearly 20% to only 64% removal compared to red blood cells resuspended in buffer with 82% total removal. Like IL-6 removal in whole blood, these results indicate an underlying mechanism responsible for the reduction in capture rates and could be attributed to the reduction in surface area due to significant white blood cell adsorption onto the bead surface.

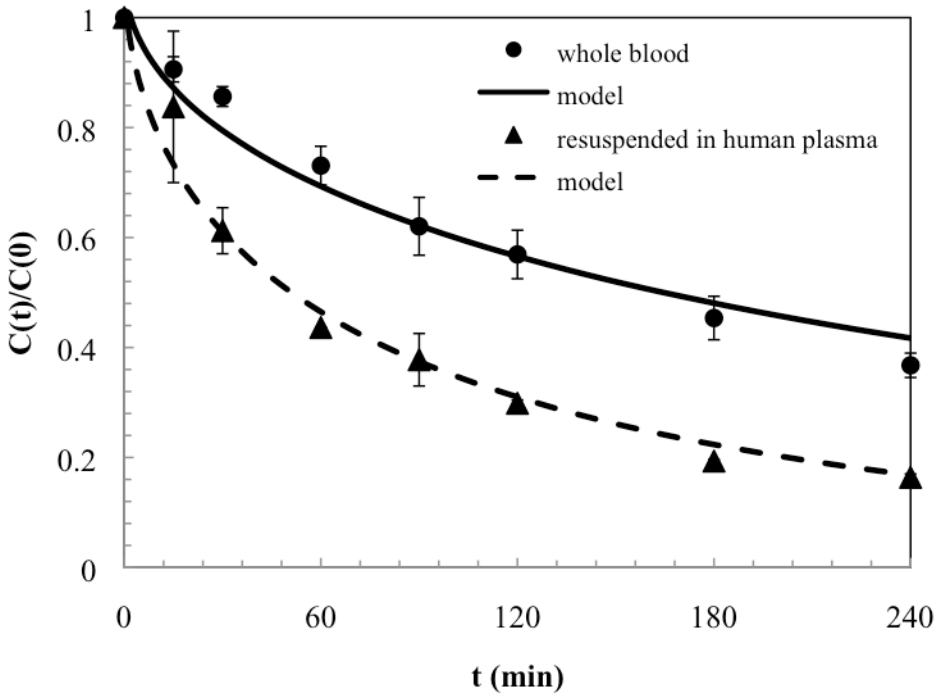


**Figure 51:** IL-10 capture in whole human blood compared to capture of red blood cells resuspended in human plasma

In conclusion, capture rates of IL-6 and IL-10 in whole blood were not as expected and had reduced removal, the mechanism behind which may include white blood cell adsorption to the bead and subsequent activation and production of white blood cells. Additional experiments of capture of TNF in whole blood were as expected and had similar removal to those in plasma. All of the data from this chapter will be included in the systems model of sepsis being developed by our colleagues.

# 6.0 SUMMARY AND CONCLUSIONS

The goal of this thesis was to characterize and compare adsorption profiles of a novel sorbent polymer used for the treatment of sepsis using different devices, suspensions, and cytokines. The specific aims included characterizing adsorption profiles and model fits of the three main cytokines of interest in buffer and serum for our original baseline polymer; characterization and comparison of adsorption during a change in bead lots as well as expanding our knowledge of adsorption by investigating other cytokines of interest; characterization of a small diameter bead lot and the subsequent development of a newly engineered device for use with the smaller polymer; and finally the characterization of cytokine capture in whole blood and red blood cell suspensions.

A mathematical model was previously developed in-house in order to guide development of the device and characteristics of the polymer used. Our mathematical model was derived in order to quantify and compare removal of cytokines from suspensions using different bead sizes, flow rates, reservoir volumes, suspensions, etc. The analysis the following simple analytic expression for the removal rate of individual cytokines:

$$-\frac{dC_i}{dt} = \frac{Q}{V_r}\left[1 - \exp\frac{-3}{\sqrt{\pi}}\frac{m_b}{Q}\frac{1}{R}\sqrt{\frac{\Gamma_i}{\rho t}}\right]C_i(t) \qquad \textbf{(8)}$$

where Q is the volumetric flow rate, $V_r$ is the suspension reservoir volume, $m_b$ is the mass of beads in the column, $R$ is the radius of bead in the column, and ρ is the density of the polymer [44]. The unknown parameter $\Gamma_i$, which is specific to the cytokine $i$ and the particular polymer, is defined as

$$\Gamma_i \equiv D_i q_i^{\max} K_i \qquad \textbf{(9)}$$

where $D_i$ is the effective diffusion coefficient of cytokine $i$ in the beads, $q_i^{max}$ is the maximum capacity of cytokine $i$ per unit mass of bead, and $K_i$ is the affinity constant from the Langmuir equilibrium adsorption isotherm [44].

Using this model, we discovered that the biocompatible baseline polymer was able to remove significant amounts of IL-6, TNF, IL-10, IL-1α, IL-1RA, HMG-B1, and IL-8 in both buffer and serum. A summary of the gamma values for our three main cytokines of interest for these experiments is shown below in Table 8.

**Table 8:** Comparison of gamma ($\Gamma_i$) values for IL-6, TNF, and IL-10 in baseline polymer for buffer and serum

| | **Buffer** | **Serum** |
|---|---|---|
| **IL-6** | 1.76E-4 | 5.08E-5 |
| **TNF** | 4.30E-5 | 4.52E-6 |
| **IL-10** | 1.86E-5 | 2.25E-5 |

Further reduction of polymer diameter resulted in faster capture rates for several of the cytokines and the resulting development of the reCAD for use with small polymer was also significant,

providing a device with reduced shear for lower hemolysis. A summary of the gamma values for our three main cytokines of interest for these experiments is shown below in Table 9.

**Table 9:** Gamma ($\Gamma_i$) values for IL-6, TNF, and IL-10 capture using small diameter polymer in the CAD and reCAD

| | **Small bead CAD** | **Small bead reCAD** | **p value** |
|---|---|---|---|
| **IL-6** | 2.60E-4 | 3.40E-6 | =0.310 |
| **TNF** | 4.77E-6 | 6.47E-6 | =0.513 |
| **IL-10** | 3.39E-5 | 1.38E-4 | =0.369 |

Finally, experimentation in red blood suspensions proved our hypothesis that the presence of red blood cells has no effect on capture; however, an underlying mechanism in capture of spiked whole blood results in a significant reduction of capture rates for both IL-6 and IL-10. Our preliminary hypothesis is that white blood cells, which interact and adsorb to the surface of the polymer, may be producing certain cytokines, therefore changing the rate of capture for some of the cytokines of interest. This mechanism will be investigated further in the future. A summary of the gamma values for our three main cytokines of interest for these experiments is shown below in Table 10.

**Table 10:** Gamma ($\Gamma_i$) values for IL-6, TNF, and IL-10 capture in healthy human whole blood

| | **IL-6** | **TNF** | **IL-10** |
|---|---|---|---|
| **Whole blood** | 1.21E-5 | 4.32E-6 | 6.27E-6 |

This characterization data is crucial not only for the validation and development of our own in-house mathematical model that will be discussed later, but also for the development and calibration of a systems model of sepsis developed by our colleagues [43]. This systems model will ultimately stimulate the development and progression of sepsis in humans and the integration of a therapeutic CAD intervention protocol into the timecourse of sepsis to improve patient outcomes. The work in this thesis provides a complete characterization of a novel sorbent polymer used for the treatment of sepsis. With the data in this thesis, optimizations and developments to both the polymer and the device can be made, further advancing hemoadsorption technology.

# APPENDIX A

# MATLAB® CODE FOR MATHEMATICAL MODEL

## A.1 ORIGINAL CODE

### A.1.1 CADs_ model_fitting.m

```
% Script file to perform nonlinear regression and analysis for the cytokine
% adsorbing device (CAD) model

% cartridge and bead parameters
global mb rho R Q Vr deltaV t_exp N
mb=1.5; % mass of adsorbing beads in the CADS (g)
rho=1.02; % density of adsorbing beads (g/ml)
R=266.58; % radius of adsorbing beads (microns)
R=R*10^-4; % work in cgs units

% device operating parameters
Q=0.8; % flowrate through device (ml/min)
Vr=8; % initial reservoir volume (ml)
deltaV=0.200; % sampling size that reduces the reservoir size at each time point
warning off all

% the experimental data below could also be inputed from a file

% input time of sampling
t_exp=[10^-4
   15
   30
   60
```

```
   90
   120
   180
   240];
N=length(t_exp);
tmax=t_exp(N)+t_exp(2);
tspan=[t_exp(1) tmax];

% input experimentally measured cytokine values
C_exp=[1
0.49929865
0.331467259
0.151037565
0.112290482
0.08093236
0.042398813
0.026708655];

% determine and evaluate initial guesses for best gamma and Ci
gamma=1.e-7; % initial guess for the gamma value describing data set
Ci=C_exp(1); % initial guess for the initial concentration value
[t_out,C_out]=ode45((@(t,C) C_dot(t,C,gamma)),tspan,Ci);


% perform nonlinear regressions to estimate best gamma and Ci
beta=[gamma Ci];
[betafit,resids,J]=nlinfit(t_exp,C_exp,'removal_predict',beta);
confident = nlparci(betafit,resids,J);% 95% confidence intervals for each parameter
gamma=betafit(1);
Ci=betafit(2);

% graphically evaluate best fit
[t_out,C_out]=ode45((@(t,C) C_dot(t,C,gamma)),tspan,Ci);
figure
plot(t_exp,C_exp,'o',t_out,C_out)
axis([0 tmax 0 C_exp(1)])
xlabel('Circulation Time (mins)')
ylabel('Cytokine Concentration')
legend('Experimental', 'Model Prediction')
%titletxt=sprintf(: Gamma_i = %.3e and C_i = %.2f',gamma,Ci);
title('Best-fit predictions versus experimental data')
labeltxt=sprintf('Gamma_i = %.3e \n C_i = %.2f',gamma,Ci);
gtext(labeltxt);

% output the final parameter values and confidence intervals
```

```
fprintf('Gamma_i = %.3e (w/ 95 percent CI from %.3e to
%.3e)',gamma,confident(1,1),confident(1,2))
fprintf('\n\n C_i = %.2f (w/ 95 percent CI from %.2f to %.2f)',Ci,confident(2,1),confident(2,2))
fprintf('\n')
```

### A.1.2 Removal_predict.m

```
function C_pred = removal_predict(beta,t);
N=length(t);
gamma=beta(1);
Ci=beta(2);
tspan=[0 t(N)];
[t_out,C_out]=ode45((@(t,C) C_dot(t,C,gamma)),tspan,Ci);
C_pred=interp1(t_out,C_out,t,'spline');
```

### A.1.3 C_dot.m

```
function y = C_dot(t,C,gamma);
% function file for computing the time-derivative of cytokine concentartion
% predicted by the model
global mb rho R Q Vr deltaV t_exp N
% adjust reservoir size for finite sampling size
Vact=Vr;
for n=1:N-2
   if t>t_exp(n+1) Vact=Vact-deltaV;
   end
end
y =-Q/Vact*(1-exp(-3/pi*mb/Q/R*sqrt(gamma/rho/t)))*C;
```

## A.2 MODIFIED CODE FOR SMALL BEAD CAPTURE

### A.2.1 reCADs_ model_fitting.m

```
% script file to perform nonlinear regression and analysis for the cytokine
% adsorbing device (CADS) model
```

```
% cartridge and bead parameters
global mb rho R Q Vr deltaV t_exp N
mb=1.5;
rho=1.02;% mass of adsorbing beads in the CADS (g)rho=1.02; % density of adsorbing beads
(g/ml)
R=46.4; % radius of adsorbing beads (microns)
R=R*10^-4; % work in cgs units
% device operating parameters
Q=0.8; % flowrate through device (ml/min)
Vr=8; % initial reservoir volume (ml)
deltaV=0.200; % sampling size that reduces the reservoir size at each time point
warning off all

% the experimental data below could also be inputted from a file
% input time of sampling
t_exp=[10^-4
15
30
60
90
120
180
240];

N=length(t_exp);
tmax=t_exp(N)+t_exp(2);
tspan=[t_exp(1) tmax];

% input experimentally measured cytokine values
C_exp=[1
0.392628866
0.29151298
0.174458939
0.121045562
0.114789769
0.078233595
0.078574256
];

% determine and evaluate initial guesses for best gamma and Ci
gamma=1.0e-7; % initial guess for the gamma value describing data set
Ci=C_exp(1); % initial guess for the initial concentration value
[t_out,C_out]=ode45((@(t,C) C_dot(t,C,gamma)),tspan,Ci);

% perform nonlinear regressions to estimate best gamma and Ci
beta=[gamma Ci];
```

```
[betafit,resids,J]=nlinfit(t_exp,C_exp,'removal_predict',beta);
confident = nlparci(betafit,resids,J);% 95% confidence intervals for each parameter
gamma=betafit(1);
Ci=betafit(2);

%r squared value and if statement to run new code
r2(1) = 1 - sum(resids.^2) / sum((C_exp - mean(C_exp)).^2);

if r2(1)<0.9999

% determine and evaluate initial guesses for best gamma and Ci
gamma=1.0e-5; % initial guess for the gamma value describing data set
Ci=C_exp(1); % initial guess for the initial concentration value
Cinf=0.0001; % initial guess for C infinity
[t_out,C_out]=ode45((@(t,C) C_smdot(t,C,gamma,Cinf)),tspan,Ci);

% perform nonlinear regressions to estimate best gamma, Ci, Cinf
beta=[gamma Ci Cinf];
[betafit,resids,J]=nlinfit(t_exp,C_exp,'sm_removal_predict',beta);
confident = nlparci(betafit,resids,J);% 95% confidence intervals for each parameter
gamma=betafit(1);
Ci=betafit(2);
Cinf=betafit(3);

r2(2) = 1 - sum(resids.^2) / sum((C_exp - mean(C_exp)).^2);

% graphically evaluate best fit
[t_out,C_out]=ode45((@(t,C) C_smdot(t,C,gamma,Cinf)),tspan,Ci);
figure
plot(t_exp,C_exp,'o',t_out,C_out)
axis([0 tmax 0 C_exp(1)])
xlabel('Circulation Time (mins)')
ylabel('Cytokine Concentration')
legend('Experimental', 'Model Prediction')
%titletxt=sprintf(: Gamma_i = %.3e and C_i = %.2f',gamma,Ci);
title('Best-fit predictions versus experimental data')
labeltxt=sprintf('Gamma_i = %.3e \n C_i = %.2f \n C_i_n_f = %.3f',gamma,Ci,Cinf);
gtext(labeltxt);

% output the final parameter values and confidence intervals
fprintf('Gamma_i = %.3e (w/ 95 percent CI from %.3e to
%.3e)',gamma,confident(1,1),confident(1,2))
fprintf('\n\n C_i = %.2f (w/ 95 percent CI from %.2f to %.2f)',Ci,confident(2,1),confident(2,2))
fprintf('\n\n R squared = %.2f; %.2f',r2(1),r2(2))
fprintf('\n')
```

```
else
[t_out,C_out]=ode45((@(t,C) C_dot(t,C,gamma)),tspan,Ci);
figure
plot(t_exp,C_exp,'o',t_out,C_out)
axis([0 tmax 0 C_exp(1)])
xlabel('Circulation Time (mins)')
ylabel('Cytokine Concentration')
legend('Experimental', 'Model Prediction')
%titletxt=sprintf(: Gamma_i = %.3e and C_i = %.2f',gamma,Ci);
title('Best-fit predictions versus experimental data')
labeltxt=sprintf('Gamma_i = %.3e \n C_i = %.2f',gamma,Ci);
gtext(labeltxt);

% output the final parameter values and confidence intervals
fprintf('Gamma_i = %.3e (w/ 95 percent CI from %.3e to
%.3e)',gamma,confident(1,1),confident(1,2))
fprintf('\n\n C_i = %.2f (w/ 95 percent CI from %.2f to %.2f)',Ci,confident(2,1),confident(2,2))
%fprintf('\n\n R squared = %.2f; %.2f',r2(1),r2(1))
fprintf('\n')
end
```

### A.2.2 Removal_predict.m

```
function C_pred = sm_removal_predict(beta,t);
N=length(t);
gamma=beta(1);
Ci=beta(2);
Cinf=beta(3);
tspan=[0 t(N)];
[t_out,C_out]=ode45((@(t,C) C_smdot(t,C,gamma,Cinf)),tspan,Ci);
C_pred=interp1(t_out,C_out,t,'spline');
```

### A.2.3 C_smdot.m

```
function y = C_smdot(t,C,gamma,Cinf)

% function file for computing the time-derivative of cytokine concentartion
% predicted by the model
global mb rho R Q Vr deltaV t_exp N
% adjust reservoir size for finite sampling size
Vact=Vr;
for n=1:N-2
```

```
    if t>t_exp(n+1) Vact=Vact-deltaV;
    end
end
y =-Q/Vact*(1-exp(-3/sqrt(pi)*mb/Q/R*sqrt(gamma/rho/t)))*(C-Cinf);
```

## BIBLIOGRAPHY


1. Vincent, J.L., J. Carlet, and S.M. Opal, *The sepsis text*. 2002, Boston: Kluwer Academic Publishers. xx, 848 p.

2. Bone, R.C., et al., *Definitions for sepsis and organ failure and guidelines for the use of innovative therapies in sepsis. The ACCP/SCCM Consensus Conference Committee. American College of Chest Physicians/Society of Critical Care Medicine.* Chest, 1992. **101**(6): p. 1644-1655.

3. Angus, D., *The effect of drotrecogin alfa (activated) on long-term survival after severe sepsis.* Crit Care Med, 2004. **32**(11): p. 2199-206.

4. Hodgin, K.E. and M. Moss, *The epidemiology of sepsis.* Curr Pharm Des, 2008. **14**(19): p. 1833-9.

5. *Centers for Disease Control: Increase in national hospital discharge survey rates for septicemia--United States, 1979-1987.* . JAMA, 1990(263): p. 937-8.

6. Kellum, J.A., *Systems Engineering of a Pheresis Intervention for Sepsis*. 2005, NIH: University of Pittsburgh.

7. Robertson, C.M. and C.M. Coopersmith, *The systemic inflammatory response syndrome.* Microbes Infect, 2006. **8**(5): p. 1382-9.

8. Rangel-Frausto, M.S., et al., *The natural history of the systemic inflammatory response syndrome (SIRS). A prospective study.* JAMA, 1995. **273**(2): p. 117-23.

9. Padkin, A., et al., *Epidemiology of severe sepsis occurring in the first 24 hrs in intensive care units in England, Wales, and Northern Ireland.* Crit Care Med, 2003. **31**(9): p. 2332-8.

10. Danai, P.A., et al., *Seasonal variation in the epidemiology of sepsis.* Crit Care Med, 2007. **35**(2): p. 410-5.

11. Jean-Baptiste, E., *Cellular Mechanisms in Sepsis.* J Intensive Care Med, 2007. **22**(2): p. 63-72.

12. Janeway, C., *Immunobiology : the immune system in health and disease*. 6th ed. 2005, New York: Garland Science. xxiii, 823 p.

13. Nylen, E.S. and A.A. Alarifi, *Humoral markers of severity and prognosis of critical illness.* Best Pract Res Clin Endocrinol Metab, 2001. **15**(4): p. 553-573.

14. Cinel, I. and S.M. Opal, *Molecular biology of inflammation and sepsis: a primer.* Crit Care Med, 2009. **37**(1): p. 291-304.

15. Tsuchida, K., et al., *Blood purification for critical illness: cytokines adsorption therapy.* Ther Apher Dial, 2006. **10**(1): p. 25-31.

16. Ventetuolo, C.E. and M.M. Levy, *Biomarkers: diagnosis and risk assessment in sepsis.* Clin Chest Med, 2008. **29**(4): p. 591-603, vii.

17. Yende, S., et al., *Inflammatory markers at hospital discharge predict subsequent mortality after pneumonia and sepsis.* Am J Respir Crit Care Med, 2008. **177**(11): p. 1242-7.

18. Kufe, D.W., et al., *Cancer medicine 6*. 6th ed. 2003, Hamilton, Ont. ; Lewiston, NY: BC Decker. 2 v. (xxiv, 2699, [40] p.).

19. Rivers, E.P., *Early goal-directed therapy in severe sepsis and septic shock: converting science to reality.* Chest, 2006. **129**(2): p. 217-8.

20. Kellum, J.A. and S. Uchino, *International Differences in the Treatment of Sepsis: Are They Justified?* JAMA, 2009. **301**(23): p. 2496-2497.

21. Hollenberg, S.M.M.D., et al., *Practice parameters for hemodynamic support of sepsis in adult patients: 2004 update.* Critical Care Medicine, 2004. **32**(9): p. 1928-1948.

22. Rivers, E., et al., *Early Goal-Directed Therapy in the Treatment of Severe Sepsis and Septic Shock.* N Engl J Med, 2001. **345**(19): p. 1368-1377.

23. Sharma, V.K. and R.P. Dellinger, *Treatment options for severe sepsis and septic shock.* Expert Rev Anti Infect Ther, 2006. **4**(3): p. 395-403.

24. Otero, R.M., et al., *Early goal-directed therapy in severe sepsis and septic shock revisited: concepts, controversies, and contemporary findings.* Chest, 2006. **130**(5): p. 1579-95.

25. Abraham, E., et al., *Double-blind randomised controlled trial of monoclonal antibody to human tumour necrosis factor in treatment of septic shock. NORASEPT II Study Group.* Lancet, 1998. **351**(9107): p. 929-33.

26. Fisher, C.J., Jr., et al., *Initial evaluation of human recombinant interleukin-1 receptor antagonist in the treatment of sepsis syndrome: a randomized, open-label, placebo-controlled multicenter trial.* Crit Care Med, 1994. **22**(1): p. 12-21.

27. Bernard, G., et al., *Efficacy and safety of recombinant human activated protein C for severe sepsis.* New Engl J Med, 2001. **344**(10): p. 699-709.

28. Annane, D., et al., *Effect of treatment with low doses of hydrocortisone and fludrocortisone on mortality in patients with septic shock.* JAMA, 2002. **288**(7): p. 862-71.

29. Opal, S., *Corticosteroids for patients with septic shock.* JAMA, 2003. **289**(1): p. 41-2.

30. Bellomo, R., *Continuous hemofiltration as blood purification in sepsis.* New Horizons, 1995. **3**(4): p. 732-7.

31. House, A.A. and C. Ronco, *Extracorporeal blood purification in sepsis and sepsis-related acute kidney injury.* Blood Purif, 2008. **26**(1): p. 30-5.

32. Kellum, J., *Immunomodulation in sepsis: the role of hemofiltration.* Minerva Anestesiol, 1999. **65**(6): p. 410-8.

33. De Vriese, A.S., et al., *Cytokine removal during continuous hemofiltration in septic patients.* J Am Soc Nephrol, 1999. **10**(4): p. 846-53.

34. Kellum, J.A. and M.K. Dishart, *Effect of hemofiltration filter adsorption on circulating IL-6 levels in septic rats.* Crit Care, 2002. **6**: p. 429-433.

35. Kellum, J.A., et al., *Diffusive vs. convective therapy: effects on mediators of inflammation in patient with severe systemic inflammatory response syndrome.* Crit Care Med, 1998. **26**(12): p. 1995-2000.

36. Oda, S., et al., *Cytokine adsorptive property of various adsorbents in immunoadsorption columns and a newly developed adsorbent: an in vitro study.* Blood Purif, 2004. **22**(6): p. 530-6.

37. Shimizu, T., et al., *Endotoxin apheresis for sepsis.* Transfus Apher Sci, 2006. **35**(3): p. 271-82.

38. Tsuchida, K., et al., *Lixelle adsorbent to remove inflammatory cytokines.* Artif Organs, 1998. **22**(12): p. 1064-7.

39. Albright, R.L., *Hemocompatible coated polymer and related one-step methods*, in http://patft.uspto.gov, U.S.P.a.T. Office, Editor. 2007, MedaSorb Corporation: United States. p. 11.

40. Song, M., et al., *Cytokine removal with a novel adsorbent polymer.* Blood Purification, 2004. **22**(5): p. 428-34.

41. Kellum, J.A., M. Song, and R. Venkataraman, *Hemoadsorption removes tumor necrosis factor, interleukin-6, and interleukin-10, reduces nuclear factor-kappaB DNA binding,*

*and improves short-term survival in lethal endotoxemia.* Crit Care Med, 2004. **32**(3): p. 801-805.

42. Kellum, J.A., et al., *Feasibility study of cytokine removal by hemoadsorption in brain-dead humans.* Crit Care Med, 2008. **36**(1): p. 268-72.

43. Daun, S., et al., *An ensemble of models of the acute inflammatory response to bacterial lipopolysaccharide in rats: results from parameter space reduction.* J Theor Biol, 2008. **253**(4): p. 843-53.

44. DiLeo, M.V., J. Kellum, and W.J. Federspiel, *A simple mathematical model of cytokine capture using a hemoadsorption device.* Annals of Biomedical Engineering, 2008. **37**(1): p. 222-229.

45. Kellum, J., et al., *Feasibility study of cytokine removal by hemoadsorption in brain-dead humans.* Crit Care Med, 2008. **36**(1): p. 268-72.

46. DiLeo, M.V., J.D. Fisher, and W.J. Federspiel, *Experimental validation of a theoretical model of cytokine capture using a hemoadsorption device.* Ann Biomed Eng, 2009. **37**(11): p. 2310-6.

47. Smith, R.A. and C. Baglioni, *The active form of tumor necrosis factor is a trimer.* J Biol Chem, 1987. **262**(15): p. 6951-4.

48. Corti, A., et al., *Oligomeric tumour necrosis factor alpha slowly converts into inactive forms at bioactive levels.* Biochem J, 1992. **284 (Pt 3)**: p. 905-10.

49. Tartaglia, L.A. and D.V. Goeddel, *Two TNF receptors.* Immunol Today, 1992. **13**(5): p. 151-3.

50. Bozza, F.A., P.T. Bozza, and H.C. Castro Faria Neto, *Beyond sepsis pathophysiology with cytokines: what is their value as biomarkers for disease severity?* Memorias do Instituto Oswaldo Cruz, 2005. **100 Suppl 1**: p. 217-21.

51. Andersson, U. and K.J. Tracey, *HMGB1 in sepsis.* Scand J Infect Dis, 2003. **35**(9): p. 577-84.

52. Hack, C.E., et al., *Interleukin-8 in sepsis: relation to shock and inflammatory mediators.* Infect Immun, 1992. **60**(7): p. 2835-42.

53. Cole, L., et al., *The effect of coupled haemofiltration and adsorption on inflammatory cytokines in an ex vivo model.* Nephrol Dial Transplant, 2002. **17**(11): p. 1950-6.

54. Hakim, R.M., *Clinical implications of biocompatibility in blood purification membranes.* Nephrol Dial Transplant, 2000. **15 Suppl 2**: p. 16-20.

55. Opatrny, K., Jr., *Clinical importance of biocompatibility and its effect on haemodialysis treatment.* Nephrol Dial Transplant, 2003. **18 Suppl 5**: p. v41-4.

56. Brandl, M., et al., *Detection of fluorescently labeled microparticles in blood.* Blood Purif, 2005. **23**(3): p. 181-189.

57. Vaslef, S.N. and R.W. Anderson, *The Artificial Lung*. 2002: Landes Bioscience.